SOME FACTORS AFFECTING FATIGUE RESISTANCE OF RUBBER SPRINGS

THESIS

presented for the degree of

DOCTOR OF PHILOSOPHY

in the

UNIVERSITY OF LONDON

and

DIPLOMA OF MEMBERSHIP

of the

IMPERIAL COLLEGE OF SCIENCE AND TECHNOLOGY

by

TEO SEN CHONG

Malaysian Rubber Producers' Research Association,
Brickendonbury,
Hertford, Hertfordshire

and

Mechanical Engineering Department,
Imperial College of Science and Technology,
London

January 1981

ABSTRACT

A fracture mechanics approach and two-dimensional finite-element analyses have been used to investigate some of the factors affecting the fatigue resistance of rubber springs.

Fatigue lives of rubber springs could be predicted provided the crack growth characteristics of rubbers under service conditions and the tearing energies (ie critical strain energy release rates) of rubber springs are known.

The crack growth characteristics of a natural rubber gum vulcanizate have been obtained at various temperatures and the fatigue lives of thin testpieces in simple extension predicted at 23 and 70°C assuming that an initial effective flaw size of 0.025 mm is present in the edges of the testpieces. For the thin testpieces used there is a reduction at relatively short times in crack growth and fatigue resistance at 100°C and above. This can be attributed mainly to oxidative effects as opposed to a lessening of strain-induced crystallization.

Since most rubber springs are substantially more bulky than the thin testpieces the effects of temperature at much longer times have been investigated using thick rubber blocks. An identation test is used to obtain the Young's modulus and puncture strength of rubber. Measurements on the blocks at the surface where oxidation occurs and at the centre where there is no oxidation show well defined variations of these two properties with ageing time at various temperatures.

The tearing energies of square-cornered bonded rubber blocks having cracks along the bonds are determined for various modes of deformation — tension, rotation and shear. The theoretical solutions

are confirmed by experiment or numerical finite-element analysis. As re-entrant square corners are undesirable in stressed components, stress and strain concentrations can be reduced by the use of fillets. Using the finite-element method the strain concentration factors of bonded rubber blocks with radiussed fillets are found to be a function of the height-to-fillet radius ratio and, in tension and rotation, also a function of shape factor ie ratio of loaded area to force free area.

ACKNOWLEDGEMENTS

The author is greatly indebted to Dr. P.B. Lindley, his Supervisor at the Malaysian Rubber Producers' Research Association and Dr. J.G. Williams, his Director of Studies at the Imperial College of Science and Technology. He is also indebted to Dr. L. Mullins, Director, and the Board of the Malaysian Rubber Producers' Research Association for the provision of experimental facilities to carry out this work.

The author's thanks are due to Dr. G.T. Knight for the radio-chemical analyses, to Dr. G.P. McSweeney for the TLC analyses and to Dr. I.R. Gelling for the oxygen uptake determinations given in Section 7.

CONTENTS

		Page
TITLE PAGE		1
ABSTRACT		2
ACKNOWLEDGEMENTS		4
CONTENTS		5
LIST OF FIGURES		10
LIST OF TABLES		18
NOTATION		19
	PART I	22
SECTION 1	GENERAL INTRODUCTION	23
SECTION 2	NATURAL RUBBER	26
2.1	Introduction	26
2.2	Chemical structure	26
2.3	Vulcanization	27
2.4	Compounding	28
2.5	Crosslinks	28
2.6	Effects of molecular structure	33
SECTION 3	THE CRACK GROWTH RESISTANCE OF NATURAL RUBBER	34
3.1	Introduction	34
3.2	Tearing of rubber	35
3.3	Crack growth characteristic	38
3.4	Mechanical crack growth limit T_o	40
3.5	Hysteresis	41
3.6	Fatigue in simple extension	44
3.7	Effect of oxygen	46
3.8	Strain concentrations	49
3.9	Crack growth in rubber components	52

		Page
	PART II	53
SECTION 4	EXPERIMENTAL METHODS FOR CRACK GROWTH AND FATIGUE STUDIES ON RUBBER	54
4.1	Apparatus	54
4.2	Preparation of rubber vulcanizate	58
4.3	Testpieces	59
4.4	Tensile force-deflection tests	61
4.5	Crack growth tests on tensile strips	63
4.6	Fatigue tests in simple extension	65
SECTION 5	TEARING ENERGY IN SIMPLE EXTENSION	66
5.1	Tearing energy for a tensile strip with an edge crack	66
5.2	Strain energy function	67
5.3	Relationship between W_1, W_2 and C_1, C_2	68
5.4	Determination of W_1 and W_2	70
5.4.1	Effect of test temperature on the W_2/W_1 ratio	74
5.4.2	Effect of time and temperature of vulcanization	74
5.4.3	Limits for W_2/W_1	79
5.5	Determination of k in simple extension	81
5.6	Numerical results	81
SECTION 6	RELAXING CRACK GROWTH AND FATIGUE AT ELEVATED TEMPERATURES	84
6.1	Effects of temperature	84
6.2	Crack growth characteristic and fatigue at 23°C	85

		Page
6.3	Fatigue of an unprotected rubber vulcanizate	90
6.4	Tensile tests at elevated temperatures	92
6.5	Ageing tests at elevated temperatures	94
6.6	Crack growth and fatigue at 70°C	97
6.7	Crack growth and fatigue at 100°C	97
6.8	Fatigue tests at 120°C and 140°C	102
6.9	Summary	105
SECTION 7	HIGH TEMPERATURE AGEING OF RUBBER BLOCKS	107
7.1	Introduction	107
7.2	Experimental method	111
7.3	Variations of stiffness and strength with time of ageing	112
7.4	Brittle skin formation	120
7.5	Oxidation of outer layer	123
7.6	Anaerobic ageing during vulcanization	128
7.7	Anaerobic ageing of bulk rubber	129
7.8	Weight losses	133
7.9	'Black hole' oxidation	135
7.10	Thickness effect	139
7.11	Summary	139
	PART III	142
SECTION 8	TEARING ENERGIES OF RUBBER SPRINGS	143
8.1	Introduction	143
8.2	Experimental method	144
8.2.1	Bonded shear springs	144
8.2.2	Shear crack growth tests	147
8.3	Numerical method	147

		Page
8.4	Simple shear with long crack	150
8.4.1	Theoretical	150
8.4.2	Numerical	152
8.4.3	Experimental	152
8.5	Simple shear with short cracks	155
8.6	Bonded disks in simple shear	160
8.7	Plane strain tension	160
8.7.1	Theoretical model	160
8.7.2	Theoretical solution	162
8.7.3	Numerical solutions	165
8.8	Disk in tension	167
8.9	Plane strain rotation	168
8.10	Summary	171
	PART IV	173
SECTION 9	STRAIN CONCENTRATION FACTORS FOR BONDED RUBBER BLOCKS WITH RADIUSSED FILLETS	174
9.1	Introduction	174
9.2	Numerical method	176
9.3	Plane stress	177
9.4	Theoretical considerations for F_s	181
9.4.1	Compression	181
9.4.2	Tension	182
9.4.3	Limiting values	183
9.4.4	Rotation	184
9.4.5	Shear	185
9.5	F_s for square-cornered blocks using finite elements	186

		Page
9.5.1	Comparison with theoretical predictions	186
9.5.2	Shear	188
9.6	Numerical results for radiussed fillets	190
9.6.1	Tension	190
9.6.2	Rotation	192
9.6.3	Shear	194
9.7	Stress concentration factors	197
9.8	Summary	197
	PART V	200
SECTION 10	GENERAL CONCLUSIONS AND SUGGESTIONS FOR FURTHER WORK	201
REFERENCES		206
	SUPPLEMENTARY REMARKS	210

LIST OF FIGURES

Figure		Page
2.1	Types of crosslinks in (a) conventional accelerated sulphur system (b) peroxide-cured system	29
3.1	Tensile strip, trousers and pure shear testpieces used for tear and crack growth testing	36
3.2	Crack growth characteristic of rubber	39
3.3	Diagram illustrating the effect of hysteresis of a rubber on its crack growth behaviour as proposed by Lake and Thomas (15). The diagram shows typical experimental results for gum vulcanizates of natural rubber (•) and SBR (o).	42
3.4	Fatigue lines for natural rubber gum vulcanizate under non-relaxing conditions: experimental points, theoretical curves (26)	47
3.5	Crack growth characteristics of protected and unprotected gum vulcanizates of natural rubber in air and vacuo (26)	48
3.6	Effect of reducing stress concentrations on the fatigue life of bonded 25 mm square x 6.3 mm thick testpieces of natural rubber (shown hatched) subjected to alternating shear deformations of $\pm$ 100% at 2 Hz (31). Large flaws became visible at the number of cycles shown	51
4.1	Dynamic testing machine for experimental investigation of crack growth and fatigue at laboratory temperature	55
4.2	Dynamic testing machine for experimental investigation of crack growth and fatigue at elevated temperatures	56

		Page
4.3	High temperature fatigue machine	57
4.4	Four types of testpieces: (a) dumbbell for fatigue testing; (b) tensile strip for crack growth testing; (c) Bongo and (d) ring testpieces for tensile strength	60
4.5	Relations of stress σ to strain e and of strain energy density W to strain e	62
5.1	Experimental variation of stress σ and extension ratio λ in the form from which the constants W_1 and W_2 can be obtained	71
5.2	Relations of experimental stress σ to strain e (X) and of strain energy density W to e (•). The full lines are theoretical curves given by eqs. (5.5) and (5.6) with $W_1 = .174$ and $W_2 = .195$	72
5.3	The effect of W_2/W_1 ratios on the shape of stress σ/E - strain curves, where E is the Young's modulus	73
5.4	The stress-strain curves of natural rubber gum vulcanizate A at elevated temperatures	75
5.5	Finite-element meshes used to represent tensile strip with the region around the crack shown enlarged	80
5.6	Variation with strain e of k in eq. (5.2) for simple extension strips determined by numerical method with different W_2/W_1 ratios. The experimental points (□) were obtained by Greensmith (10)	82
6.1	Crack growth characteristic for natural rubber gum vulcanizate A at 23°C. Experimental points. Full line relating crack growth rate dc/dn with	86

		Page
	tearing energy T given by eqs. (6.1) - (6.4)	
6.2	Dependence of fatigue life N of vulcanizate A on strain e at 23°C: experimental points; curve ab is predicted curve given by eqs. (6.1) - (6.4). Curve ac is the best line through the experimental points	89
6.3	Dependence of fatigue life N on strain e of unprotected natural rubber gum vulcanizate B. Experimental points. Curve ac is that at 23°C (Fig. 6.2)	91
6.4	Dependence of tensile strength on temperature for vulcanizate A. Experimental points	93
6.5	Tensile hysteresis loops at elevated temperatures	95
6.6	Crack growth characteristic for vulcanizate A at 70°C. Experimental points. The full line is that at 23°C (Fig. 6.1)	98
6.7	Dependence of fatigue life N on strain e of vulcanizate A at 70°C. Experimental points. Curve ac is that at 23°C (Fig. 6.2)	99
6.8	Crack growth characteristic for vulcanizate A at 100°C. Experimental points. The full line is that at 23°C (Fig. 6.1)	100
6.9	Dependence of fatigue life N on strain e of vulcanizate A at 100°C. Experimental points; curve ac is that at 23°C (Fig. 6.2)	101
6.10	Dependence of fatigue life N on strain e of vulcanizate A at 120°C. Experimental points; curve ac is that at 23°C (Fig. 6.2)	103

		Page
6.11	Dependence of fatigue life N on strain e of vulcanizate A at 140°C. Experimental points; curve ac is that at 23°C (Fig. 6.2)	104
7.1	Two pieces of rubber which have been aged for the same time: the thicker piece is still flexible, even at the surface, but the thinner one has become hard and brittle	109
7.2	A typical curve showing the relationship between the indentation force and the depth of indentation	113
7.3	Variation of Young's modulus E and puncture strength P (with ½ mm indentor) of the surface (X) and bulk (●) of rubber disks 25 mm diameter by 8 mm thick with time of ageing in air ovens at 70°C. Unaged values are indicated by the horizontal broken lines at the left	114
7.4	Details as Fig. 7.3 but with ageing at 100°C	115
7.5	Details as Fig. 7.3 but with ageing at 100°C	116
7.6	Details as Fig. 7.3 but with ageing at 125°C	117
7.7	Details as Fig. 7.3 but with ageing at 150°C	118
7.8	Details as Fig. 7.3 but with ageing at 150°C. At this temperature there was no abrupt drop in force when the indentor penetrated the surface for P values below about 6N, until the hard skin formed. To determine P the indentor was loaded and unloaded with gradually increasing maximum values, until a surface puncture could be seen	119
7.9	Curves from Figs. 7.3-7.8 representing surface values of E and P	121

		Page
7.10	Curves from Figs. 7.3-7.8 representing bulk values of E and P	122
7.11	Arrhenius plots of the time for the brittle skin to form (t^*) and the square of the depth of the discoloured surface layer after one day (h_1^2) against temperature. The abscissa covers the reciprocal of the absolute temperature linearly from 0.002 to 0.003	124
7.12	Percentage weight losses as a function of the square root of time in air at different temperatures of 50 x 50 x 25 mm blocks	134
7.13	Two different sections of the same block (aged for 15 days at 175°C). 'Black hole' oxidation	137
8.1	Double shear spring. Each of the two individual bonded rubber blocks (which corresponds to a single shear unit) is shown sheared by an amount he under shear force F. In the case of a double cylindrical shear unit, w is the diameter of the rubber disks	145
8.2	The shear stress-strain curve for natural rubber gum vulcanizate A	146
8.3	Finite-element representation of a section or part section of a rubber block. In all cases AB is a bond line and cracks are 'grown' from A. For a full section the height AD = h and the width AB = w; the depth, normal to the plane of the figure, is taken as unity in the analyses	149
8.4	Spring in simple shear at strain e (a) with no crack and (b) with a crack along the bond from the bottom left corner	151

		Page
8.5	Variation of energy loss U with crack length c (which also equals the crack area A) in plane strain simple shear. The points (w/h values as Fig. 8.7) were obtained using plane-strain finite-element analysis with w = 10 and 40, h = 1, G = 1 and e = 0.01. The slope of the line is given by eq. (8.4)	153
8.6	Experimental crack growth rate (dc/dn) against tearing energy (T) characteristic obtained using simple extension testpieces (Fig. 3.1 and eq. (3.4)) and rectangular cross-section springs in simple shear (Fig. 8.4 and eq. (8.4)). For the latter c > 3h.	154
8.7	Variation of the square root of the energy loss ($U^{\frac{1}{2}}$) with crack length c in simple shear. Finite-element data: h = 1, w/h as shown, G = 1 and e = 0.01. The full line has the form of eq. (8.6)	156
8.8	Variation of energy loss U with crack length c in simple shear for c $\leqslant$ h. Finite-element data: h = 1, w as Fig. 8.7, G = 1 and e = 0.01	157
8.9	Variation of tearing energy T with crack length c derived from finite-element analyses in simple shear (Figs. 8.7 and 8.8). Wh is the value of T for c > 3h	159
8.10	Experimental crack growth data obtained using double cylindrical shear springs in simple shear, with T from eq. (8.7) and simple extension testpieces	161

		Page
8.11	Theoretical model. The shaded areas are assumed to represent the volume of rubber from which all the energy is lost due to the crack(s)	163
8.12	Variation of the parameter u, eq. (8.17), with c/w for plane-strain sections in tension. Values of shape factor S (= w/2h) are shown alongside the curves. The scale for u is the same as that for c/w; the scale in square brackets applies to S = 0.2 and 20. The full lines are drawn through points obtained from finite-element analyses. The dotted lines are theoretical relations (u = c/w) for $K_1 = 1$. Significant departures from the latter, when K_1 is given by eq. (8.13), are represented by broken lines	166
8.13	Rotation of a plane-strain section. PP' is the tensile displacement of P caused by the transfer from P to Q of the centre of rotation of the top plate when cracks of length c are introduced at the left corners	169
9.1	Model section. For plane strain, the depth dimension normal to the plane of this section is infinite. For the purpose of calculation a section of unit depth is assumed. For disks w is the diameter	175
9.2	Part sections analysed numerically; in some cases a full section was analysed in shear. The strains are defined as shown for the three modes of deformation	178

		Page
9.3	Variation of strain concentration factor k for rubber sheets in tension with the height-to-radius ratio (h/r) for three width-to-height ratios (w/h). (Plane stress data from Lindley (33).)	180
9.4	Variation of effective strain concentration factors k at square corners with shape factor S for plane-strain sections in different modes of deformation and for disks in tension. For clarity the k values in shear have been multiplied by 10. (Numerical results)	187
9.5	Variation of F_s with shape factor S on logarithmic scales	189
9.6	Variation of (k - 0.4)/S with h/r on logarithmic scales for plane-strain sections and disks in tension a w/h = 1 (disks) b w/h = 1 (plane-strain section) c w/h = 2 (disk)	191
9.7	Numerical values of strain concentration factor k in tension plotted on logarithmic scales against the height-to radius ratio h/r for different shape factors S. The full-line curves are given by eq. (9.18)	193
9.8	Numerical results showing linear relation between corresponding values of k for rotation and k for tension	195
9.9	Variation of k with the height-to-radius ratio h/r for plane-strain sections in shear	196

LIST OF TABLES

Table		Page
2.1	Sulphur and accelerator concentrations (pphr) (1)	31
2.2	Type of crosslinks and its effect on the properties of natural rubber vulcanizates (3)	32
5.1	Values of W_1, W_2 and C_1, C_2 at elevated temperatures	76
5.2	Values of W_1, W_2 and C_1, C_2 at different combinations of time and temperature of vulcanization	77
5.3	Effect of vulcanization time at 140°C	78
6.1	Effect of ageing on properties of natural rubber vulcanizate A	96
7.1	Depth of oxidized layer after 1 day (h_1) and at longer times of ageing (h_{max})	126
7.2	Effect of vulcanization time at 150°C	130
7.3	Comparison of properties of air-aged and vacuum-aged rubber pellets	131
7.4	Properties of vacuum-aged 1 mm thick rubber sheet	132
7.5	Analysis of aged disks	136

NOTATION

A area of one surface of the crack measured in the unstrained state

A_o relaxing crack growth constant, eq. (3.7)

A_1 function of λ, eq. (5.19)

A_2 function of λ, eq. (5.20)

a constant in eq. (9.1)

B relaxing crack growth constant, eq. (3.8)

C_1 constant in eq. (5.8)

C_2 constant in eq. (5.8)

c crack length

c_c crack length corresponding to T_c

c_o length of flaw from which failure initiates

d unstressed crack tip diameter, eq. (3.10)

d diameter of a flat-ended indentor, eq. (7.1)

E Young's modulus

E_a activation energy, eq. (7.3)

E_c compression modulus

E_r rotation modulus

e strain

e_o mechanical fatigue limit in simple extension

e_1 compressive strain in Section 8.9

e_p maximum edge strain

e_{sc} shear strain at bond due to compressive strain e

e_x strain in the x direction

e_y strain in the y direction

e_z strain in the z direction

F indentation force

F_r function of h/r in eq. (9.1)

F_s function of w/h in eq. (9.1)

G shear modulus, first Lamé constant

G_e effective shear modulus

h unstrained rubber thickness or height

h_1 thickness of discoloured layer after 1 day ageing

h_{max} thickness of discoloured layer after ageing for long times

h^* thickness of discoloured layer when hard skin forms

I_1 strain invariant

I_2 strain invariant

K_1 function of W_2/W_1, eq. (5.23)

K_1 function of S, eq. (8.13)

K_2 function of W_2/W_1, eq. (5.24)

K_2 function of S, eq. (8.15)

K_3 function of S, eq. (8.20)

K_4 function of S, eq. (8.21)

K_5 function of S, eq. (8.26)

k function of strain, eq. (3.4)

k rate of reaction, eq. (7.3)

k strain concentration factor (Section 9)

k' stress concentration factor

k_s constant, eq. (8.5)

l_o undeformed length

M couple to maintain the rotation, eq. (8.23)

m number of corners at which there are cracks

N fatigue life, cycles

n number of cycles

P puncture strength

p relaxing crack growth constant, eq. (3.8)

p normal stress at the bonds, eq. (9.6)

p' limiting value of normal stress at the bond

p'' normal stress at the centre of the bond

P_y normal stress in the y direction

Q function of λ, eq. (5.14)

R gas constant, eq. (7.3)

r	radius of fillet
r_z	crack growth constant, eq. (3.7)
S	function of λ, eq. (5.16)
S	shape factor (cross-sectional area/force-free area)
T	tearing energy
T	absolute temperature
T_c	catastrophic tearing energy
T_i	initial tearing energy
T_o	relaxing mechanical crack growth limit
T_t	transition tearing energy
U	energy loss due to a crack
U_c	total elastic energy with a crack
U_o	total elastic energy without a crack
u	maximum displacement of edge
u	parameter proportional to U/T_i, eq. (8.17)
V	volume of rubber block
W	strain energy density
W_1	material constant, eq. (5.4)
W_2	material constant, eq. (5.4)
W_b	strain energy density at break
w	width of plane strain section or diameter of disk
x	function of c/w, eq. (8.8)
x	distance parallel to bond from square edge
y	distance from and normal to bond
θ	angle of rotation, eq. (8.23)
λ	extension ratio (1 + e)
λ	second Lamé constant
λ_1	principal extension ratio, eq. (5.2)
λ_2	principal extension ratio, eq. (5.2)
λ_3	principal extension ratio, eq. (5.2)
σ	stress

PART I

		Page
Section 1	General Introduction	23
Section 2	Natural rubber	26
Section 3	The crack growth resistance of natural rubber	34

SECTION 1 GENERAL INTRODUCTION

In the last two decades the importance of rubber as an engineering material has grown considerably. The demand for it and the range of its applications in all branches of engineering show a steady increase.

Rubber differs from other solid engineering materials in having a very low shear modulus combined with large extensibility and deformability. In addition it is relatively incompressible with its bulk modulus two or three orders of magnitude greater than its shear modulus. This is of particular relevance in the design of components which require a very high ratio of stiffness in one direction to that in another. The combination of these properties makes rubber a unique material for many engineering applications.

It is widely used in springs which range from small engine mountings to massive bearings for buildings. In springs, the rubber is usually bonded between more rigid materials which can then be bolted to a structural member. The main function of the springs is to absorb the harmful effects of vibration by attenuating the magnitudes of the transmitted forces or deformations. The repeated deformation to which the springs are subjected may lead to fatigue failure which, as in other materials, is due to the growth of cracks.

There are many factors that can affect the fatigue resistance of rubber springs. They can be broadly classified into three categories, namely the strength properties such as crack growth resistance of rubber, the design of springs and how they are manufactured.

Crack growth in rubber has been extensively studied using a fracture mechanics approach which has proved extremely useful in understanding the strength properties of vulcanized rubbers. The approach is based on a concept of tearing energy which is the energy

available for crack growth. It is also known as critical strain energy release rate. If the crack growth rate of the rubber is expressed in terms of this parameter, it is independent of shape and size of test piece and type of deformation. It is thus an intrinsic property of the material. The relationship between the crack growth rate and the tearing energy defines the crack growth characteristics of rubber.

Nowadays, more and more rubber springs are required to operate intermittently, and occasionally continuously, at temperatures substantially higher than normal ambient. Oxidative degradation is generally considered to be the most serious problem in the use of rubber at high temperatures. Consequently many investigations have been carried out on thin strips of rubber to understand either the oxidative ageing behaviour of rubber or the basic chemical process of oxidation. There is, however, little information available on the effect of elevated temperature on the crack growth characteristics of rubber or on the ageing behaviour of bulky rubber springs. An experimental investigation aimed at providing such information is described in Part II.

The fracture mechanics approach can in principle be applied to predict the fatigue life of rubber springs. However, a major difficulty is to determine the relationship between the tearing energy and the crack size and/or the overall applied forces. With the aid of computers, a numerical approach offers a solution. A numerical method based on two dimensional finite-element analyses has been used to determine the energy for crack growth at the bonds of rubber springs. This is described in Part III.

When a rubber spring is deformed, a non-uniform distribution of strain is introduced in the spring. A peak value of strain, ie a strain concentration, may therefore be expected in the vicinity of the bonds. Fatigue failure usually initiates at sites of high strain concentration. It is thus essential that the peak value should be reduced to a safe level. In the design of metal components, there are many published data to help designers evaluate strain concentration factors so as to enable them to improve their strength calculations, better balance their designs, and reduce the number of failures of machine parts and structural elements. However, no major general guidelines have been provided in the design of rubber components. Studies undertaken to obtain design data on strain concentrations in rubber springs are described in Part IV. Here again the finite-element method has been used.

The main aim of the work to be described in this thesis is to further the knowledge and understanding of the factors affecting the fatigue resistance of rubber springs, so that the engineer may design rubber springs which, when manufactured, will perform exactly as he intended and for as long.

SECTION 2 NATURAL RUBBER

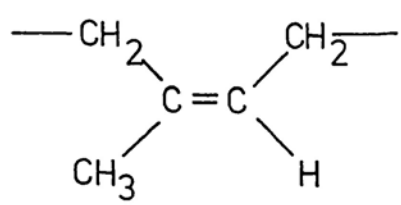
2.1 Introduction

Polymers are a class of materials characterised by their long molecular chain structure which is built up by the regular or irregular repetition of one or more types of chemical units - monomers. Some members of this class have the ability to undergo large deformations and to recover rapidly and substantially on release of the deforming forces. These are the characteristics of a rubber. There are many types of rubber which differ from one another in the chemical structures of their basic monomer units and this gives rise to different properties.

Natural rubber, one of the most widely used rubbers, is the material used for the experimental studies in this thesis.

2.2 Chemical structure

Natural rubber is cis-1,4-polyisoprene, its empirical formula being $(C_5H_8)_n$ where n is of the order of 10 000 and C_5H_8 is the monomer isoprene. The configuration of the isoprene unit is



Every fourth bond in the chain is a double bond, and every fourth carbon atom has attached to it the methyl (CH_3) group. Gutta-percha, a hard plastic material, has the same empirical formula as natural

rubber, the difference being solely in the arrangement of the single C-C bonds adjacent to the double bond. In natural rubber these single bonds both lie on the same side of the double bond, ie , forming the cis-configuration, whilst in gutta-percha the single bonds lie on opposite sides of the double bond, ie , to form the trans-configuration.

2.3 Vulcanization

Natural rubber is commonly obtained from the latex of 'Hevea brasiliensis', a large tree which is indigenous to the Amazonian rain forests of Brazil and has been cultivated mainly in South East Asia and West Africa. Raw rubber is obtained by coagulation of the latex with acid, followed by washing and drying. At this stage the raw rubber has little practical use. To make it so, it has to undergo the chemical reaction of vulcanization, a process by which the long flexible rubber chains are chemically crosslinked at intervals along their lengths with adjacent rubber chains to form a three dimensional network. This process transforms the raw rubber into a resilient, highly elastic material of considerable strength,and stable over a wide range of temperatures.

The vulcanization (or curing) process is generally carried out under pressure in metal moulds at a temperature in excess of 100^{o}C and takes from a few minutes to several hours depending upon the type of vulcanization system used and the size of the component.

Vulcanized rubber is generally referred to as 'rubber' or 'vulcanizate'.

2.4 Compounding

Several chemicals can be used as vulcanizing agents for natural rubber. Sulphur, however, is still the paramount agent for effecting crosslinking, as it has been since the inception of vulcanization. Recent developments in vulcanizing systems for natural rubber have been extensively reviewed by Elliott and Tidd (1).

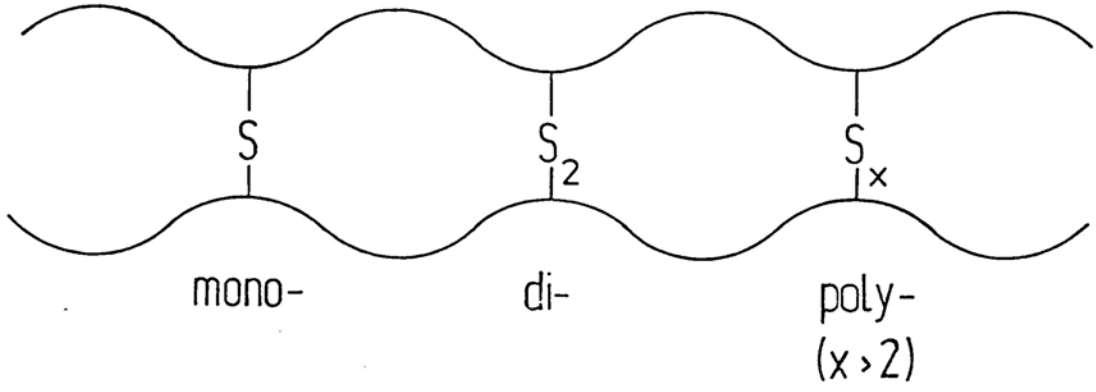
In addition to the crosslinking agents, other chemicals are incorporated in the rubber mix prior to vulcanization. The main additives are accelerators usually in combination with activators to catalyse and speed up the vulcanization process. Antidegradants are added to protect the rubber against oxidation and ozone attack. Reinforcing filler, notably carbon black, is added to increase the stiffness and strength properties such as the tear and abrasion resistance of the vulcanizate. Processing oils may be added to facilitate mixing these chemicals with the raw rubber. Other chemicals may be added to soften, cheapen and colour the vulcanizate.

Mixing is usually carried out on an open two-roll rubber mill or, more commonly, in a Banbury internal mixer. To ensure good physical properties the ingredients must be well dispersed in the rubber to form a homogeneous mix. The maldispersion of the ingredients can have a marked effect on tensile strength at elevated temperature (2).

2.5 Crosslinks

Different vulcanization systems produce different types of crosslinks. In accelerated sulphur systems, three types of crosslinks are formed, namely mono-, di- and poly-sulphidic crosslinks (Fig. 2.1a). The proportions of each group formed depends largely on the ratio of sulphur to accelerator concentration

(a). sulphidic crosslinks



(b). carbon-carbon crosslinks

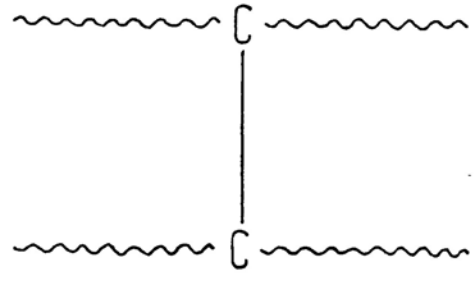


Fig. 2.1 Types of crosslinks in (a) conventional accelerated sulphur system (b) peroxide-cured system.

and on both the time and temperature of vulcanization (1). This ratio is used to classify accelerated sulphur systems into conventional systems which contain a much higher concentration of sulphur than accelerator, EV (efficient vulcanizing) systems which contain a much lower concentration of sulphur than accelerator, and the intermediate, semi-EV systems. The approximate concentrations of sulphur and accelerator in the three systems are given in Table 2.1. The type and proportion of sulphidic crosslinks for each system are given in Table 2.2. (3).

In sulphurless systems, organic peroxides such as dicumyl peroxide are commonly used as crosslinking agents: these form carbon-carbon crosslinks (Fig. 2.1b).

The type of vulcanization system employed has a significant effect on the properties of natural rubber vulcanizates. Conventional sulphur vulcanization systems give rubber with higher tensile and tear strengths than rubbers vulcanized with EV systems, and these are stronger than peroxide-cured rubbers (4). The ranking of vulcanized rubber to heat resistance is, however, in reverse order to that based on its strength properties. This is because carbon-carbon crosslinks are more stable to heat than mono-sulphidic crosslinks, poly-sulphidic crosslinks being the least stable (5) as shown in Table 2.2.

In this thesis, a vulcanizate (Vulcanizate A) based on EV system is used for the high temperature experimental studies described later because of its good heat resistance at elevated temperatures. Even though peroxide cured system has a higher degree of thermal stability, it is not a good practical compound in terms of poor strength and a slow rate of curing. Also, the rubber surface tends to become very sticky during the cure and the vulcanizate has an unpleasant odour.

Table 2.1 Sulphur and accelerator concentrations (pphr)* (1)

	Sulphur	Accelerator
Conventional	2.0 to 3.5	0.4 to 1.0
Semi-EV	1.0 to 1.7	1.0 to 2.5
EV	0.3 to 0.8	2.5 to 6.0

* pphr - parts per hundred of rubber

Table 2.2 Type of crosslinks and its effect on the properties of natural rubber vulcanizates (3)

	Conventional	Semi-EV	EV	Peroxide
Crosslinks				
Poly and Di $-S_x-$, $-S_2-$	95%	50%	20%	-
Mono -S-	5%	50%	80%	-
Carbon C-C	-	-	-	100%
Heat resistance	——— increasing ———→			
Strength	←——— increasing ———			

2.6 Effects of molecular structure

The molecular structural network of natural rubber gives rise to two important features. One is due to the regular structure of its long chain molecules. When the rubber is stretched to high strains, portions of the molecular chains become aligned in the direction of the extension giving rise to strain-induced crystallization. This phenomenon also occurs in some synthetic rubbers, such as polybutadiene and polychloroprene but not in others. Styrene-butadiene rubber (SBR) for example, is a copolymer of randomly arranged butadiene and styrene units which inhibit crystallization.

The other feature, common to most general purpose rubbers, is due to the presence of highly-reactive double bonds in the molecules which enable vulcanization process to take place. However, the double bond is also very reactive with other chemicals notably oxygen and ozone.

These two features - strain induced crystallization which is beneficial and susceptibility to oxygen and ozone which is not - greatly influence the fatigue and crack growth resistance of natural rubber and will be discussed more fully in later sections.

SECTION 3 THE CRACK GROWTH RESISTANCE OF NATURAL RUBBER

3.1 Introduction

Theoretically, the strength of rubber or any materials is the stress required to rupture its chemical bonds. In practice, however, most materials fail under tensile loading at a stress one or more orders of magnitude below the theoretical strength. The discrepancy between the theoretical strength and actual fracture strength was first explained by Griffith (6). He postulated that solids normally contain imperfections such as inhomogeneities or flaws which act as stress raisers creating localized stresses much greater than those in the bulk. It is at such a site of high stress concentration that failure usually initiates to form a crack which may ultimately propagate through the material under the action of the applied forces and environmental conditions. Thus the fundamental failure mechanism is that of crack propagation.

According to Griffith a crack present in a stressed specimen will propagate when the strain energy released by the crack growth exceeds the surface free energy created by the formation of the new surfaces, but this criterion applies reasonably well only in the fracture of certain brittle materials such as glass (6). In other materials additional energy is required to take into account other forms of energy dissipation such as plastic flow or mechanical hysteresis (7). In the tearing of rubber, energy is being dissipated irreversibly, ultimately as heat (8) and not appearing exclusively as surface energy as in brittle material. Thus some modification of Griffith's theory is necessary when applied to the tearing of rubber.

3.2 Tearing of rubber

Rivlin and Thomas (9) extended the Griffith energy balance approach to a highly elastic material such as rubber. They introduced the concept of tearing energy T which is defined for a strained testpiece containing a crack as the elastic strain energy dissipated per unit area of crack growth, i.e.

$$T = -\left(\frac{\partial U}{\partial A}\right)_1 \qquad (3.1)$$

where U is the total elastic stored strain energy in the testpiece, A the area of one surface of the crack measured in the unstrained state, and the suffix 1 denotes that the differentiation is carried out at constant deformation so that no work is done by the applied forces. It represents the rate of release of strain energy as the crack propagates and can be considered as the energy available for crack growth.

This criterion is seen to be similar to the Griffith criterion for brittle materials, but T is no longer to be interpreted as surface energy because the energy dissipation occurs irreversibly in a highly localized region around the crack tip. It is therefore to be expected that T will be substantially independent of the overall shape of the testpiece but be governed by the properties of the rubber at the localised zone around the crack tip and by the geometrical form of the tip.

In order to verify the criterion, Rivlin and Thomas carried out tear tests using testpieces of different size and shape for which T could be calculated from readily measured forces or strains. Three such testpieces are shown in Fig. 3.1; their tearing energies are as follows (9):

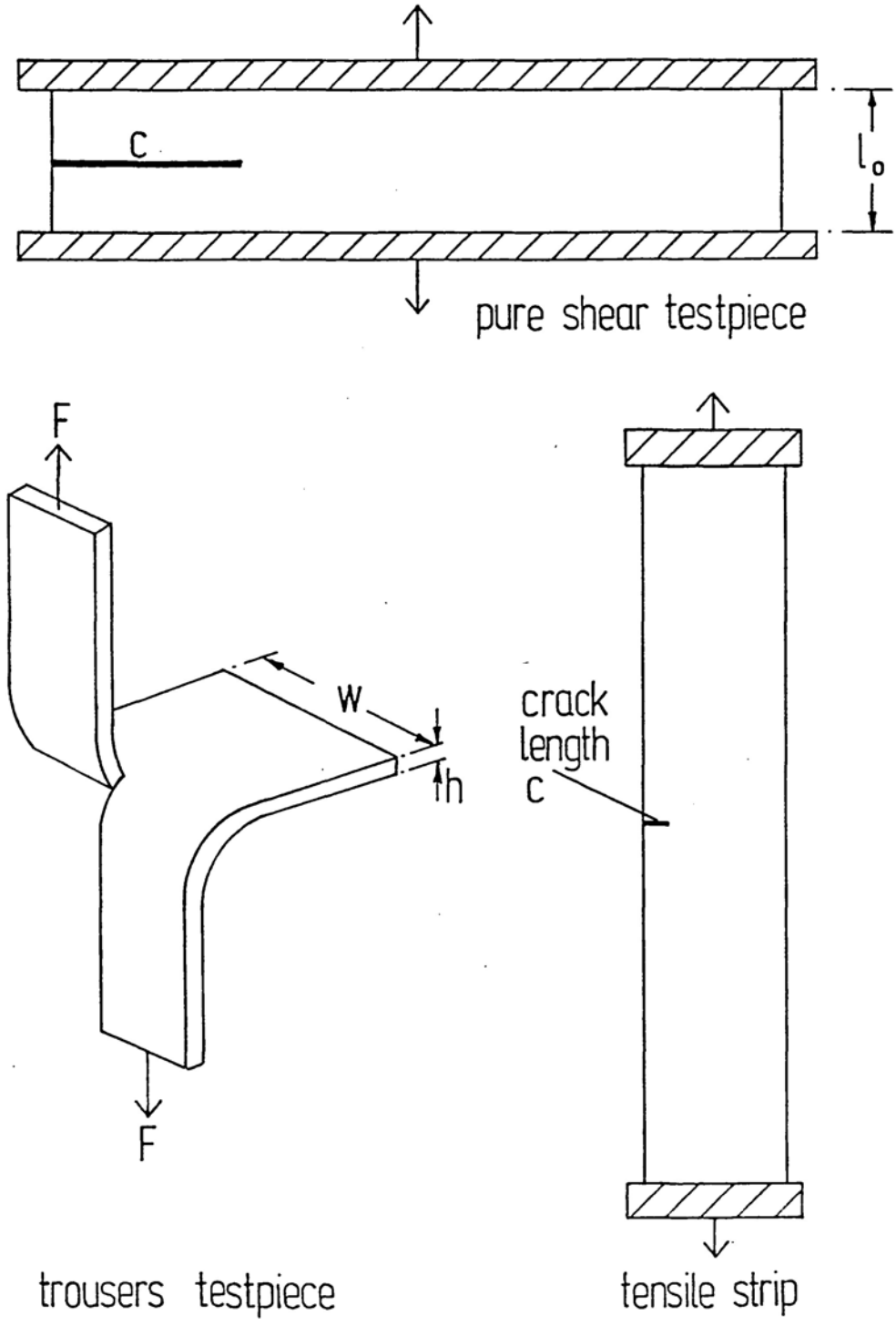


Fig. 3.1 Tensile strip, trousers and pure shear testpieces used for tear and crack growth testing.

(i) pure shear testpiece

$$T = Wl_o \qquad (3.2)$$

where W is the strain energy density in pure shear and l_o the undeformed length between the clamps;

(ii) 'trousers' testpiece

$$T = \frac{2F\lambda}{h} - wW \qquad (3.3)$$

where F is the applied force, λ the extension ratio, h the thickness, w the width and W the strain energy density;

(iii) tensile strip with an edge crack of length c

$$T = 2kWc \qquad (3.4)$$

where W is the strain energy density in the bulk of the testpiece (i.e. remote from the crack), and k a non-dimensional function of strain. The variation of k with strain e has been determined experimentally by Greensmith (10) and Lindley (11) on a limited range of natural rubber vulcanizates. For strains up to 200% the equation (11)

$$k = (2.95 - 0.08e)/(1+e)^{\frac{1}{2}} \qquad (3.5)$$

is a satisfactory approximation for the derived values of k.

From the results of tear tests carried out using these testpieces on a range of natural rubber vulcanizates, a characteristic value T_c of tearing energy was found for each vulcanizate at which catastrophic tearing occurred; the crack suddenly increasing the length by a substantial amount. This verified the Rivlin and Thomas criterion for tearing in rubber. T_c is thus a strength parameter and is known as tear strength. The magnitude found for T_c is of the order of 1-10 kN/m which is at least a thousand times greater than surface free energies of materials (8). Thus the irreversible dissipation energy referred to earlier dominates the tear behaviour of rubber.

3.3 Crack growth characteristic

For a crystallizing rubber such as natural rubber, large scale crack growth occurs if T_c is exceeded. However, if the testpiece is subjected to repeated stressing, the load being alternately removed and re-applied, crack growth occurs at values of tearing energy lower than T_c. The crack growth takes place during the load increasing part of each cycle; there is no crack growth when the load is held constant. This is in contrast to the crack growth behaviour of a non-crystallizing rubber such as SBR, for which crack growth is a time dependent process, i.e. the crack will continue to propagate even though the deformation is held constant. Thus for natural rubber, the amount of growth depends primarily on the number of cycles rather than the period of cycling.

When the amount of crack growth per cycle, dc/dn, is expressed in terms of the maximum tearing energy T attained during each cycle it is found (12, 13) that the results are independent of the form of the testpiece used. This further illustrates the validity of the tearing energy concept. The relation between crack growth rate and tearing energy is therefore an intrinsic property of the material, and will be referred to as the crack growth characteristic of the material.

Crack growth characteristics have been obtained (13) for various rubbers. For many rubber vulcanizates the relationship between dc/dn and T can be described by the following empirical equations, shown in Fig. 3.2 on logarithmic scales:-

$$\frac{dc}{dn} = r_z \qquad T \leqslant T_o \qquad (3.6)$$

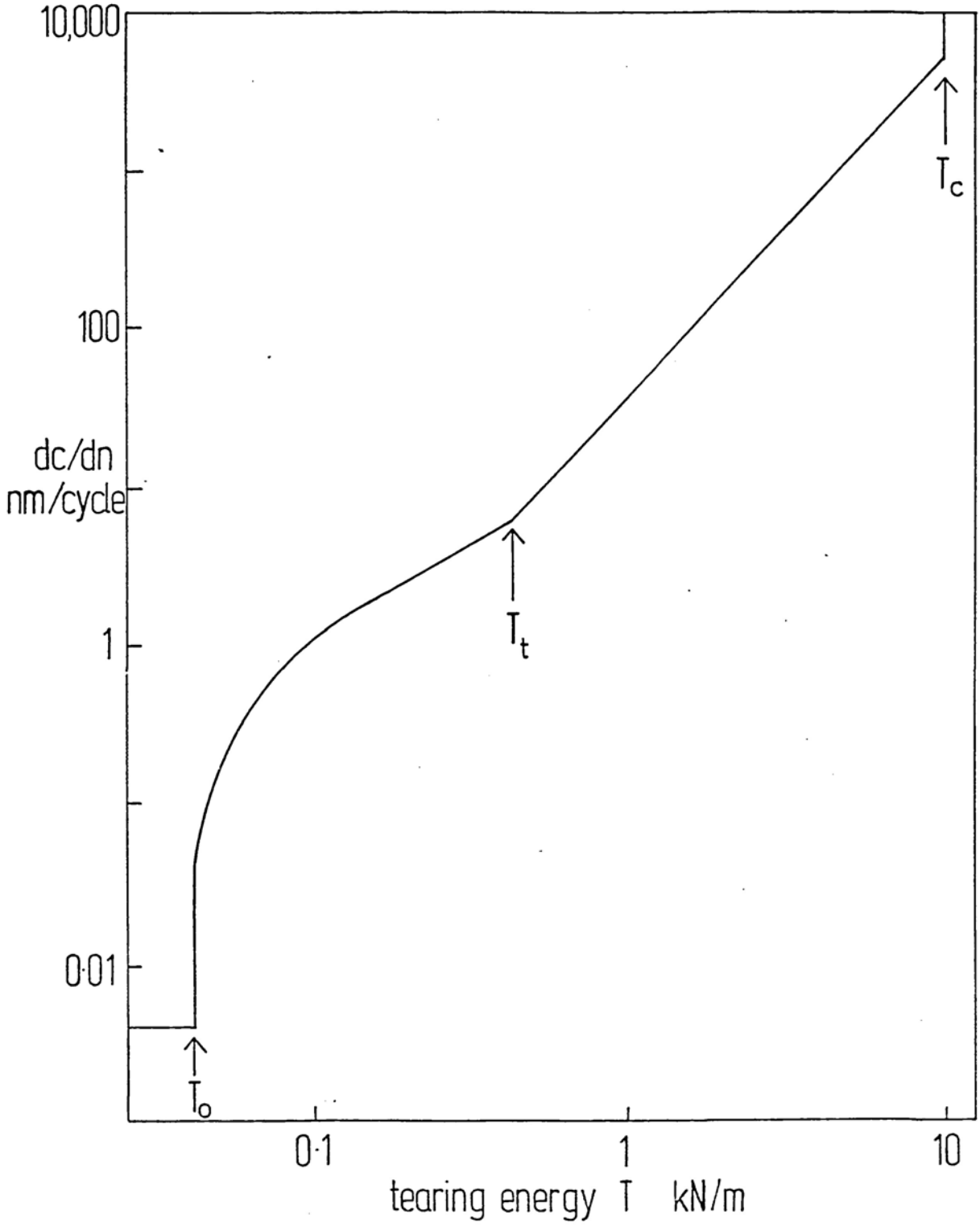


Fig. 3.2 Crack growth characteristic of rubber.

$$\frac{dc}{dn} = A_o(T - T_o) + r_z \qquad T_o < T \leqslant T_t \qquad (3.7)$$

$$\frac{dc}{dn} = BT^P \qquad T_t < T < T_c \qquad (3.8)$$

$$\frac{dc}{dn} = \infty \qquad T_c \leqslant T \qquad (3.9)$$

where r_z, A_o, B, p, T_o, T_t and T_c are crack growth constants. The values of these constants are different for different vulcanizates. T_c is the catastrophic tearing energy or tear strength of rubber described in Section 3.2.

It is evident from Fig. 3.2 that T_o is an important parameter. Below T_o the rate of growth given in eq. (3.6), is independent of tearing energy and it has an extremely low value. Immediately above T_o there is a very rapid increase in the crack growth rate which varies linearly with increasing T, eq. (3.7). At the transition point T_t the rate changes over to a power law dependence on T, eq. (3.8) until catastrophic failure occurs at T_c.

3.4 Mechanical crack growth limit T_o

T_o, known as the mechanical crack growth limit, is the lowest tearing energy for crack growth to occur due to mechanical rupture. The crack growth below T_o is attributed solely to the effects of ozone (13).

The magnitude of T_o is found (14) to be in the region of 0.05 kN/m for a wide range of rubbers, including both crystallizing and non crystallizing rubbers which differ widely in other strength properties such as tear and tensile strengths (10). This suggests that T_o may be related to the molecular strength of rubbers. Lake and Thomas (15) showed that T_o can be related to the primary bond strength and molecular structure of a vulcanizate. An estimate of the value of

T_o can be made using the following equation (16)

$$T = W_t d \qquad (3.10)$$

where W_t is the strain energy density at the crack tip and d the unstrained tip diameter. In the Lake and Thomas theory for T_o it is assumed that d has the minimum possible value, ie the distance between adjacent crosslinks in the unstrained state. It is also assumed that W_t has the maximum possible value which is given by multiplying the number of single bonds per unit volume by the energy stored by each single bond at its rupture point. The predicted value for T_o is less than a factor of three below the experimentally observed values in vacuo. The agreement is considered good in view of the approximations in the theory.

3.5 Hysteresis

It would appear from the above discussions that once T_o is reached, the rubber would be expected to rupture catastrophically since T_o marks the commencement of mechanical crack growth. However, this is not the case in practice. As discussed in Section 3.3, the catastrophic failure does not occur until the tear strength T_c is reached, and there is stable crack growth at tearing energies above T_o. Lake and Thomas (15) suggested that this behaviour is governed by the mechanical hysteresis properties of the rubber at very high strains. For an ideally elastic rubber, having no hysteresis, catastrophic tearing would occur at T_o. In practice all rubbers are to some extent hysteresial. As the hysteresis of rubber increases, T_o is virtually unaffected but the rate of crack growth is reduced and T_c is increased, Fig. 3.3.

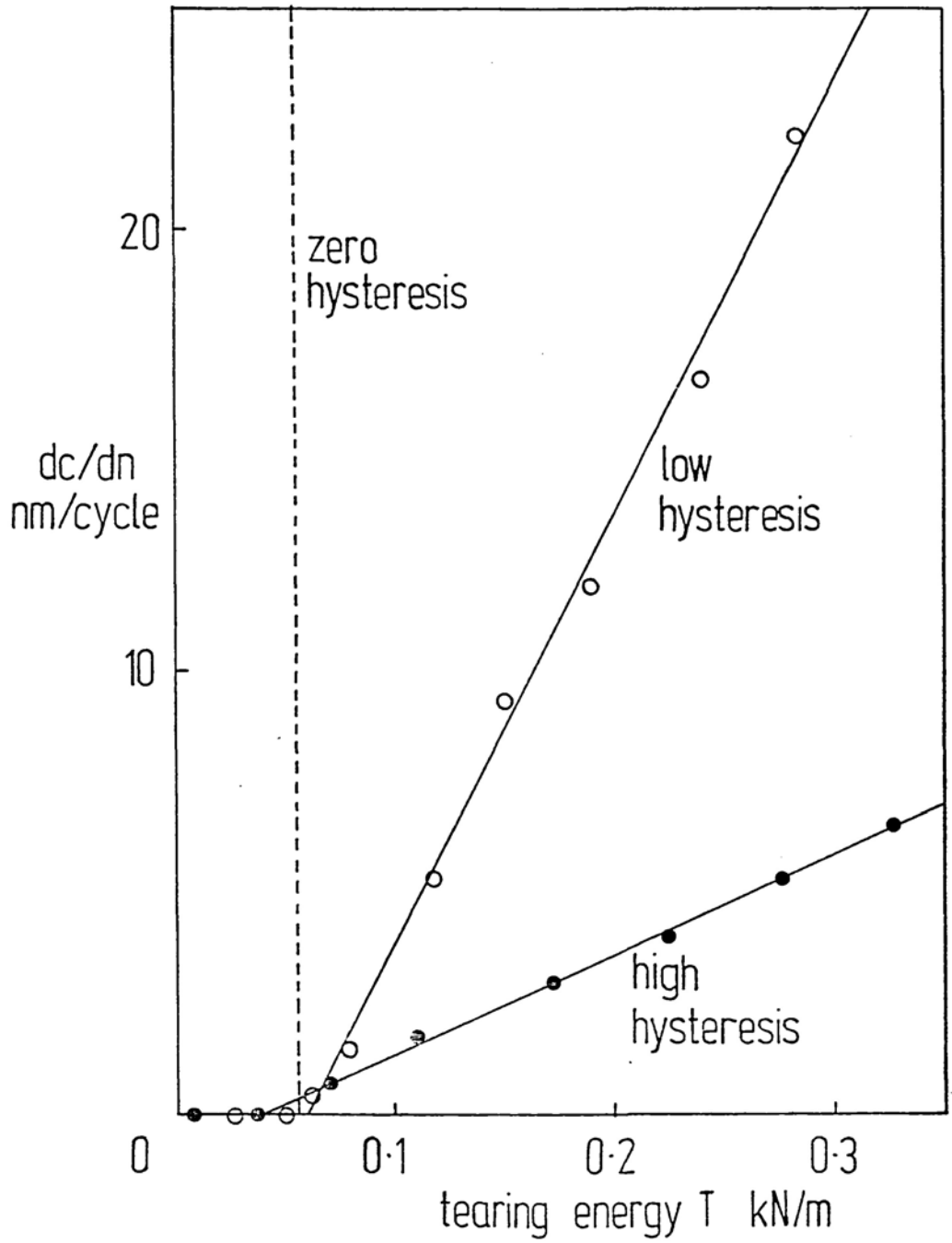


Fig. 3.3 Diagram illustrating the effect of hysteresis of a rubber on its crack growth behaviour as proposed by Lake and Thomas (15). The diagram shows typical experimental results for gum vulcanizates of natural rubber (●) and SBR (O).

The physical basis for the above hypothesis is as follows. If a testpiece containing a crack is extended, the stress at the crack tip increases until T_o is reached when the rubber is on the point of breaking. Up to this point the stresses at the tip are governed by the extension stress-strain curve. Crack growth begins to occur with further extension, causing relaxation of a region of highly strained rubber around the tip. The relaxation is governed by the retraction stress-strain curve and influences the stress at the new tip. The stress at the tip will be substantially lower in a hysteresial rubber than in a perfectly elastic rubber (17, 18). Thus the greater the hysteresis, the more difficult it is for the crack to propagate.

There are three main types of hysteresis that can occur in rubbers —— that due to visco-elasticity, that due to strain-induced crystallization and that due to the presence of reinforcing fillers such as carbon black. Natural rubber exhibits strain-induced crystallization which gives rise to pronounced hysteresial effects at high strains.

It is evident from Fig. 3.3 that the strength properties of rubbers are greatly influenced by their hysteresial properties; the higher the hysteresis, the greater the strength. This is consistent with experimental observations, for example (i) crystallizing rubbers have higher tear and tensile strengths than those of non-crystallizing rubbers (19, 20), (ii) the tear and tensile strengths of non-crystallizing rubbers are enhanced by reinforcing fillers (21, 22), and (iii) swelling decreases the strength of rubber (23). The influence of hysteresis on strength should thus depend on the extent of the crack propagation which is involved in the strength measurement.

The most undesirable consequence of hysteresis is heat build-up, the temperature rise resulting from energy dissipation during repeated deformation. For large rubber articles that are deformed vigorously such as truck tyres, the temperature in the interior of the article may rise to a sufficiently high value to cause chemical degradation of the rubber and may lead to catastrophic failure. This type of failure will not be considered in this thesis. For relatively small or thin samples, heat build-up is usually negligible.

3.6 Fatigue in simple extension

If a piece of rubber is repeatedly deformed and relaxed, it will ultimately fail even though the maximum stress is much less than the breaking stress as normally measured. In the absence of heat build-up (discussed in Section 3.5), fatigue failure occurs through the growth of one or more cracks across the testpiece, and this suggests that fatigue in rubber is essentially a crack growth process initiated by small flaws in the sample. Fatigue failure in simple extension has been studied extensively using the fracture mechanics approach (12, 13, 24).

The fracture mechanics approach can, in principle, be applied to the prediction of the fatigue life of rubber components provided the tearing energy of the component is known, the crack growth characteristic of the rubber used has been obtained and the initial flaw size is known or assumed.

Consider a tensile strip, Fig. 3.1, subjected to repeated deformation in simple extension. The tearing energy is given by eq. (3.4), ie

$$T = 2kWc \qquad (3.4)$$

The crack growth characteristic (Section 3.3) is the dependence of the crack growth rate on T, ie

$$\frac{dc}{dn} = f(T) \qquad (3.11)$$

Substituting for T and on integration, this gives the number of cycles n needed for a crack to grow from one length c_o to another c as

$$n = \int_{c_o}^{c} \frac{dc}{f(2kWc)} \qquad (3.12)$$

For many natural rubber vulcanizates the crack growth rate can be approximated at moderate to high T values by the relation (25)

$$\frac{dc}{dn} = BT^2 \qquad (3.13)$$

where B is a constant.

Using this relation, equation (3.12) gives

$$n = \frac{1}{B(2kW)^2} \left[\frac{1}{c_o} - \frac{1}{c}\right] \qquad (3.14)$$

If the number of cycles to fail, N, is required and the initial crack length c_o is small compared with the final crack length c, then 1/c can be neglected in comparison with $1/c_o$ and thus

$$N = \frac{1}{B(2kW)^2 c_o} \qquad (3.15)$$

Equation (3.15) has been applied to tensile strips with initial razor cuts of known size, good agreement being found (24). The fatigue of dumbbell testpieces containing no intentionally introduced flaws has also been studied. The fatigue lives were obtained for the moderate to high strain region over which eq. (3.13)

holds. A plot of the life N against 2kW on logarithmic scales gave the slope of -2 predicted by eq. (3.15). The initial effective flaw size c_o was deduced to be about 0.025 mm for unfilled natural rubber vulcanizates. Flaws of this magnitude can be observed in the die-stamped dumbbells (24).

The mechanical crack growth limit T_o is the tearing energy below which the crack growth rate is extremely slow. Similarly in a fatigue test there is a particular strain e_o, known as mechanical fatigue limit (13), corresponding to T_o below which the fatigue life increases rapidly.

Lindley (26) showed that this approach can be applied to predict the fatigue lives of dumbbells under non-relaxing conditions in which the testpieces are not completely relaxed on each cycle. Fig. 3.4 shows the experimental fatigue results and the corresponding predicted curves. The agreement is considered good. Increasing the minimum strain increases the fatigue life considerably. The marked increase in fatigue life of natural rubber under non-relaxing conditions has also been observed by Cadwell, Merrill, Sloman and Yost (27) who used cylindrical, not flat, dumbbells.

3.7 Effect of oxygen

When the tearing energy exceeds T_o, crack growth occurs due to mechanical rupture, the extent of which is considerably increased in the presence of oxygen as shown in Fig. 3.5 (26), and is thus referred to as mechanico-oxidative crack growth. The value of T_o for unprotected rubber in air is about half that in vacuo.

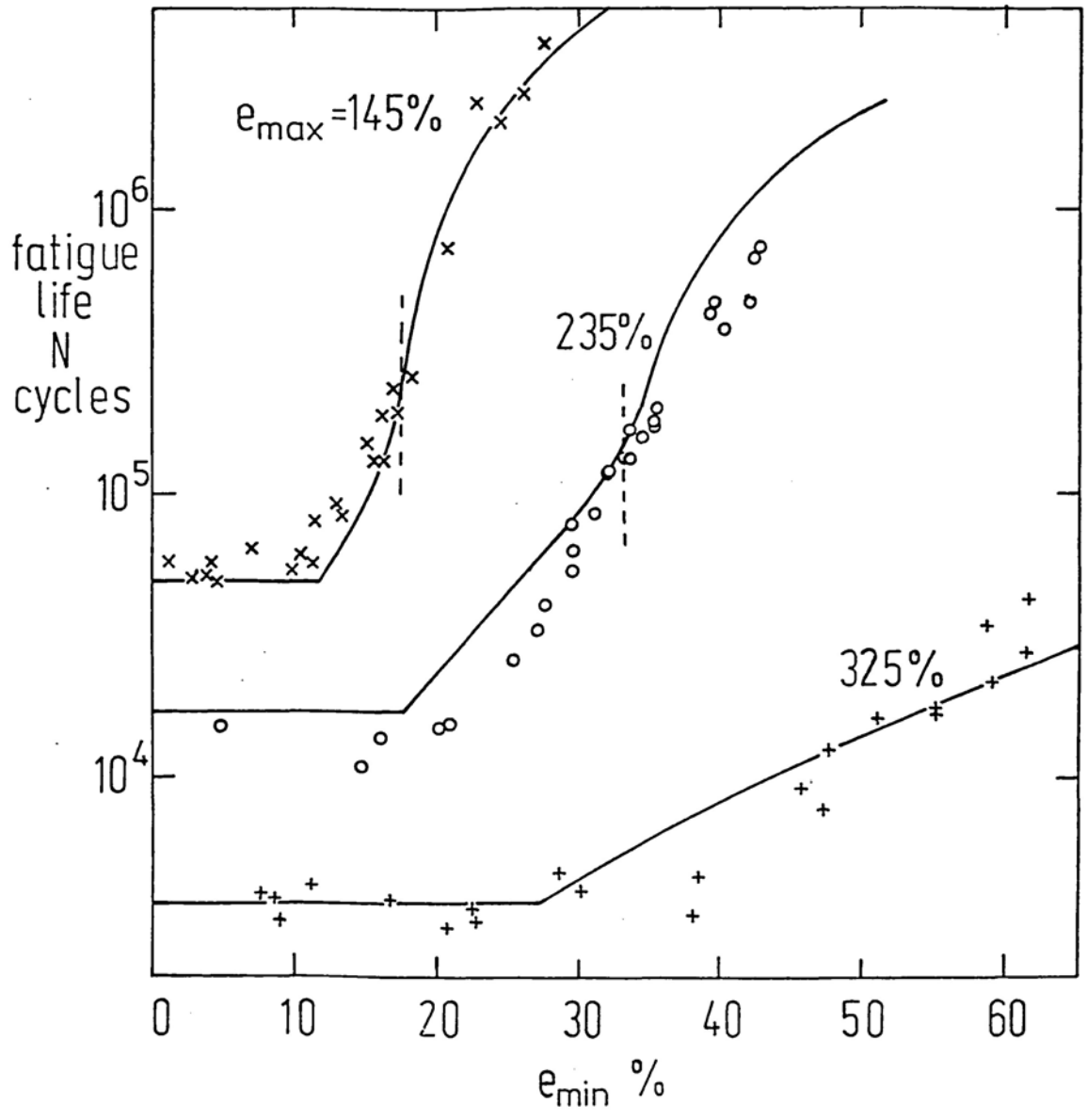


Fig. 3.4 Fatigue lives for natural rubber gum vulcanizate under non-relaxing conditions: experimental points, theoretical curves (26).

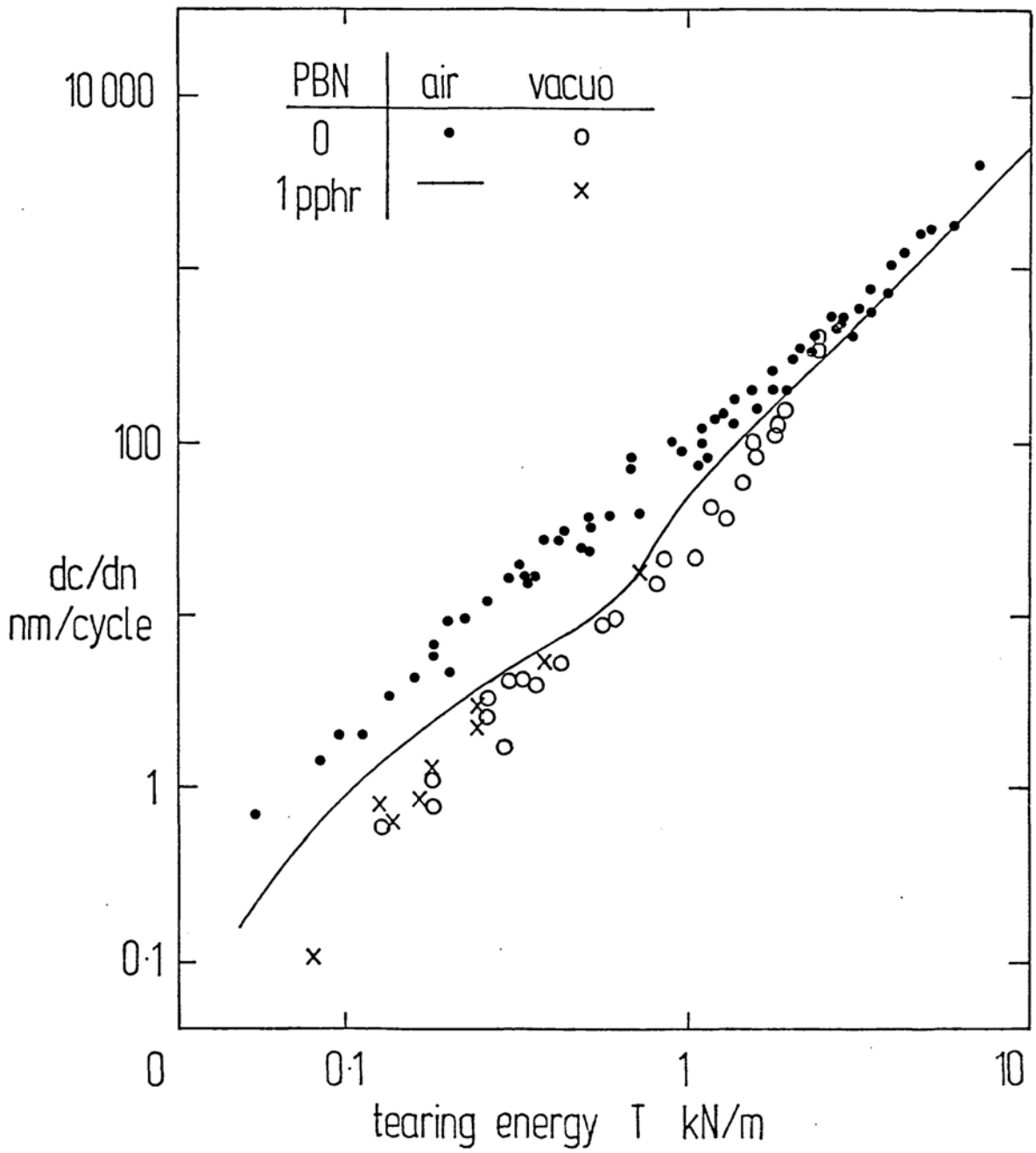


Fig. 3.5 Crack growth characteristics of protected and unprotected gum vulcanizates of natural rubber in air and vacuo (26).

The mechanism of the oxidative effect appears to be due to a reduction in the energy required for bond scission. This is inferred from the theory of T_o described in Section 3.4, and is consistent with the crack growth behaviour at low tearing energies. However this does not explain the diminution of the oxidative contribution at high tearing energies (Fig. 3.5). Lake (28) has suggested that the oxidative component arises because the very high mechanical energy in the rubber at the tip of a crack accelerates the rate of oxidative scission in a way similar to high temperature ageing under which the oxygen can cause main chain or crosslink scission. This implies that the oxidative component in crack growth is time-dependent and may become negligible at high tearing energies because the mechanical crack growth rate is rapid. Crack growth tests carried out at various frequencies (26) provide supporting evidence for this hypothesis.

At elevated temperatures, the effect of oxygen will be expected to be more dominant because the rate of oxidation has been shown (29, 30) to increase with increasing temperature. There is virtually no information on the crack growth characteristic of rubbers at elevated temperatures. Further work has now been undertaken and will be discussed in later sections of this thesis.

At laboratory temperature, the effect of oxygen can be reduced by the inclusion in rubber of suitable antioxidants (26).

3.8 Strain concentrations

It was mentioned in Section 3.1 that failure usually initiates at sites of high strain concentration. It is well known in the design of machine parts that sharp variations in

their cross-sections are to be avoided, as abrupt changes give rise to high stress concentrations which can lead to fatigue cracking.

In rubber springs, the soft rubber is usually bonded to rigid materials such as steel. Not all bonded rubber components have deliberately introduced corner fillets, but the method of manufacture invariably ensures that there is one, albeit small. The presence of the corner fillets can have a marked improvement on the fatigue life of rubber components. This is illustrated in Fig. 3.6 (31). In all cases cracking started at the surface of the rubber, but not at the rubber-metal bond.

The distribution of strain over the surface of a rubber component may be studied experimentally by imprinting a grid on the rubber surface. By taking measurements of the grid in both the strained and unstrained states of the component, the maximum and minimum extension ratios in the plane of the surface can be obtained. Gent (32) used this technique to measure the surface strain distributions for bonded rubber pads in compression and showed that the strain concentrations could be reduced by modifying the shape of the metal end-pieces.

There is little quantitative information on strain concentrations in rubber components. Some data were obtained by Lindley (33) on the strain concentrations at the corners of stretched rubber sheets with various corner fillets. He found that strain concentration factors are approximately proportional to the cube root of the relative size of the fillet, and also that the strain at the corner of the rubber sheet is reduced to zero by introducing corner wedges with angles of less than 45 degrees.

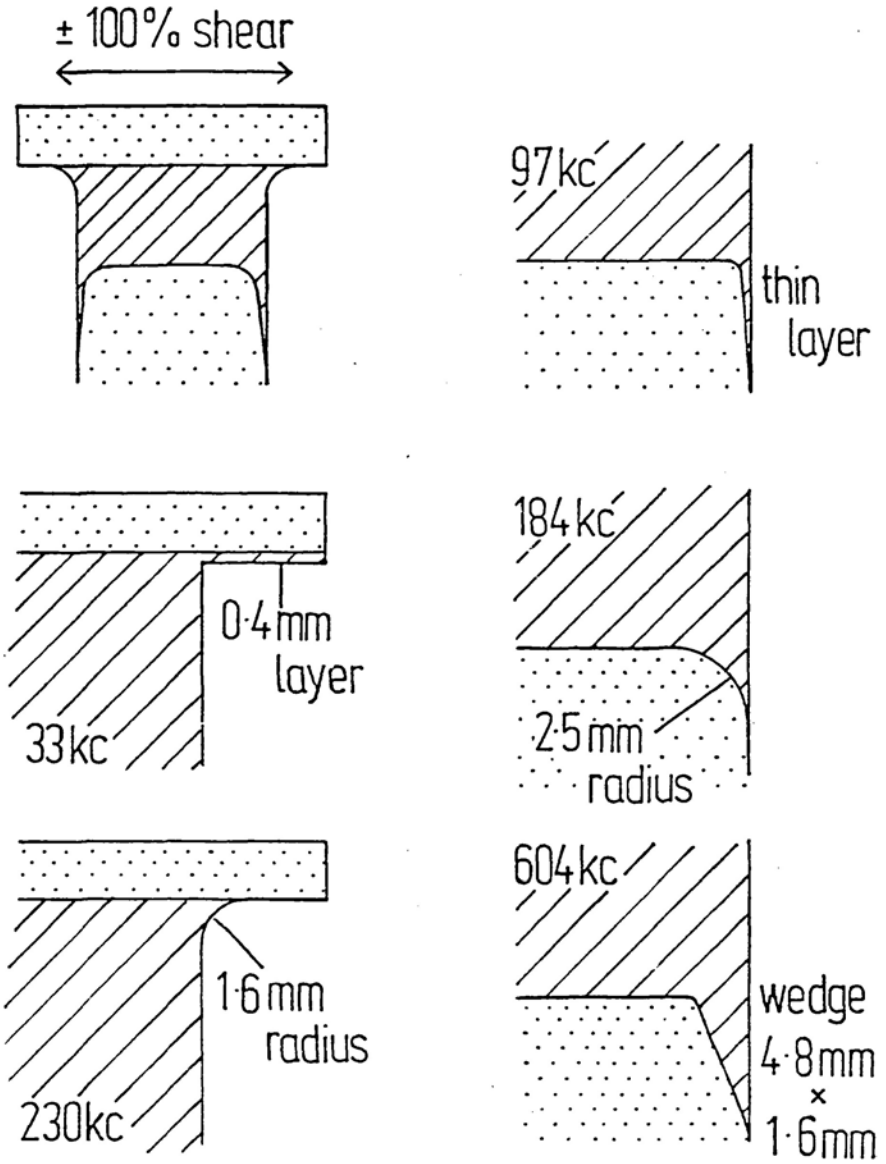


Fig. 3.6 Effect of reducing stress concentrations on the fatigue life of bonded 25 mm square x 6.3 mm thick testpieces of natural rubber (shown hatched) subjected to alternating shear deformations of ± 100% at 2 Hz (31). Large flaws became visible at the numbers of cycles shown.

3.9 Crack growth in rubber components

As indicated in Section 3.6, the fracture mechanics approach can in principle be used to predict the fatigue life of rubber components in service, since the crack growth characteristic is independent of sample shape or size. A major difficulty in practice is to determine the relation between the tearing energy, crack size and overall applied forces or deformations for a rubber component which may be of complex shape and structure. Calculation of this relation is prohibitively difficult except for certain simple shapes. Lindley (11) used a numerical method based on finite element analysis to determine the tearing energies in plane-stress testpieces of complex shape and the findings were confirmed by experiments.

Lake (34) used tensile strip and pure shear testpieces (Fig. 3.1) containing central cracks to verify an experimental method of determining the tearing energy from measurements of the amount by which a crack opens under stress. This crack opening technique, also known as crack surface displacement method has been applied successfully to the practical problem of groove cracking in truck tyres (35). The tearing energy relation for a tyre groove, obtained by the crack opening technique, approximates to that for the tensile strip when the crack length is short and to that for the pure shear testpiece when the crack length is long. Using the crack growth characteristics of the tyre tread rubber, the predicted rates of growth are in good agreement with the measurements of groove cracking in bus tyres in service.

PART II

		Page
Section 4	Experimental methods for crack growth and fatigue studies on rubber	54
Section 5	Tearing energy in simple extension	66
Section 6	Relaxing crack growth and fatigue at elevated temperatures	84
Section 7	High temperature ageing of rubber blocks	107

SECTION 4 EXPERIMENTAL METHODS FOR CRACK GROWTH AND FATIGUE STUDIES ON RUBBER

4.1 Apparatus

Two machines were specially made for carrying out crack growth and fatigue experiments at laboratory and elevated temperatures. The main features of these machines are that they

(1) provide a wide range of amplitudes

(2) have easy adjustment of amplitudes

(3) have good recording counters for each individual testpiece, and

(4) operate at a frequency of about 2 Hz.

Fig. 4.1 shows a photograph of the machine for testing at laboratory temperature. It has 16 stations to allow 16 samples to be tested at the same time. The counters, one for each station, are shown on the right of the photograph. The amplitude of this machine can be varied from about 20 to 200 mm. When rubber is stretched, its cross-sectional dimensions reduce to maintain approximately constant volume. The brass clamps, by means of which the testpieces are attached to the machines, have small horizontal rods soldered to one inner face which press into the rubber to prevent slip during testing.

A general view of the machine for testing at elevated temperatures is shown in Fig. 4.2,and Fig. 4.3 shows the general lay-out and the working mechanism of the machine. The reciprocating movement is obtained through the pneumatic air cylinder by means of the flip-flop switch shown on the left hand top of Fig. 4.3. The stroke of the piston can be varied from about 30 mm to 280 mm by simple adjustment of the two stops shown on the left of the Fig. 4.3. The main

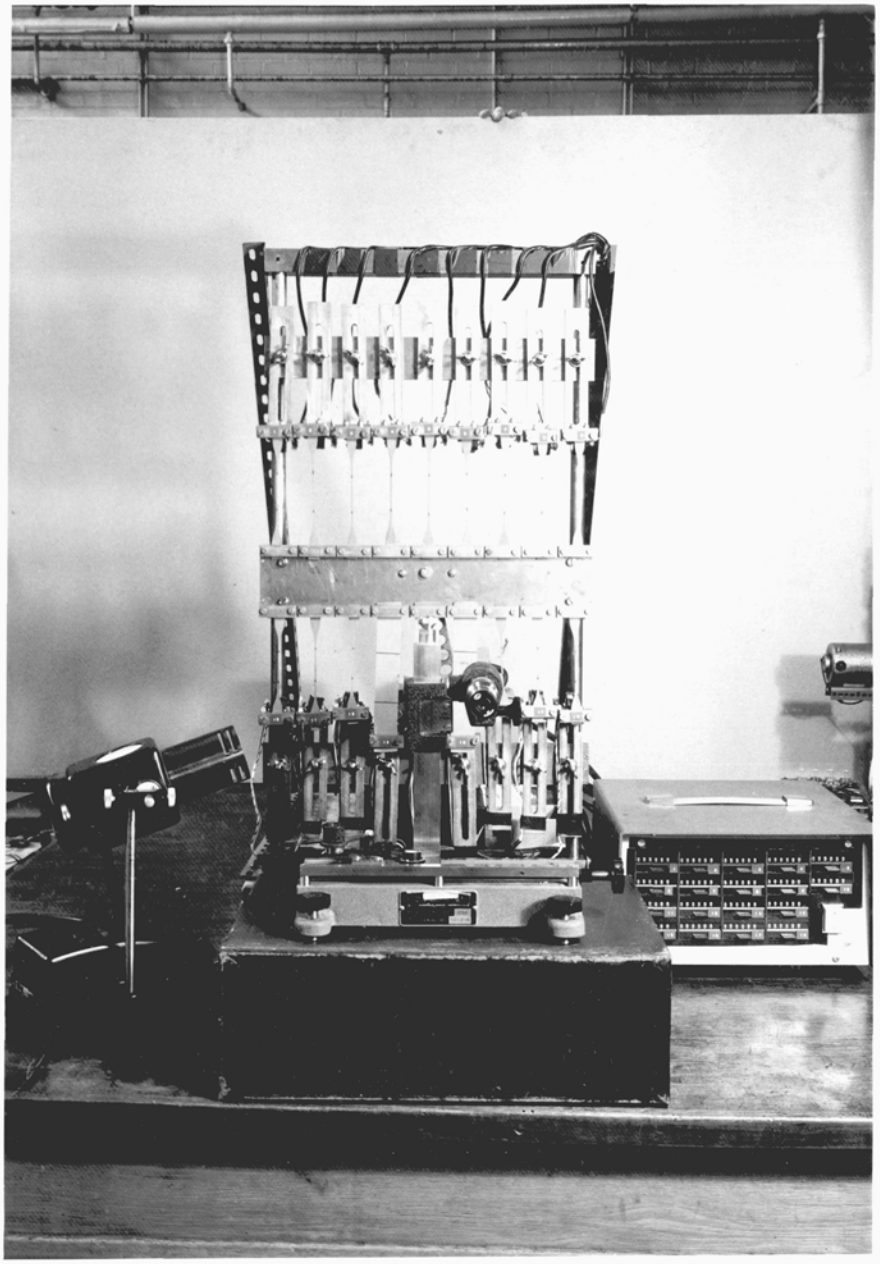


Fig. 4.1 Dynamic testing machine for experimental investigation of crack growth and fatigue at laboratory temperature



Fig. 4.2 Dynamic testing machine for experimental investigation of crack growth and fatigue at elevated temperatures

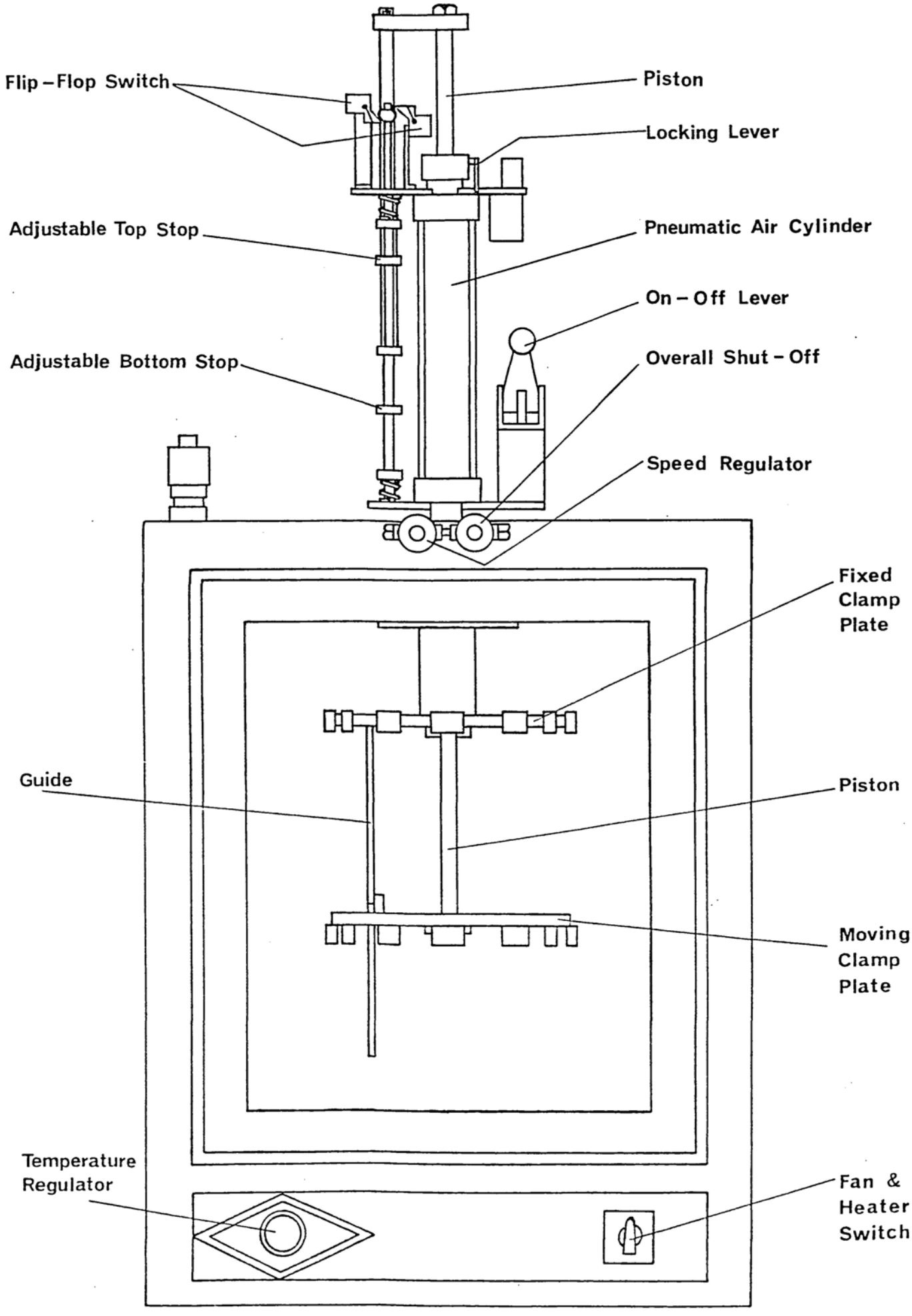


Fig. 4.3 HIGH TEMPERATURE FATIGUE MACHINE

feature of this machine is the ease and convenience of adjusting these stops to any position, which is particularly useful for non-relaxing fatigue and crack growth tests. The maximum operating temperature of this machine is 180°C. The temperature around the main testing area is quite uniform and can be set to the nearest 1°C.

The oven door is double glazed and is further lagged with fibre-glass wool wrapped with aluminium foil between the glass. There is a viewing slot in the door to enable crack lengths to be measured by means of a travelling microscope. The whole reciprocating assembly can be rotated to bring any testpiece up to the viewing slot.

There are 12 stations to allow 12 samples to be tested at the same time. (The counting devices are similar to those shown in Fig. 4.1). The machine stops automatically when all the samples have failed.

4.2 Preparation of rubber vulcanizate

All the experimental work was carried out on a natural rubber gum vulcanizate (vulcanizate A) compounded according to the following formulation (in parts by weight):

SMR5 CV	100
Zinc oxide	5
Zinc 2-ethyl-hexanoate	2
Sulphur	0.7
OBS[1]	1.7
TBTD[2]	0.7
Antioxidant[3]	2

1. N-oxydiethylenebenzothiazole-2-sulphenamide; Santocure MOR (Monsanto) was used.
2. Tetrabutylthiuram disulphide.
3. N-isopropyl-N'-phenyl-p-phenylenediamine (IPPD); Nonox ZA was used.

Mixing was carried out in laboratory 'BR' Banbury. The sequence is as follows:

0 min : add rubber

2 min : add zinc oxide, zinc 2-ethyl-hexanoate and antioxidant

3.5 min : add sulphur

5 min : discharge

OBS and TBTD were added on a cold mill.

Vulcanization was effected by heating in a mould under pressure for 90 minutes at 140°C. The rubber was moulded, generally in sheets of 300 x 300 x 1 mm against polished or smoothly ground steel plates. The testpieces were prepared from these sheets.

4.3 Testpieces

After moulding, every sheet was left at laboratory temperature and in the dark for at least 24h before any testpieces were prepared from it.

Four types of testpiece were used. These are shown in Fig. 4.4. The type C dumbbell (BS 903 Part A2, Fig. 4.4a) was used for the fatigue tests. The cutter used to diestamp the dumbbells from the moulded sheets had the cutting edges of its central region maintained in near-perfect condition to prevent flaws due to the cutter occurring on the central parallel-sided parts of the testpieces where fatigue flaws initiated. The testpieces on which crack growth tests were carried out were parallel-sided tensile strips 25 mm wide and 150 mm long (Fig. 4.4b). 'Bongo' testpieces (Fig. 4.4c) having a parallel-sided strip 100 mm long and 2 mm wide between the tabs, and 'ring' testpiece (Fig. 4.4d) with inner diameter of 15 mm and outer diameter of 17 mm were used only for determining tensile stress-strain properties of the rubber, although tensile stress-strain tests were

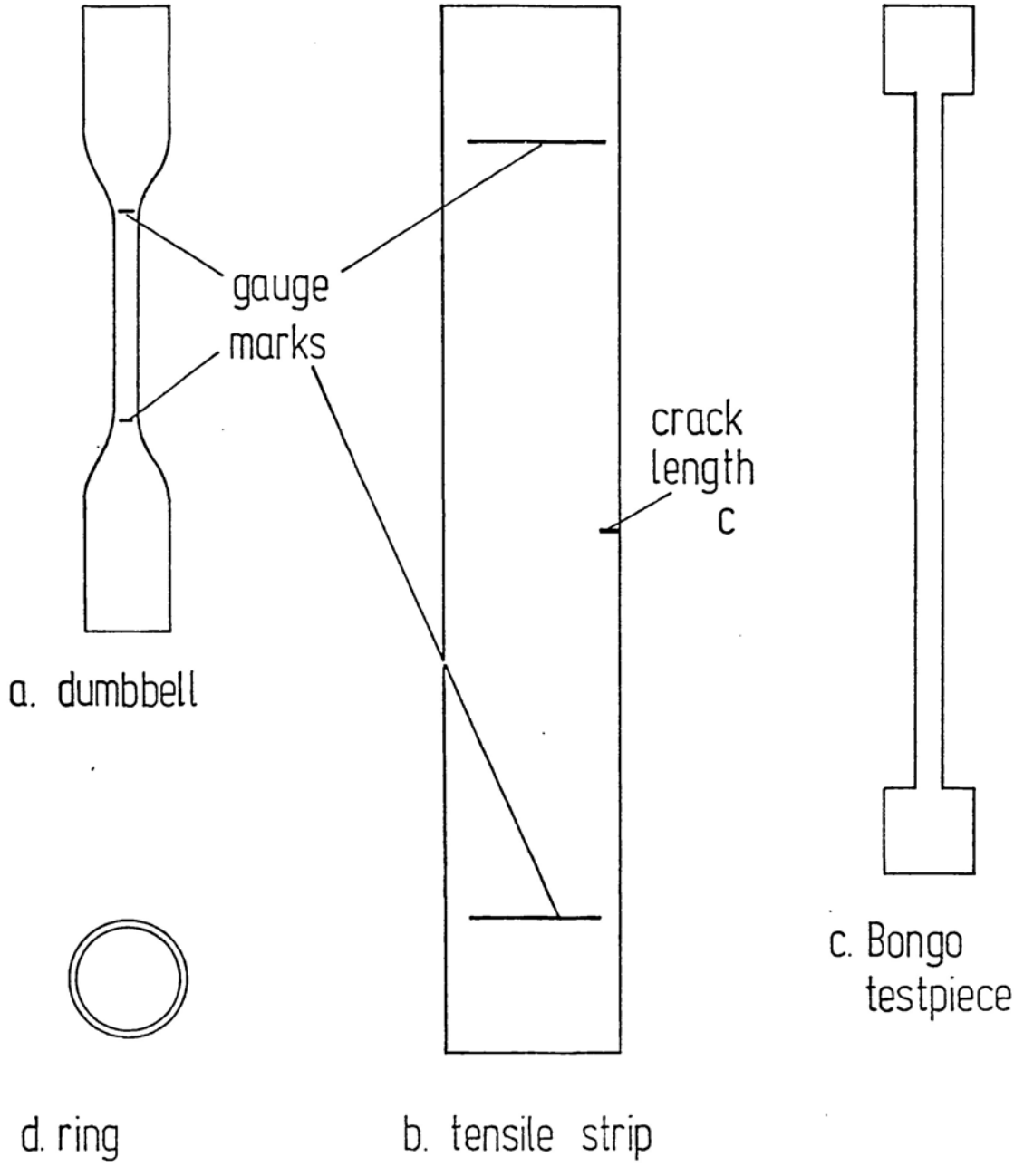


Fig. 4.4 Four types of testpieces: (a) dumbbell for fatigue testing; (b) tensile strip for crack growth testing; (c) Bongo and (d) ring testpieces for tensile testing.

also carried out using dumbbells and tensile strips. The tensile strips and Bongo testpieces were also diestamped from the sheet rubber but the cutters for these did not require such careful maintenance as those for the dumbbells and ring testpieces.

To enable the extensions of the testpieces to be measured, reference lines were drawn on the dumbbells and tensile strips, as shown in Fig. 4.4, using a fine-writing ball point pen and a steel rule. The gauge length of the Bongo testpieces was the distance (100 mm) between the tabs. For the ring testpieces the original length was given by the mean circumference of the ring (π x 16 mm).

4.4 Tensile force-deflection tests

There are two main objectives in carrying out tensile tests. The first one is to obtain the values of strain energy density W at various strains required for the evaluation of tearing energy of a tensile strip, (eq. 3.4) viz.

$$T = 2kWc \qquad (3.4)$$

Tensile force deflection tests were carried out on a simple extensometer described by Lake and Lindley (13), or on an Instron tensile machine. The latter has anoven cabinet to allow testing at elevated temperatures. A test was carried out on at least one and sometimes three testpieces diestamped from each sheet. The values of W were then calculated from the area of stress-strain curve (σ - e) based on the unstrained dimensions. A typical stress-strain curve for vulcanizate A and the derived W-e curve are shown in Fig. 4.5.

It was found that the σ - e and, hence, W-e curves for vulcanizate A were not affected significantly by the type of testpiece used, by the rate of deformation up to frequencies equivalent to 5 Hz,

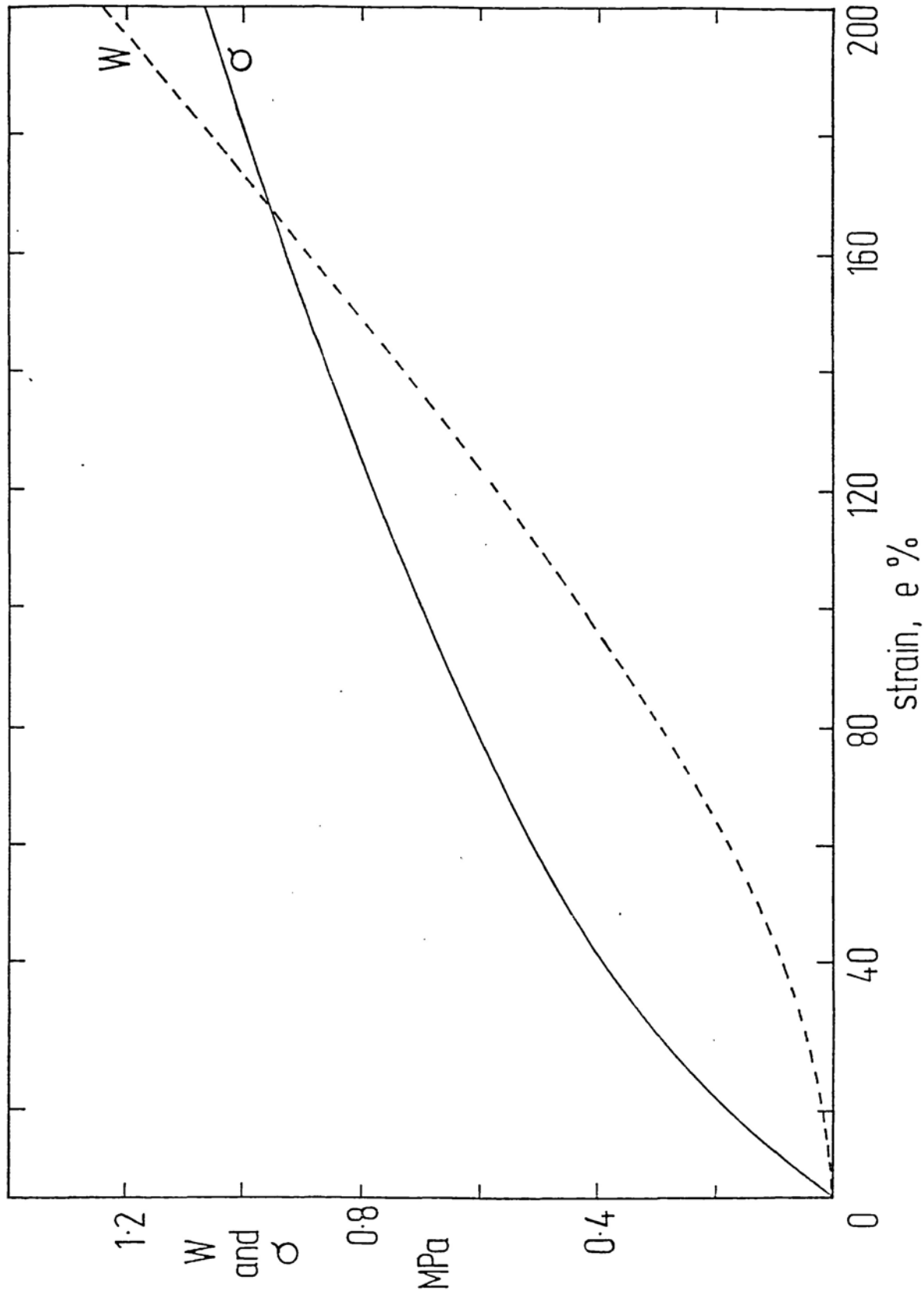


Fig. 4.5 Relations of stress σ to strain e and of strain energy density W to strain e

and by repeated deformation provided that allowance was made for a small amount of set which occurred.

The second objective is to obtain the tensile strength of vulcanizate A at elevated temperatures. The tensile tests for this were carried out mainly with ring testpieces on the Instron machine.

4.5 Crack growth tests on tensile strips

Any type of testpiece for which tearing energy can be evaluated can, in principle, be used to obtain the crack growth characteristics. The tensile strip has been found to be most suitable because (13)

(i) it is easy to prepare and set up, and the crack length can be readily measured,

(ii) it can be tested on the same machines, and at the same time as dumbbell fatigue testpieces,

(iii) a very wide range of tearing energy can be covered,

(iv) a series of results at different tearing energies is obtained from each test.

Tensile strips were die-stamped from sheets of vulcanized rubber. After the load-deflection characteristics had been obtained for a strip, a small incision about 0.5 mm long was made in the centre of one edge with a razor blade. The testpiece was then clamped on to one of the machines and cycled to a pre-determined extension, the strain being determined by measuring the separation of the reference marks with a rule. For relaxing crack growth tests, the testpiece was allowed to return to the unstressed state during each deformation cycle.

The crack length c in the unstrained state was measured initially and at suitable intervals of the number of cycles n using a travelling microscope fitted with an eyepiece scale, and with the

strip slightly strained to facilitate observation. The graticule in the eyepiece had 100 divisions, each corresponding to 0.01 mm or more depending on the objective lens used. The crack lengths could be read to the nearest half scale division.

The rate of crack growth per cycle (dc/dn) was calculated from the difference between successive readings of crack length, Δc divided by the number of cycles in the interval, Δn. The corresponding tearing energy at the maximum deformation of the cycle given by eq. (3.4), viz

$$T = 2kWc \qquad (3.4)$$

was taken as that at the average crack length in the interval Δn. The fractional increase in crack length was normally 10 to 20%. This ensured reasonable accuracy in Δc while keeping the change in tearing energy small. The maximum error in dc/dn was $\pm$ 10% which is small in relation to the inherent variability of crack growth results.

The theory on which eq. (3.4) is based requires the crack length to be small in relation to the testpiece width, but large relative to its thickness (9). In practice reliable results were obtained for crack lengths up to 40% of the testpiece width but an upper limit of 20% was rarely exceeded.

The crack growth results were normally expressed as the crack growth rate dc/dn versus the tearing energy T at the maximum deformation of the cycle.

Allowance was made for set occurring during the course of a test which effectively reduced the maximum strain of a testpiece.

4.6 Fatigue tests in simple extension

For the fatigue tests dumbbell testpieces were used in order to avoid failure at the clamps. Each dumbbell was repeatedly cycled to a fixed maximum extended length and was allowed to relax during each cycle. The strain was measured from the gauge marks on the central parallel-sided section of the dumbbell. The measured strains tended to decrease slightly during the course of the test owing to the set, particularly at elevated temperatures, and allowance was normally made for this, as in the crack growth tests.

The dumbbells were cycled until fracture occurred at the central parallel-sided section; the number of cycles,ie the fatigue life N, was recorded. The die-stamping of dumbbells introduces flaws in the edges,and failure usually occurs from one of these. Occasionally, however, failure occurs from a flaw in the major surfaces suggesting that imperfections in moulded surfaces are similar in magnitude to those in the edges.

SECTION 5 TEARING ENERGY IN SIMPLE EXTENSION

5.1 Tearing energy for a tensile strip with an edge crack

For a tensile strip containing an edge crack of length c, it can be deduced on dimensional grounds (9) that the energy loss U due to the presence of the crack is proportional to c^2, to the strip thickness t and to the strain energy density W in the rubber far removed from the crack ie

$$U = U_o - U_c$$
$$= kc^2tW \qquad (5.1)$$

where U_c and U_o are the total elastic energies in the rubber with and without the crack, and k is a strain dependent term.

Differentiating the energy loss U with respect to the crack area A (= ct) gives the relation for tearing energy T, viz

$$T = 2kWc \qquad (5.2)$$

Thus T is related to the crack length c via the two strain dependent parameters W and k.

Values of W can be obtained experimentally as described in Section 4.4. Alternately W can be evaluated from relations containing the elastic constants of the rubber, which will be discussed later. Values of k have been determined experimentally by Greensmith (10) and numerically by Lindley (11). The determination of k was carried out only on a limited number of natural rubber vulcanizates and at laboratory temperature. The determination of k has now been extended to cover both (i) a wider range of vulcanizates, and (ii) temperatures above laboratory temperature.

5.2 Strain energy function

For plane stress deformations, rubber is usually treated analytically as highly elastic incompressible material. Rivlin (36) has proposed that for a highly elastic incompressible material such as rubber, the strain energy density W is a function of two strain invariants I_1 and I_2 where

$$\begin{aligned} I_1 &= \lambda_1^{\,2} + \lambda_2^{\,2} + \lambda_3^{\,2} \\ I_2 &= \lambda_1^{\,-2} + \lambda_2^{\,-2} + \lambda_3^{\,-2} \end{aligned} \tag{5.2}$$

and λ_1, λ_2 and λ_3 are the principal extension ratios. The incompressible condition is expressed by

$$\lambda_1\lambda_2\lambda_3 = 1 \tag{5.3}$$

The form of strain energy density function, W used by Lindley in the finite element computer program for plane stress analysis of rubber at high strains (up to 200% strain) is that proposed by Gent and Thomas (37), ie

$$W = W_1 (I_1 - 3) + W_2 \ln (I_2/3) \tag{5.4}$$

where W_1 and W_2 are constants.

In simple extension $\lambda_1 = \lambda$, $\lambda_2 = \lambda_3 = \lambda^{-\frac{1}{2}}$, and

$$W = W_1 (\lambda^2 + 2\lambda^{-1} - 3) + W_2 \ln((\lambda^{-2} + 2\lambda)/3) \tag{5.5}$$

The stress σ ($= \partial W/\partial\lambda$) is

$$= 2 (\lambda - \lambda^{-2}) (W_1 + W_2/(\lambda^{-1} + 2\lambda^2)) \tag{5.6}$$

Differentiating σ with respect to λ and putting $\lambda = 1$ gives the Young's modulus E as

$$E = 6W_1 + 2W_2 \tag{5.7}$$

In practice, however, the form of W proposed by Mooney (38) is more commonly used in simple extension, ie

$$W = C_1 (I_1 - 3) + C_2 (I_2 - 3) \qquad (5.8)$$

where C_1 and C_2 are constants, C_1 being a measure of crosslink density of rubber (39).

In simple extension

$$W = C_1 (\lambda^2 + 2\lambda^{-1} - 3) + C_2 (\lambda^{-2} + 2\lambda - 3) \qquad (5.9)$$

from which the stress is

$$\sigma = \frac{\partial W}{\partial \lambda} = 2(\lambda - \lambda^{-2}) (C_1 + C_2/\lambda) \qquad (5.10)$$

and Young's modulus is

$$E = 6C_1 + 6C_2 \qquad (5.11)$$

When W_2 in eq. (5.4) and C_2 in eq. (5.9) are zero, there is no I_2 term and both equations reduce to that for the simple kinetic theory of rubber elasticity, ie

$$W = C_1 (I_1 - 3) = W_1 (I_1 - 3) \qquad (5.12)$$

5.3 Relationship between W_1, W_2 and C_1, C_2

Approximate relations between the constants W_1, W_2 in eq. (5.4) and C_1, C_2 in eq. (5.8) can be obtained by applying the least squares method to the stresses as follows.

Equating the Young's modulus in eq. (5.7) and eq. (5.11) gives

$$W_2 = 3(C_1 + C_2 - W_1) \qquad (5.13)$$

Re-arranging eq. (5.6) gives

$$\sigma_W / 2(\lambda - \lambda^{-2}) = W_1 + Q W_2 \qquad (5.14)$$

where $Q = \lambda/(1 + 2\lambda^3)$

and re-arranging eq. (5.10) gives

$$\sigma_c/2(\lambda - \lambda^{-2}) = C_1 + C_2/\lambda \qquad (5.15)$$

The difference S in the left hand sides of eq. (5.14) and eq. (5.15) is

$$S = W_1 (1 - 3Q) - C_1 (1 - 3Q) - C_2 (\lambda^{-1} - 3Q) \qquad (5.16)$$

Minimising the sum of the squares of S, differentiating with respect to W_1 and equating to zero gives

$$\frac{\partial S^2}{\partial W_1} = 0 = \sum \left\{ W_1 (1 - 3Q)^2 - C_1 (1 - 3Q)^2 - C_2(\lambda^{-1} - 3Q)(1 - 3Q) \right\} \qquad (5.17)$$

whence

$$W_1 = C_1 + A_1 C_2 \qquad (5.18)$$

where $A_1 = \sum (\lambda^{-1} - 3Q)(1 - 3Q) / \sum (1 - 3Q)^2 \qquad (5.19)$

substituting into eq. (5.13)

$$W_2 = 3 (C_1 + C_2 - C_1 - A_1C_2)$$
$$= A_2C_2 \qquad (5.20)$$

where $A_2 = 3 (1 - A_1)$

By taking the summation in eq. (5.19) over different ranges of λ, different values of A_1 and A_2 can be obtained.

Over the range $1 \leqslant \lambda \leqslant 3$, the values of A_1 and A_2 are found to be 0.21 and 2.37 respectively.

Whence

$$W_1 = C_1 + 0.21 C_2 \qquad (5.21)$$

$$W_2 = 2.37 C_2 \qquad (5.22)$$

The values of the ratio C_2/C_1 quoted for most practical rubber vulcanizates are less than 1.2 which gives W_2/W_1 ratio of 2.27.

5.4 Determination of W_1 and W_2

The constants W_1 and W_2 can be obtained from a tensile load-deflection experiment as described in Section 4.4 and a plot of the data in the form

$$\frac{\sigma}{2(\lambda - \lambda^{-2})} \quad \text{against} \quad \frac{1}{\lambda^{-1} + 2\lambda^2}$$

This gives, approximately, a straight line, the slope and intercept of which are W_2 and W_1 respectively.

Fig. 5.1 shows the experimental data for the vulcanizate A plotted in this way from which W_1 and W_2 values of .174 and .195 respectively were obtained. Using these values, the values of stress and strain-energy density have been calculated for strains up to 200%. These are compared in Fig. 5.2 with the experimental data and are seen to be in excellent agreement.

Different shapes of stress-strain curve can be obtained by varying the ratios W_2/W_1 or C_2/C_1. Fig. 5.3 shows the effects of varying the W_2/W_1 on the shape of the stress-strain curve. For convenience the non-dimensional stress σ/E is plotted where E is the Young's modulus ($=6W_1 + 2W_2$). Very similar curves are obtained using the equivalent C_1, C_2 values derived in Section 5.3 where the maximum error in σ/E between these equations over a range of λ from 1 to 3 is found to be less than 1.7%.

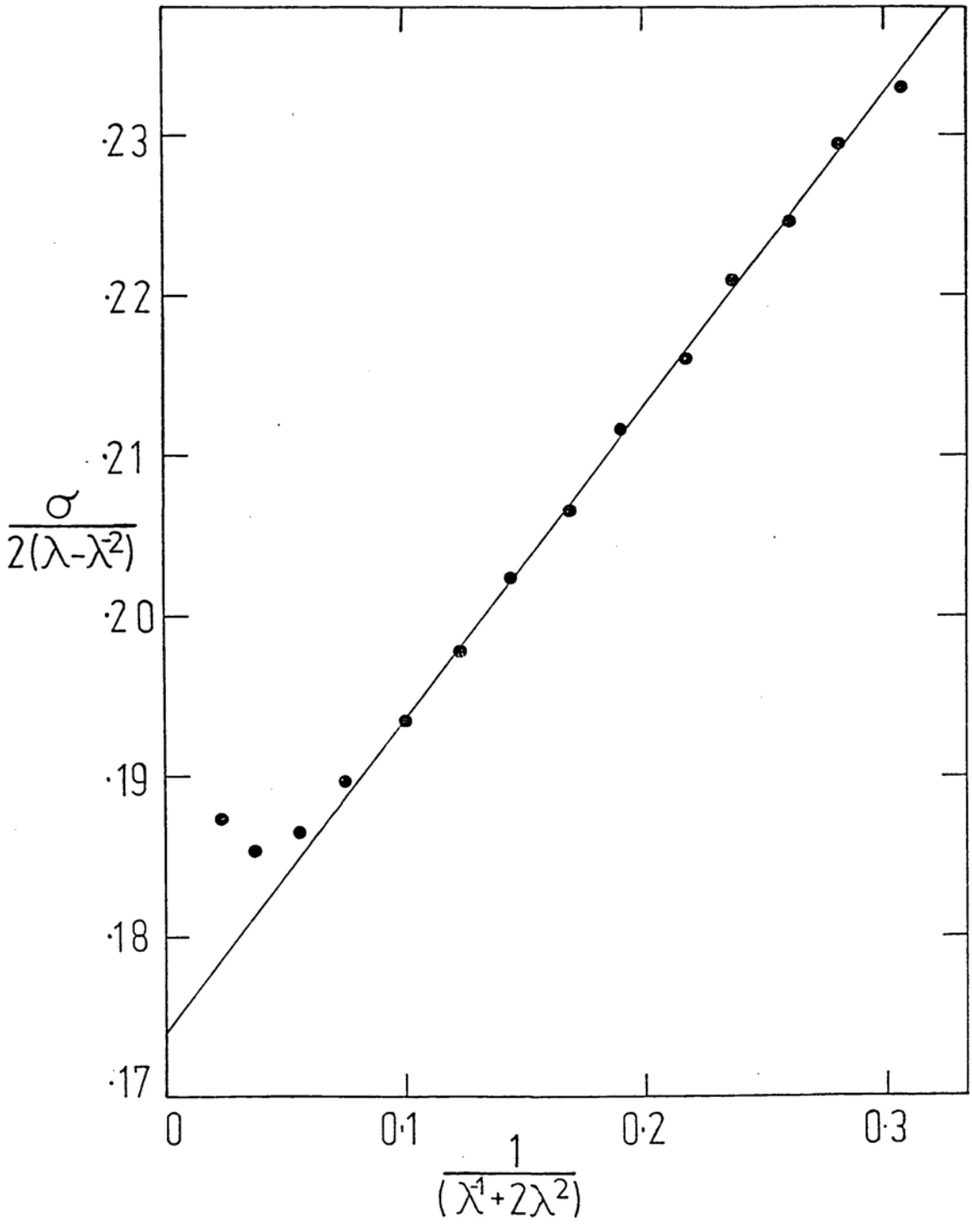


Fig. 5.1 Experimental variation of stress σ and extension ratio λ in the form from which the constants W_1 and W_2 can be obtained.

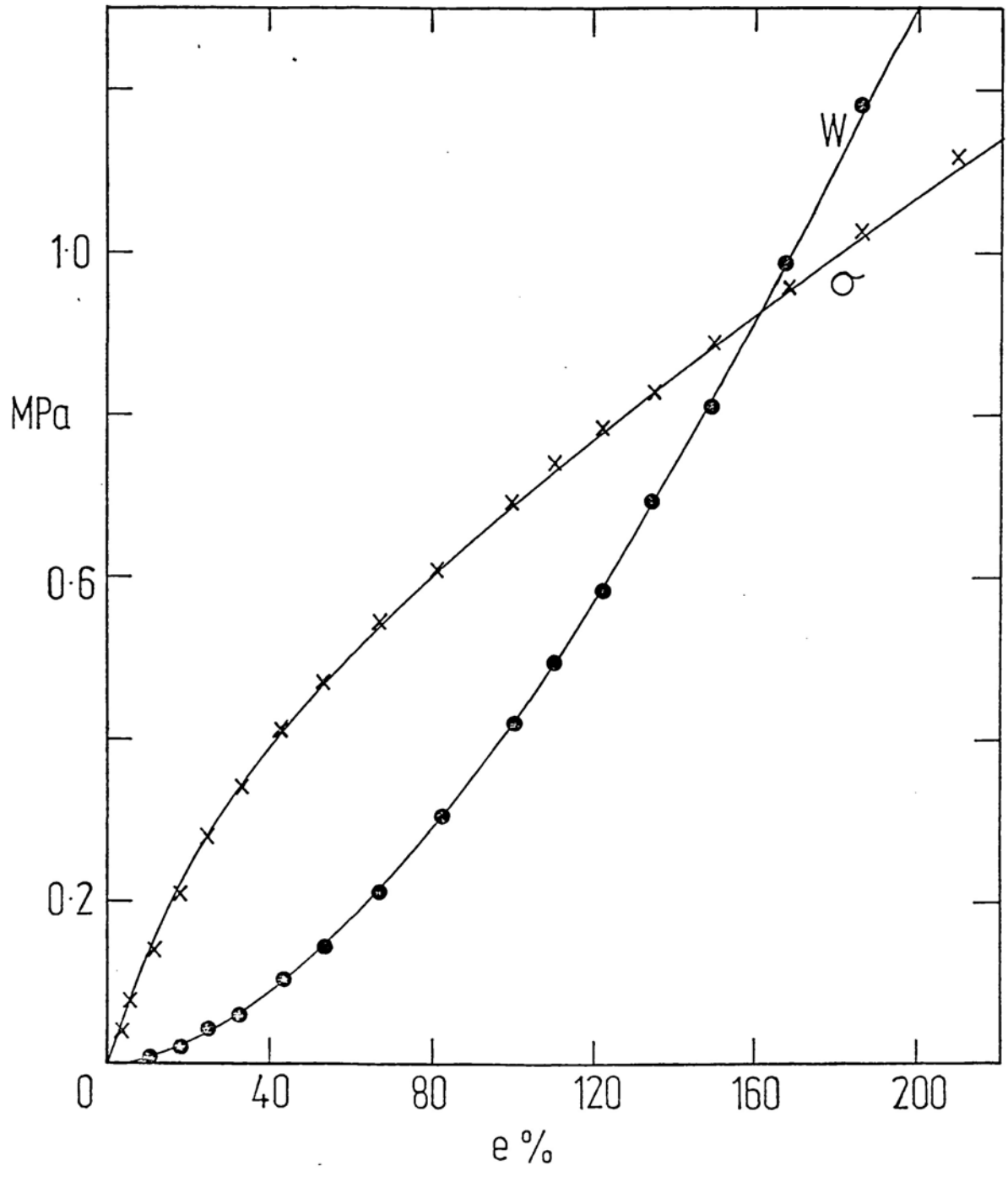


Fig. 5.2 Relations of experimental stress σ to strain e (x) and of strain energy density W to e (●). The full lines are theoretical curves given by eqs. (5.5) and (5.6) with $W_1 = .174$ and $W_2 = .195$.

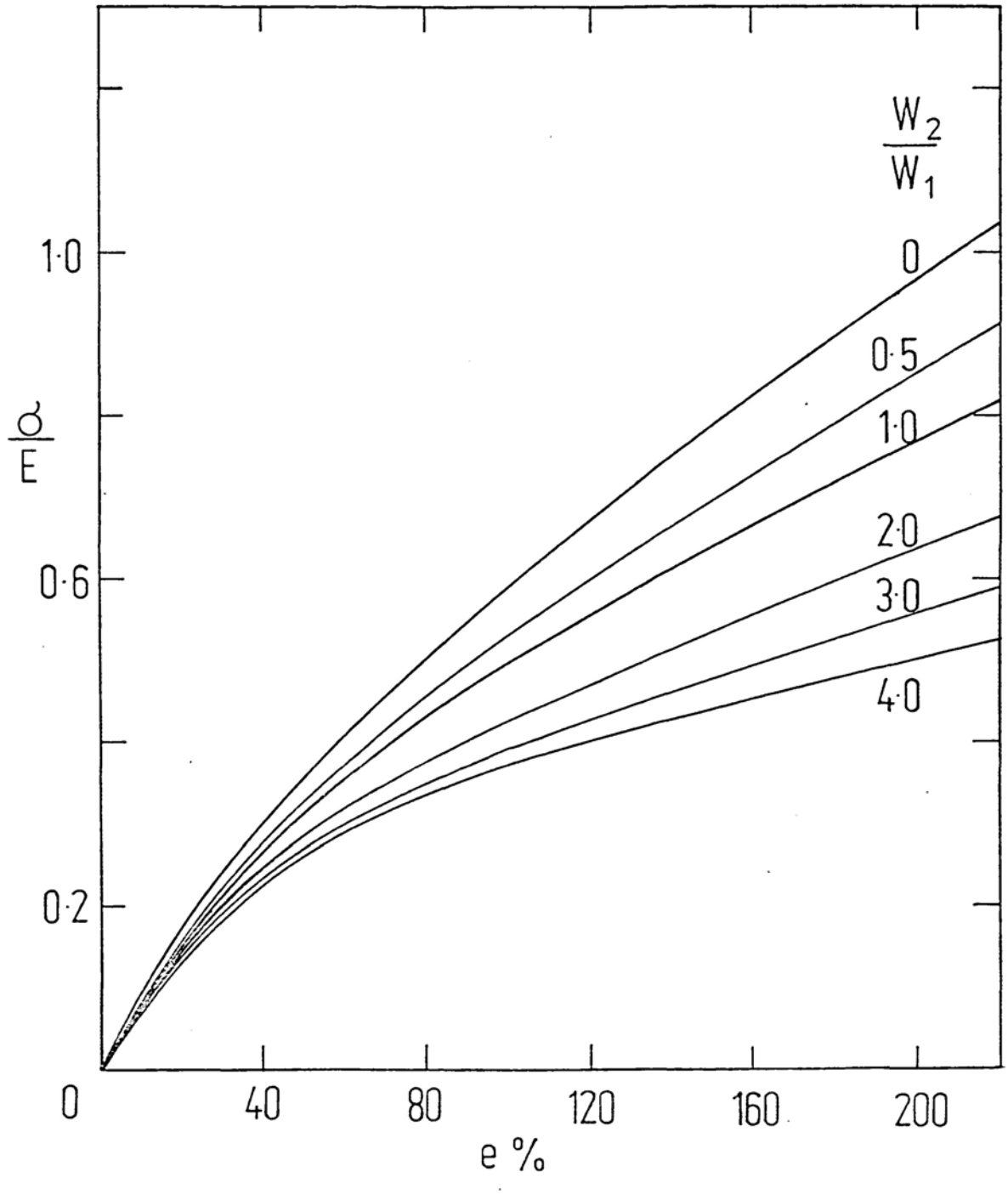


Fig. 5.3 The effect of W_2/W_1 ratios on the shape of stress σ/E - strain curves, where E is the Young's modulus.

5.4.1 Effect of test temperature on the W_2/W_1 ratio

Tensile tests were also carried out on vulcanizates A at temperatures of 70, 100, 120 and 140°C. Fig. 5.4 shows the stress-strain curves for various temperatures. The values of W_1 and W_2 and those derived for C_1 and C_2 for each temperature are tabulated in Table 5.1. All the values of W_2/W_1 ratio shown in Table 5.1 are less than 1.7. The duration of each test was less than 20 minutes. There is a gradual increase in the derived C_1 values with increasing temperature indicating that further crosslinking is taking place.

5.4.2 Effect of time and temperature of vulcanization

The values of W_1 and W_2 quoted in Section 5.4 for vulcanizate A were obtained on rubber sheets vulcanized at 140°C for 90 minutes. Tensile tests were also carried out on rubber sheets having different combinations of time and temperature of vulcanization. The results are tabulated in Table 5.2 showing the values of W_1 and W_2 and those derived for C_1 and C_2. Lower values of C_1 were obtained with increasing temperature or time of vulcanization indicating that chain or crosslink scission process dominates over the crosslinking process (39). This is consistent with the measured properties of the rubber vulcanized at 140°C for various lengths of time, Table 5.3, both hardness and tear strength decreasing with increasing time of vulcanization.

The highest W_2/W_1 ratio obtained for all times and temperatures of vulcanization is less than 1.9 (Table 5.2).

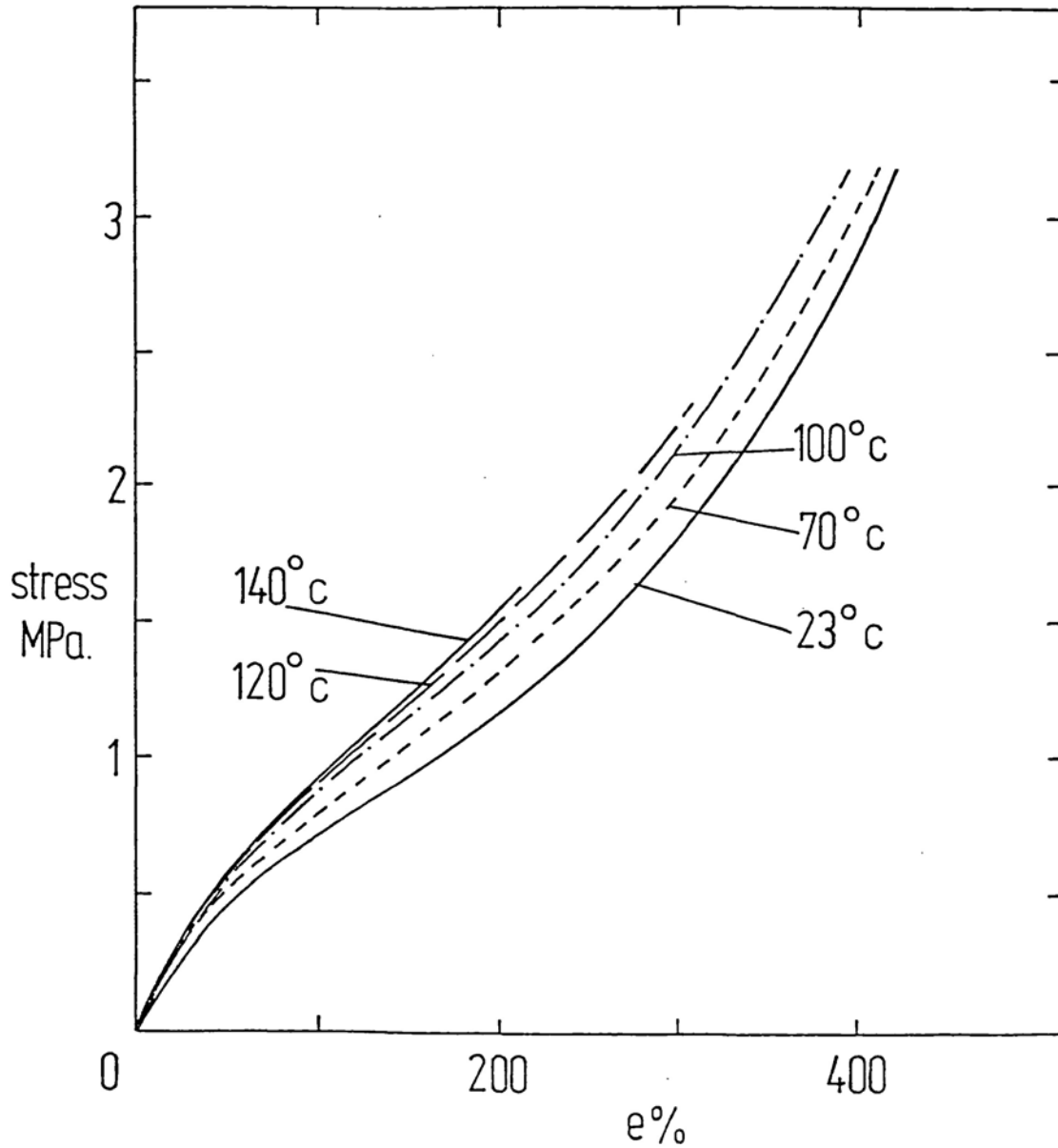


Fig. 5.4 The stress-strain curves of natural rubber gum vulcanizate A at elevated temperatures.

Table 5.1 Values of W_1, W_2 and C_1, C_2 at elevated temperatures

Temperature ^oC	W_1 N/mm^2	W_2 N/mm^2	$\frac{W_2}{W_1}$	C_1 N/mm^2	C_2 N/mm^2	$\frac{C_2}{C_1}$
23	.174	.195	1.661	.157	.082	.522
70	.205	.113	.551	.197	.039	.198
100	.225	.065	.289	.219	.027	.123
120	.231	.090	.390	.223	·038	.170
140	.246	.054	.220	.241	.023	.095

Table 5.2 Values of W_1, W_2 and C_1, C_2 at different combinations of time and temperature of vulcanization

Temperature of vulcanization °C	Time of vulcanization minutes	W_1 N/mm^2	W_2 N/mm^2	$\frac{W_2}{W_1}$	C_1 N/mm^2	C_2 N/mm^2	$\frac{C_2}{C_1}$
150	30	.159	.204	1.283	.141	.086	.610
	60	.157	.209	1.331	.138	.088	.638
	180	.144	.187	1.299	.127	.079	.622
	420	.141	.201	1.426	.123	.085	.691
200	20	.086	.149	1.732	.073	.063	.863
	45	.079	.145	1.835	.066	.061	.924
	90	.068	.119	1.750	.057	.050	.877
	180	.055	.092	1.673	.047	.039	.830
	420	.038	.059	1.553	.033	.025	.758

Table 5.3 Effect of vulcanization time at 140°C

Time hours	Microhardness IRHD	Tear strength kN/m
1.5	38	17.0
3	37.5	13.5
6	37.5	12.0
20	36.5	11.7
65	34.5	9.0

5.4.3 Limits for W_2/W_1

As k can only be a non-dimensional function of the elastic stress-strain behaviour of a vulcanizate, it can only vary from one vulcanizate to another, or one temperature to another with the ratio W_2/W_1 (or C_2/C_1). From Sections 5.3 and 5.4 W_2/W_1 was not found to exceed 2.3 and was positive, ie

$$0 \leqslant W_2/W_1 \leqslant 2.3$$

5.5 Determination of k in simple extension

A numerical method based on finite elements and the minimization of the total energy of the deformed rubber sheet is used. This method made use of a computer program written for the plane-stress analysis of rubber at high strains (40).

The strain energy function used in the program is that given in eq. (5.4). The analysis gives the total energy U, edge strains and the deformed positions of the nodal points of the triangular elements, and hence their energies and the principal stresses and strains throughout the testpiece.

The model used is that of a tensile strip 5 units long and 1 unit wide, divided into different sizes of triangular finite elements. Fig. 5.5 shows one half of the model. The effects of cracks of various lengths can be simulated simply by changes in the boundary conditions. The arrows in the figure indicate the position of the crack tip for crack lengths of 0 and .16. The .16 crack length was found by Lindley (34) to be most convenient.

The value of k can be evaluated using eq. (5.1), ie

$$k = (U_o - U_c)/c^2 t\, W \qquad (5.21)$$

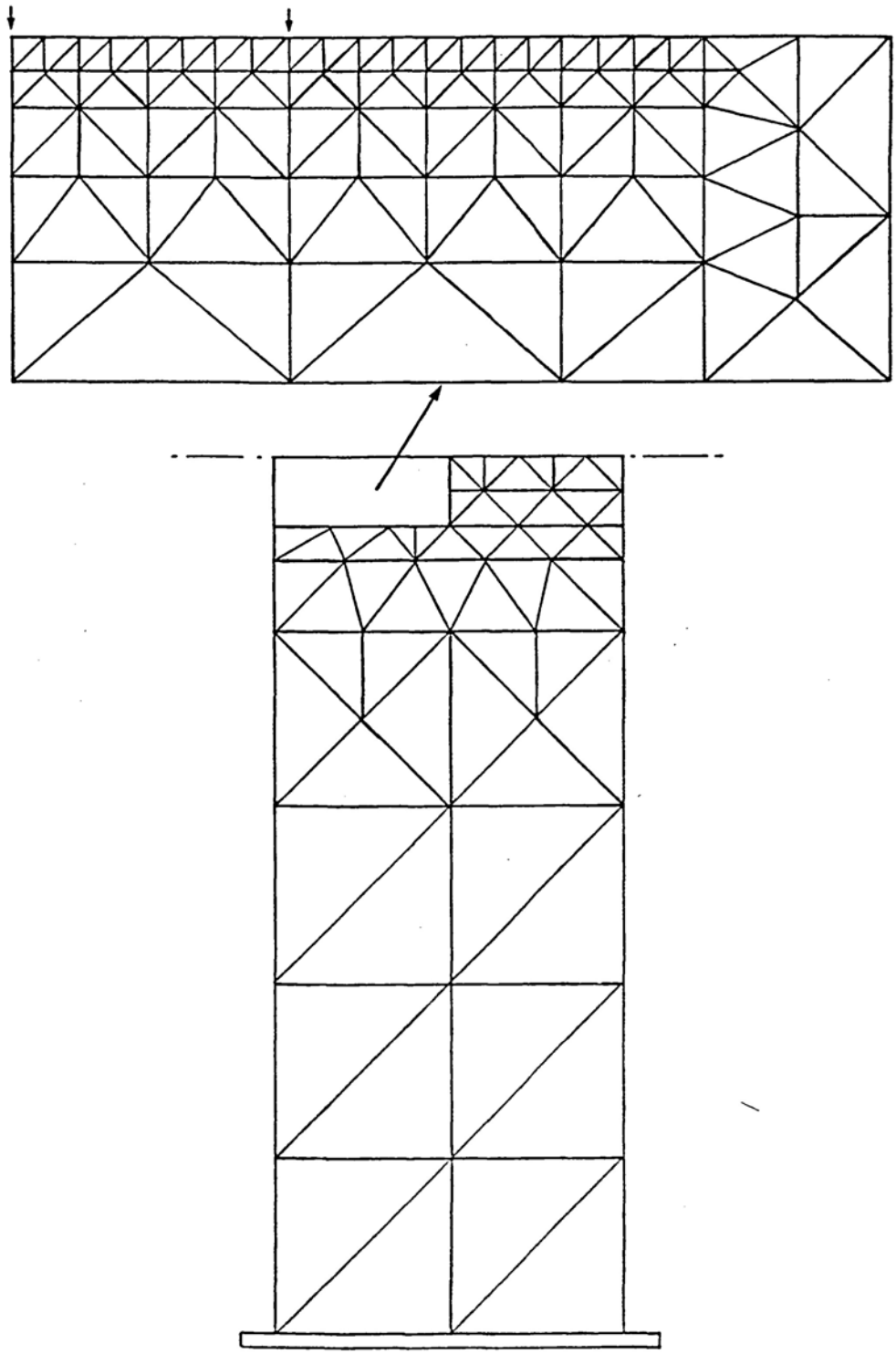


Fig. 5.5 Finite-element meshes used to represent tensile strip with the region around the crack shown enlarged.

For convenience in the program (40), a non-dimensional strain energy density W/E is used. Eq. (5.4) may then be re-written as

$$\frac{W}{E} = K_1 (I_1 - 3 + K_2 \ln(I_2)) \qquad (5.22)$$
$$(\frac{2}{3})$$

Since $E = 6W_1 + 2W_2$ from eq. (5.7), the coefficients K_1 and K_2 can be expressed in terms of the W_2/W_1 ratio, ie

$$K_1 = W_1/E = 1/(6 + 2\ W_2/W_1) \qquad (5.23)$$

$$K_2 = W_2/W_1 \qquad (5.24)$$

Section 5.4.3 gave limiting values for the ratio W_2/W_1, but in order to cover a possible wider range of vulcanizates and temperatures, this range has been widened to

$$0 \leqslant W_2/W_1 \leqslant 4$$

5.6 Numerical results

Values of k up to 200% strain obtained numerically for W_2/W_1 ratios between 0 and 4 are shown in Fig. 5.6. These results are compared in Fig. 5.6 with the experimental data of Greensmith (10) and the agreement is extremely good. The full line in Fig. 5.6 is given by eq. (3.5), ie

$$k = \frac{2.95 - 0.08e}{(1 + e)^{\frac{1}{2}}} \qquad (5.25)$$

This equation gives a reasonable fit with the results over the range 0-200% strain. This is useful for the evaluation of k in the relation, eq. (5.2), for the tearing energy of a tensile strip with an edge crack.

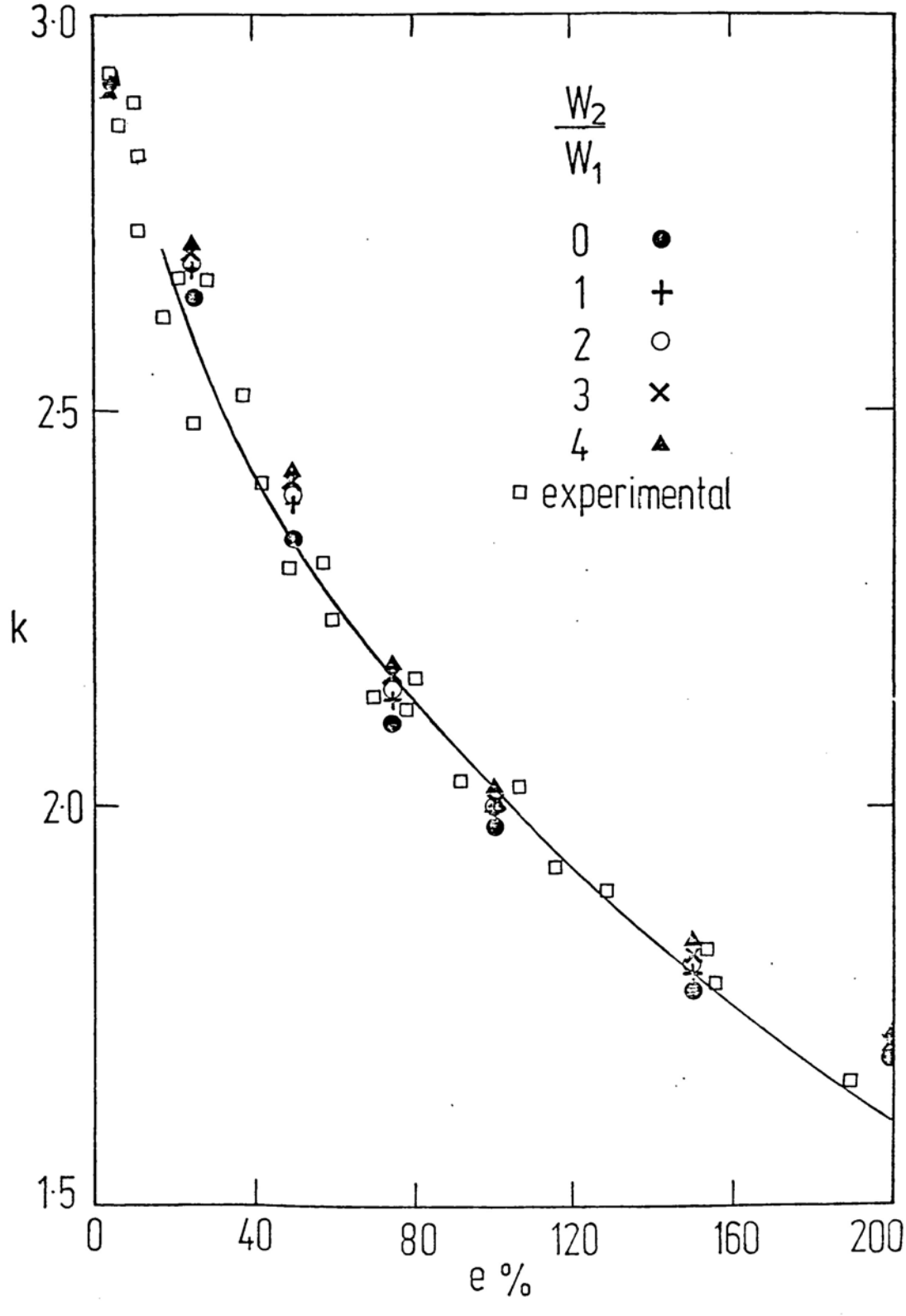


Fig. 5.6 Variation with strain e of k in eq. (5.2) for simple extension strips determined by numerical method with different W_2/W_1 ratios. The experimental points (□) were obtained by Greensmith (10).

The results in Fig. 5.6 indicate that k can be treated as a function of strain e only and is independent of both temperature and vulcanizate.

This conclusion is of considerable practical significance. It means that the tensile strip with a single edge crack - the most versatile of the various testpieces which can be used for obtaining plane stress crack growth characteristics - can be employed for this purpose for all vulcanizates and environmental conditions without the uncertainty hitherto present in the value of k, since it will be shown in Section 8 that there is no significant difference between the plane stress and plane strain crack growth characteristic of rubber.

SECTION 6 RELAXING CRACK GROWTH AND FATIGUE AT ELEVATED TEMPERATURES

6.1 Effects of temperature

Oxidative degradation is generally considered to be the most serious problem in the use of rubber at high temperatures. A small amount of oxygen (ca 1% by weight) absorbed by a natural or synthetic rubber vulcanizate has a pronounced effect on its physical properties (41).

Crack growth experiments at laboratory temperature carried out by Lake and Lindley (13) on natural rubber gum vulcanizates with and without antioxidant showed that in air both have a lower resistance to crack growth than in vacuo but that the protected rubber is noticeably better than the unprotected one. The differences are most marked at low tearing energies but become small at high tearing energies approaching those of conventional tear strength. An oxidation resistant rubber, butyl, does not show such differences in the presence and absence of oxygen. They therefore attributed the reduction of the crack growth resistance in natural rubber to oxidation.

In the investigation into the high temperature strength of natural rubber, Harwood, Payne and Whittaker (42) found that the failure criterion relating strain energy to break and hysteresis over a range of temperature for amorphous rubbers did not apply to natural rubber within a certain temperature range, about 80 to 140°C. The strain energy to break decreased dramatically, from the values up to 80°C, between these temperatures and showed a wide scatter. They suggested that between these temperatures the bulk of the rubber is nearly amorphous, but the highly strained region around the inherent flaws in the samples gives rise to crystallization as has been shown by Andrews (43).

Lake and Lindley (13) showed that as the temperature is increased from 0^{o} to $100^{o}C$, there is only a fourfold decrease in the relaxing fatigue life at 250% strain of a natural rubber gum vulcanizate compared with a 10 000-fold decrease in that of SBR. They attributed the difference to the ability of natural rubber to maintain its strain-induced crystallization over this temperature range.

Previous findings thus appear to be that there can be a pronounced effect of oxygen on crack growth resistance at laboratory temperature and a pronounced effect due to reducing ability to strain-crystallize as temperature is increased. As there should be, also, an increasing effect due to oxidation as the test temperature increases, it is possible that this may be the more dominant effect at elevated temperatures. This possibility is explored further in this section.

6.2 Crack growth characteristic and fatigue at $23^{o}C$

The results of all the crack growth experiments are expressed as crack growth rate dc/dn versus the tearing energy T at the maximum deformation of the cycle. This relationship will be referred to as the crack growth characteristic of the vulcanizate.

The crack growth characteristic of vulcanizate A at laboratory temperature is shown on logarithmic scales in Fig. 6.1. As with many other rubber vulcanizates, the characteristic can be represented by the following simple mathematical relations:-

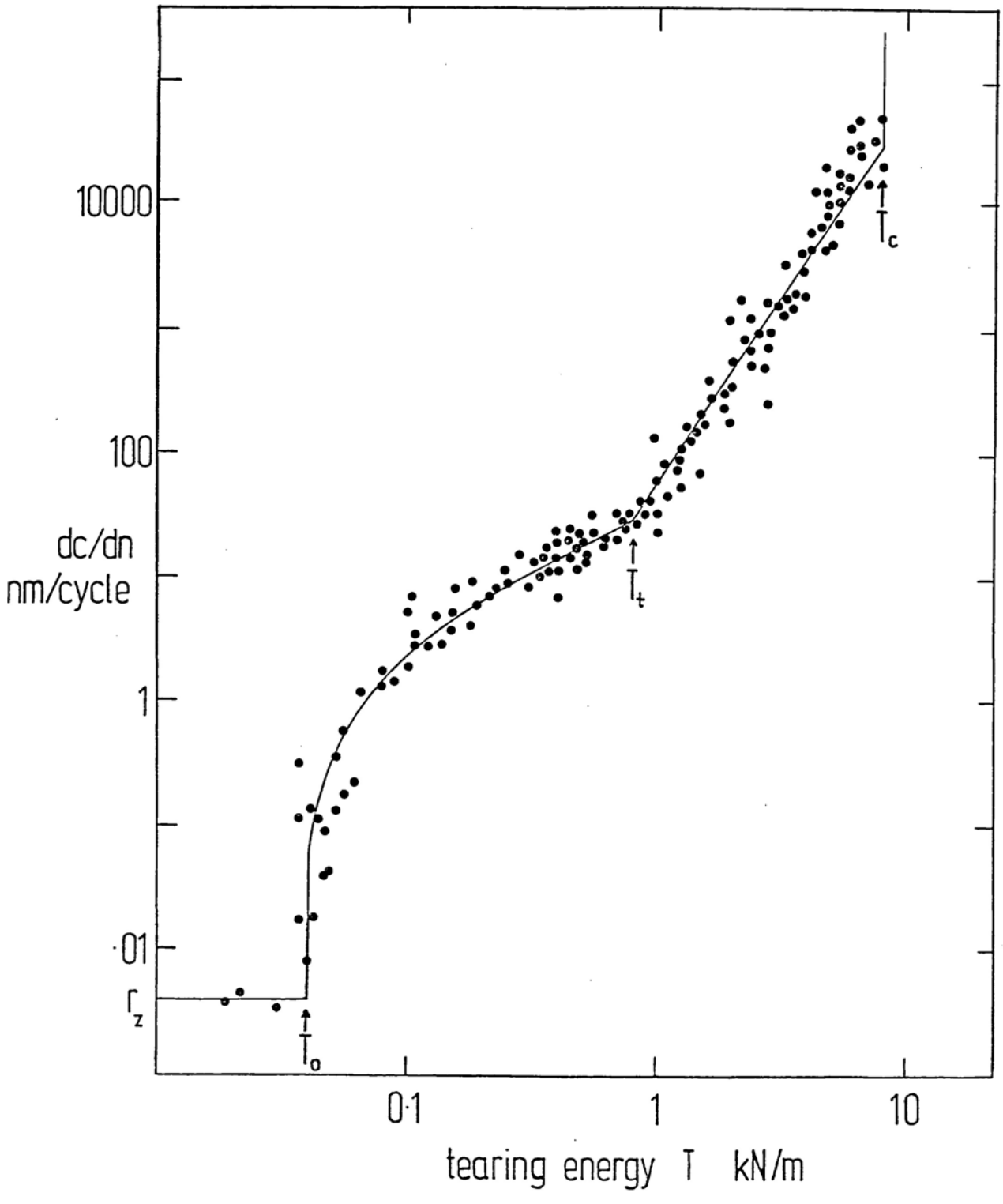


Fig. 6.1 Crack growth characteristic for natural rubber gum vulcanizate A at 23°C. Experimental points. Full line relating crack growth rate dc/dn with tearing energy T given by eqs. (6.1)-(6.4).

$$\frac{dc}{dn} = r_z \qquad T \leqslant T_o \qquad (6.1)$$

$$\frac{dc}{dn} = A_o(T-T_o) + r_z \qquad T_o < T \leqslant T_t \qquad (6.2)$$

$$\frac{dc}{dn} = BT^P \qquad T_t \leqslant T < T_c \qquad (6.3)$$

$$\frac{dc}{dn} = \infty \qquad T_c \leqslant T \qquad (6.4)$$

where r_z, A_o, B, p, T_o, T_t and T_c are constants.

The full lines in Fig. 6.1 are given by the above equations where the constants are

r_z = 0.004 nm/c

A_o = 20 (nm/c)/(kN/m)

B = 25 $(nm/c)/(kN/m)^3$

P = 3

T_o = 0.04 kN/m

T_t = 0.8 kN/m

T_c = 8 kN/m

T_o defines the mechanical crack growth limit below which the rate of growth r_z is due solely to ozone (13); r_z is independent of tearing energy. T_c is the conventional tear strength of rubber at which the crack grows catastrophically. T_t is a transition tearing energy at which the linear dependence of the crack growth rate on tearing energy, eq. (6.2) changes over to the power relationship as given in eq. (6.3). It may be noted that p for this vulcanizate A is higher than that found for other NR vulcanizates (24, 25).

It was mentioned in Section 3 that the relaxing crack growth characteristic is a unique relationship between crack growth rate dc/dn and the tearing energy T at the maximum deformation of the cycle, and it is independent of the shape and size of test pieces, and mode and amount of deformation, viz

$$\frac{dc}{dn} = f(T) \qquad (6.5)$$

For the tensile strip, the tearing energy is given in eq. (3.4) as 2kWc. Thus eq. (6.5) becomes

$$\frac{dc}{dn} = f(2kWc) \qquad (6.6)$$

As the values of k and W are known for a given strain it is possible to calculate the number of cycles required for a crack to grow from one length c_1 to another c_2 by integration of eq. (6.6), ie

$$N = \int_o^n dn = \int_{c_1}^{c_2} \frac{dc}{f(2kWc)} \qquad (6.7)$$

A specific application of eq. (6.7) is the fatigue failure of dumbbells subjected to repeated deformation. The number of cycles for the failure to occur defines the fatigue life N at a given strain, the crack growing from an initial crack length c_o to length c_c when the catastrophic tearing energy T_c is reached. The initial crack length c_o is the effective size of edge imperfections or flaws produced by the cutter during die-stamping of the dumbbells. The value of c_o was found [24] to be 0.025 mm for gum vulcanizates of natural rubber. The value of c_c is taken as the test piece width w when it is less than $T_c/2kW$. Strictly c_c should not be greater than 20-30% of w for the tearing energy equation [9] to hold. However, as most of the life is spent in the early stages of growth where growth rates are relatively slow, this restriction has been ignored when predicting fatigue life.

Fatigue lives of diestamped dumbbells of vulcanizate A have been determined experimentally at various maximum strains, the samples being allowed to relax to zero strain at each cycle. The results, plotted as fatigue life, N against strain, e, are shown in Fig. 6.2. The line ab

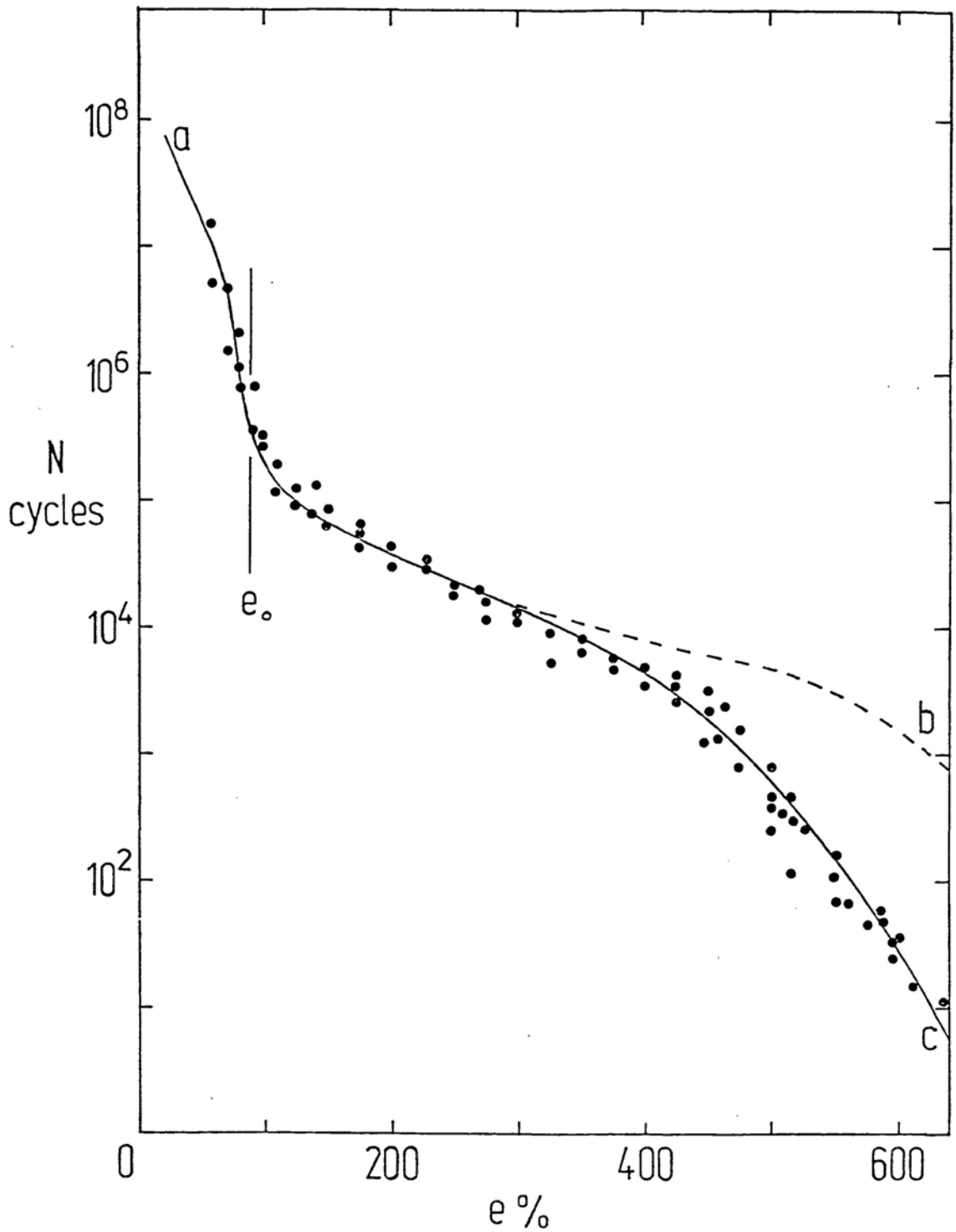


Fig. 6.2 Dependence of fatigue life N of vulcanizate A on strain e at 23°C: experimental points; curve ab is predicted curve given by eqs. (6.1)-(6.4). Curve ac is the best line through the experimental points.

in the figure corresponds to the N-e relationship predicted from eq. (6.7) with c_o = 0.025 mm. It is in satisfactory agreement with the experimental data up to 225% strain. At higher strains, the experimental points fall below the predicted curve. The departures increase with increasing strain. Lindley (26) suggested that this could be due to insufficient number of cycles for the crack tip, which is initially sharp, to roughen to its natural state. It is observed in crack growth experiments that the crack growth rate initially from the sharp razor cut is noticeably faster than rough growth at the same tearing energy.

The strain e_o shown on Fig. 6.2 is the mechanical fatigue limit at which, with c_o = 0.025 mm, the initial tearing energy correspond to the mechanical crack growth limit T_o. Below this strain cracks grow only by ozone attack (13).

The agreement between the theory and the experimental results for strains up to 225% indicates that the fatigue failure is essentially a crack growth process. For diestamped dumbbells, the process takes place from small flaws or stress raisers of effective size 0.025 mm. The points of failure of the test pieces were randomly distributed along the narrow central region indicating that the die-stamping action did not introduce an isolated flaw.

6.3 Fatigue of an unprotected rubber vulcanizate

Fatigue tests at 23°C were carried out on vulcanizate B which is similar to vulcanizate A but without the antioxidant, Nonox ZA. The results in Fig. 6.3 show that the fatigue life of the vulcanizate B is about half that of the protected vulcanizate B at low strains, but at strains above 500% there is no difference in fatigue life. This is consistent with the claim by Lake and Lindley (13) that oxidation can reduce the crack growth resistance.

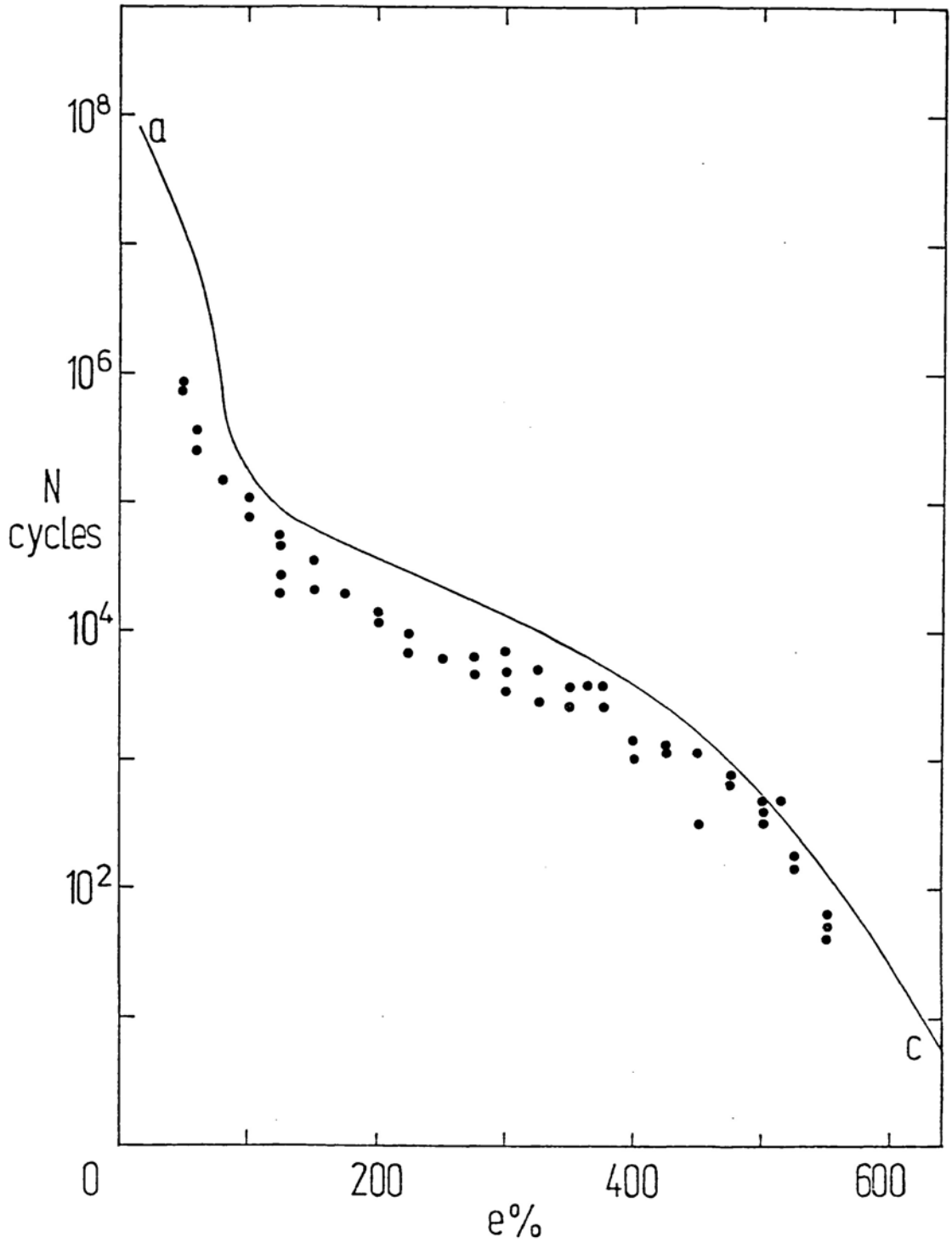


Fig. 6.3 Dependence of fatigue life N on strain e of unprotected natural rubber gum vulcanizate B. Experimental points. Curve ac is that at 23°C (Fig. 6.2).

Bell measured the oxygen uptake of stretched natural rubber vulcanizates and found it to increase with strain (44). However, the maximum strain at the crack tip, when growth is occurring, is always the breaking strain. Strains of the magnitude of the breaking strain occur in the neighbourhood of the crack tip for time periods which depend on the growth rate so that oxygen uptake there, and its deleterious effect, will have an inverse dependence on the crack growth rate. Lake (28) has already suggested this explanation for the increase in crack growth resistance at constant maximum tearing energy as the test frequency is increased. The same explanation is consistent with the reducing difference between the fatigue resistance of protected and unprotected vulcanizates in Fig. 6.3 as the maximum strain increases.

6.4 Tensile tests at elevated temperatures

Tensile tests were carried out on unaged test pieces of vulcanizate A at different elevated temperatures. The effect of temperature on tensile strength is shown in Fig. 6.4. Up to 70°C, the tensile strength remains high, but there is a dramatic decrease in the strength between 100° and 140°C. At 140°C the strength has fallen to only one tenth of that at 70°C. Above 140°C, the strength remains almost constant. The results show a wide scatter between 70° to 140°C. This observation is very similar to that made by Harwood, Payne and Whittaker (42). They suggested that up to 70°C, the rubber is crystallizing and above 140°C, amorphous. Between these temperatures, the rubber retains its ability to crystallize only around the high strained regions in the vicinity of the crack tip while the bulk of the polymer remains amorphous.

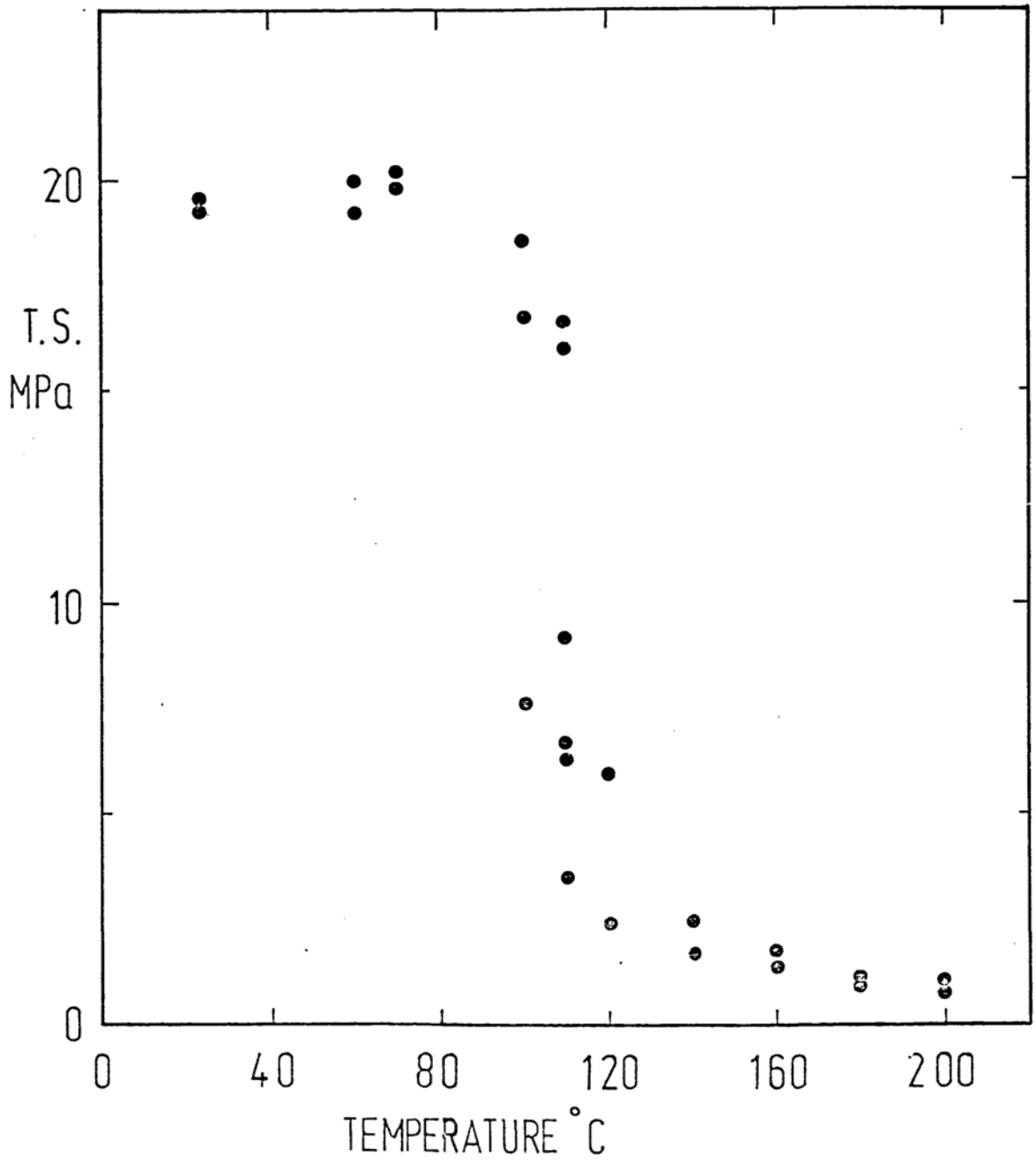


Fig. 6.4 Dependence of tensile strength on temperature for vulcanizate A. Experimental points.

Fig. 6.5 illustrates the effects of temperature on tensile hysteresis loops. Each loop was obtained near the breaking condition at the test temperature. With increasing temperature the area of the loop decreases and the slope of the retraction curve becomes less steep, thus indicating a lessening of crystallization which can occur at a crack tip during growth.

6.5 Ageing tests at elevated temperatures

Before crack growth and fatigue experiments are carried out at elevated temperatures, it is necessary to establish the length of time for which tests be continued on the same piece of rubber before there is a significant change in the material properties due to oxidation.

Table 6.1 gives the results of ageing at various temperatures. There is no oxidative degradation at 70°C. In fact, the increase in hardness of the rubber indicates that further crosslinking process may be taking place. At higher temperatures, both the hardness and the tensile strength decrease very markedly after certain periods of ageing thus illustrating the deleterious effects of oxidation. Based on these results, the maximum test period allowed at each temperature was as follows:-

Temperature of tests	Maximum period
70°C	3 months or longer
100°C	5 days
120°C	1 day
140°C	3 hours

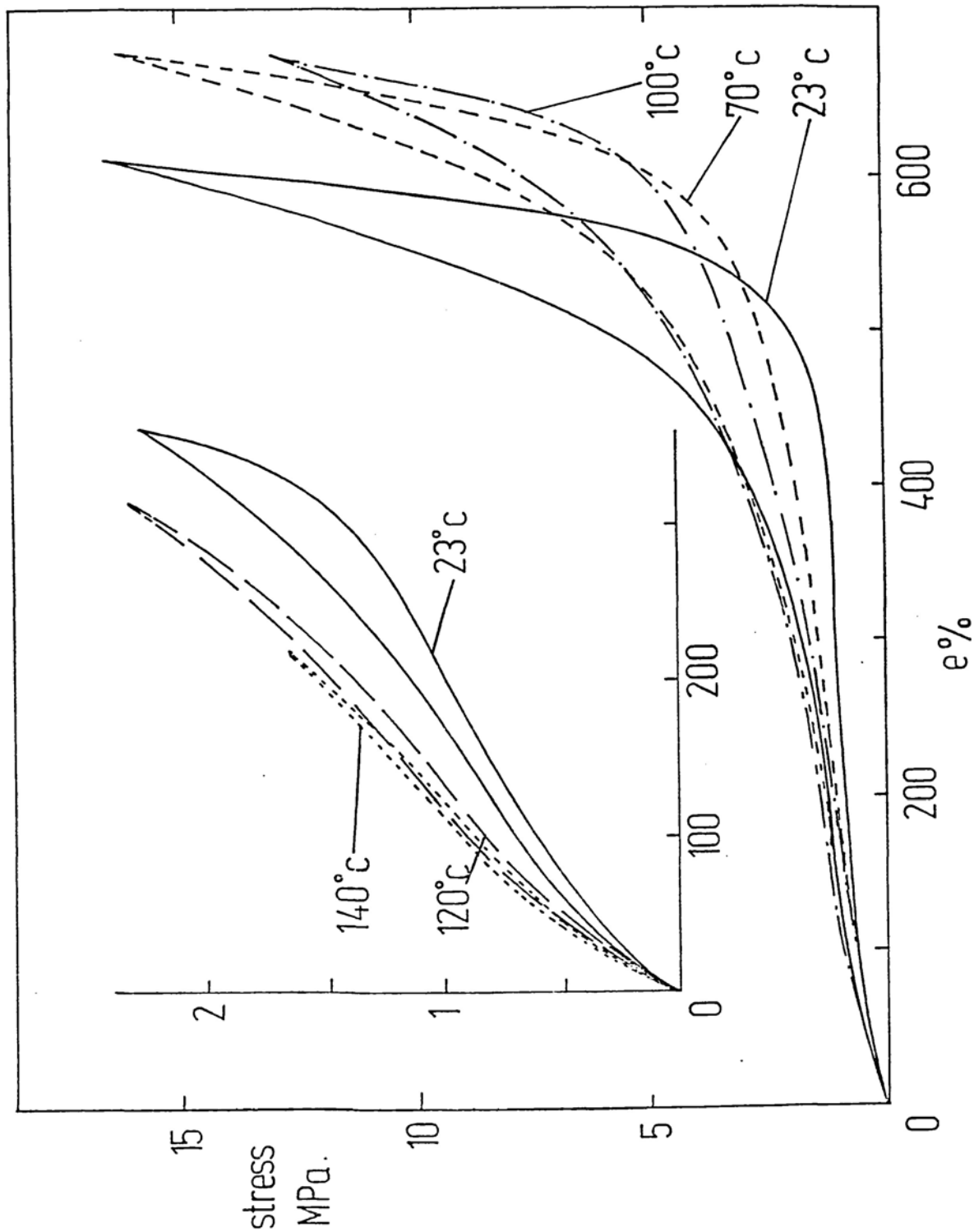


Fig. 6.5 Tensile hysteresis loops at elevated temperatures.

Table 6.1 Effect of ageing on properties of natural rubber vulcanizate A

Temperature of ageing	Time of ageing	0	1hr	3hr	5hr	1d	2d	5d	1wk	2wk	4wk	8wk	12wk
	Hardness, IRHD	37	-	-	-	37	-	-	37	38	39	39	39
70°C	TS, MPa	28	-	-	-	29	-	-	30	29	27	25	24
	E_b, %	721	-	-	-	730	-	-	712	710	650	635	633
	Hardness, IRHD	38	-	-	-	37	-	36	34	32	30	-	-
100°C	TS, MPa	30	-	-	-	28	-	26	18	15	10	-	-
	E_b, %	715	-	-	-	690	-	642	592	568	493	-	-
	Hardness, IRHD	38	-	-	38	36	32	-	<28	-	-	-	-
120°C	TS, MPa	29	-	-	26	21	13	-	5	-	-	-	-
	E_b, %	709	-	-	680	670	621	-	507	-	-	-	-
	Hardness, IRHD	38	37	35	29	<<28	-	-	-	-	-	-	-
140°C	TS, MPa	28	23	21	12	2	-	-	-	-	-	-	-
	E_b, %	709	680	657	596	477	-	-	-	-	-	-	-

Note TS —— tensile strength

E_b —— elongation at break

6.6 Crack growth and fatigue at 70°C

The results of crack growth experiments on vulcanizate A at 70°C are shown in Fig. 6.6. The full line in the figure is the same as that drawn through the 23°C results in Fig. 6.1. The results of fatigue tests at 70°C are shown in Fig. 6.7. The full line is the curve drawn through the experimental points at 23°C as shown in Fig. 6.2. In both cases there is excellent agreement between the experimental points and the full line. Thus, an increase in temperature from 23°C to 70°C has no effect on the fatigue and crack growth behaviour of vulcanizate A.

6.7 Crack growth and fatigue at 100°C

The results of crack growth tests at 100°C are shown in Fig. 6.8. The full line is that of 23°C in Fig. 6.1. The results at 100°C show more scatter than those at 23°C, although the scatter is still much less than is observed (13) on amorphous rubber at 23°C, suggesting that some strain-induced crystallization is still present at 100°C.

Owing to the restriction of the time period of 5 days, it was not possible to obtain the full crack growth characteristic at this temperature. However, the results in Fig. 6.8 indicate that the crack growth resistance is about a factor of two lower than at 23°C.

A limited amount of testing carried out at longer terms and at initial tearing energies much lower than those shown in Fig. 6.8 indicated that the crack growth limit T_o was also reduced by a factor of about two from its value at 23°C.

The results of the fatigue tests at 100°C are shown in Fig. 6.9. The scatter is similar to that of crack growth results in Fig. 6.8. At low and moderate strains, the fatigue lives are about half those

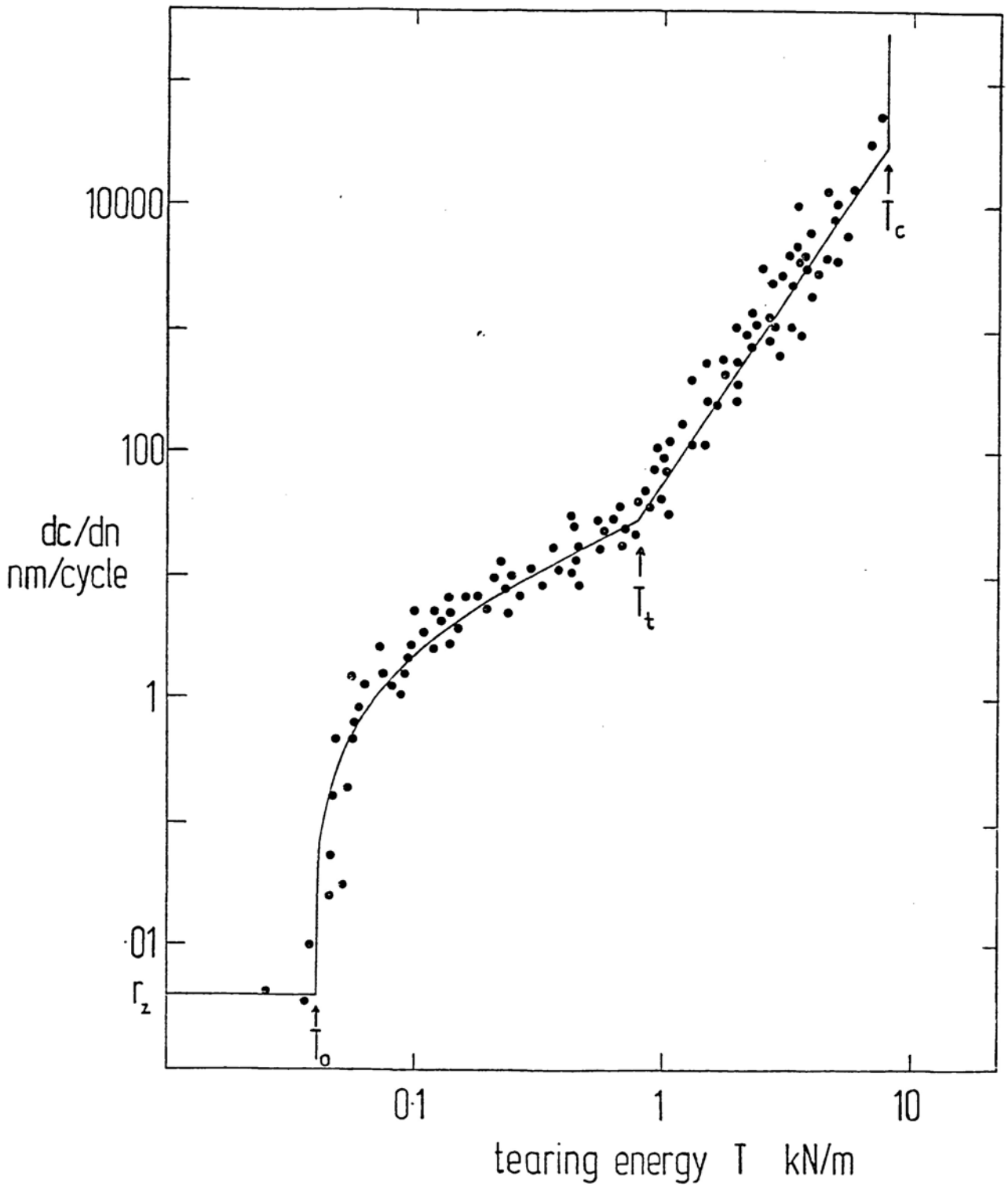


Fig. 6.6 Crack growth characteristic for vulcanizate A at 70°C. Experimental points. The full line is that at 23°C (Fig. 6.1).

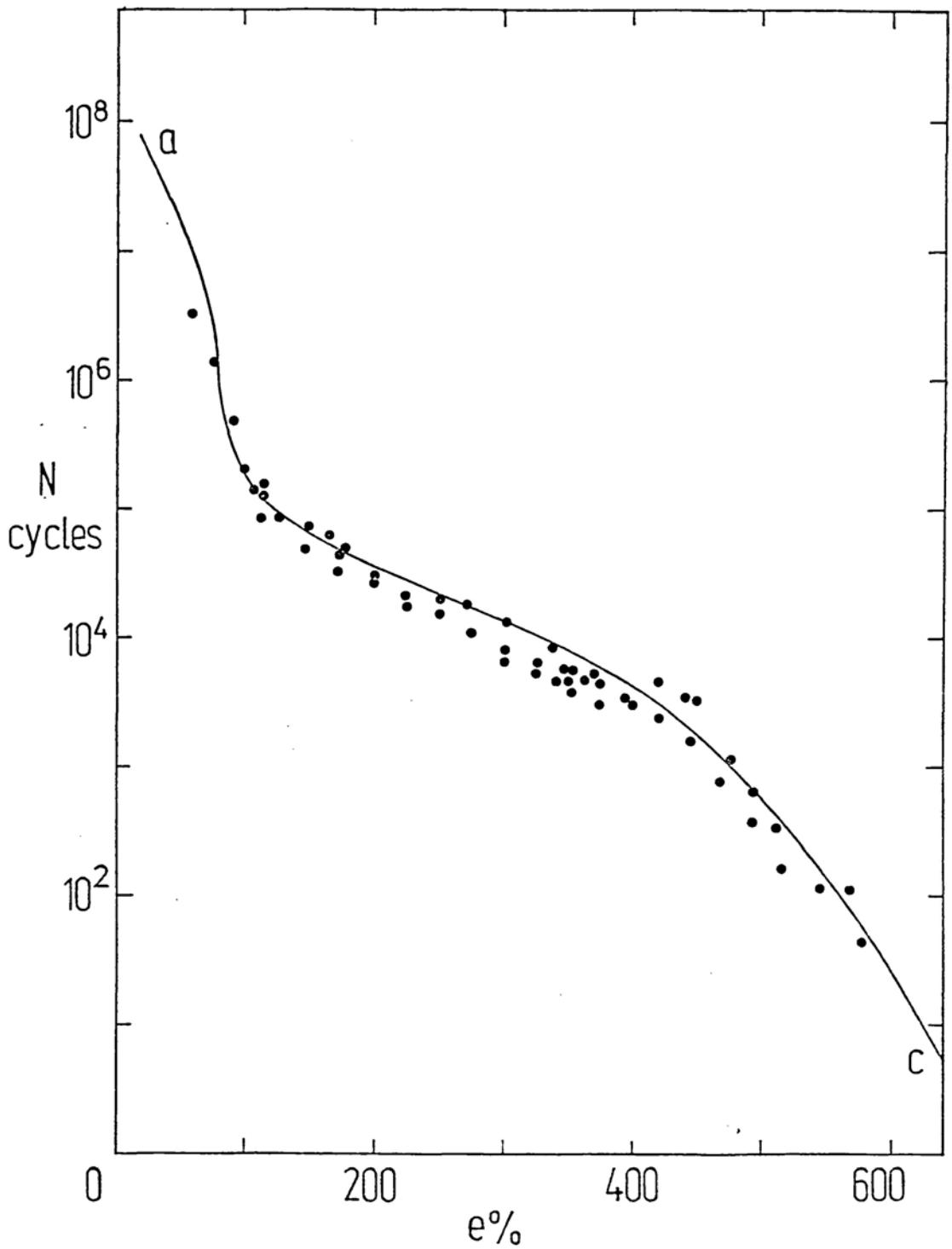


Fig. 6.7 Dependence of fatigue life N on strain e of vulcanizate A at 70°C. Experimental points. Curve ac is that at 23°C (Fig. 6.2).

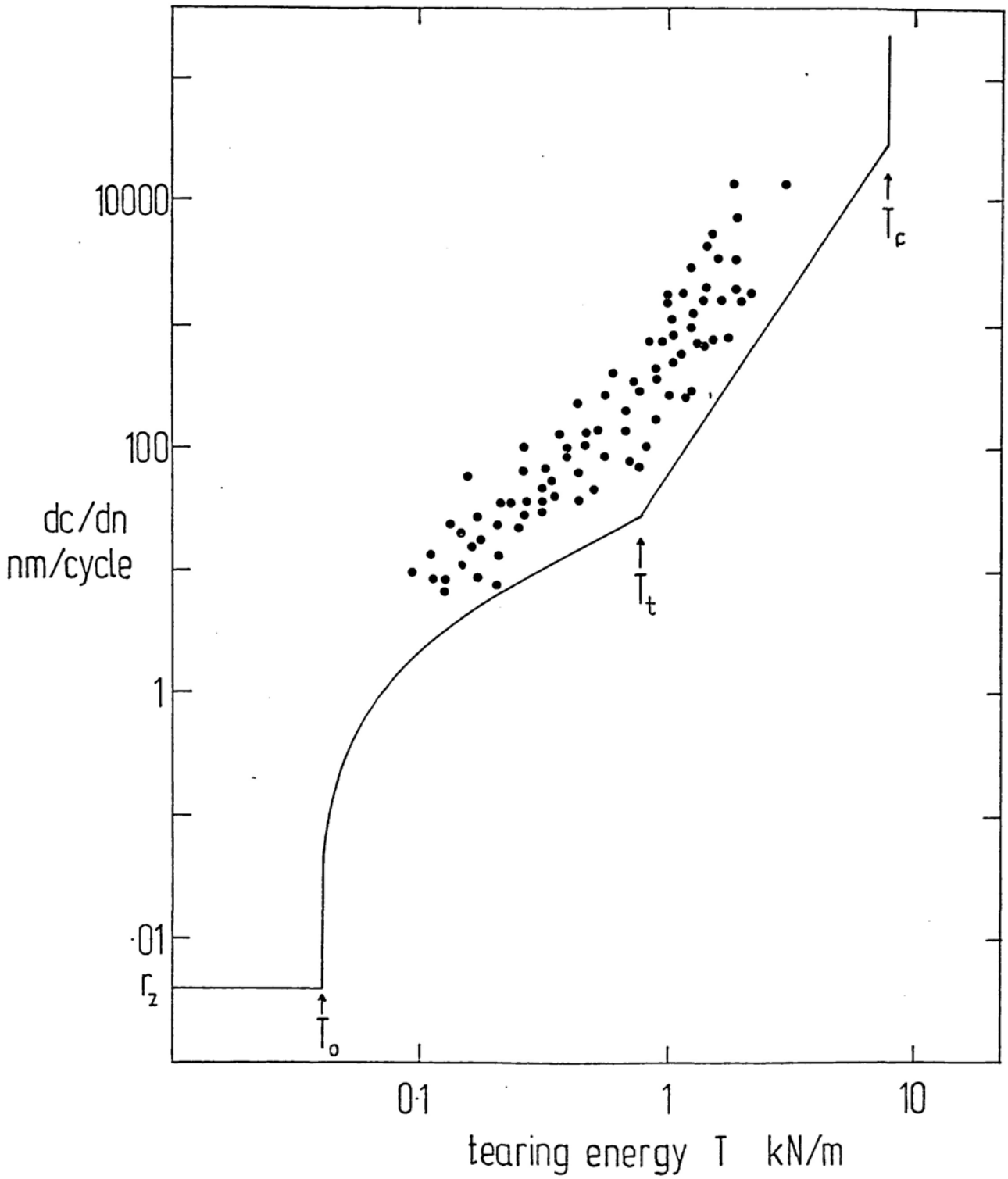


Fig. 6.8 Crack growth characteristic for vulcanizate A at 100°C. Experimental points. The full line is that at 23°C (Fig. 6.1).

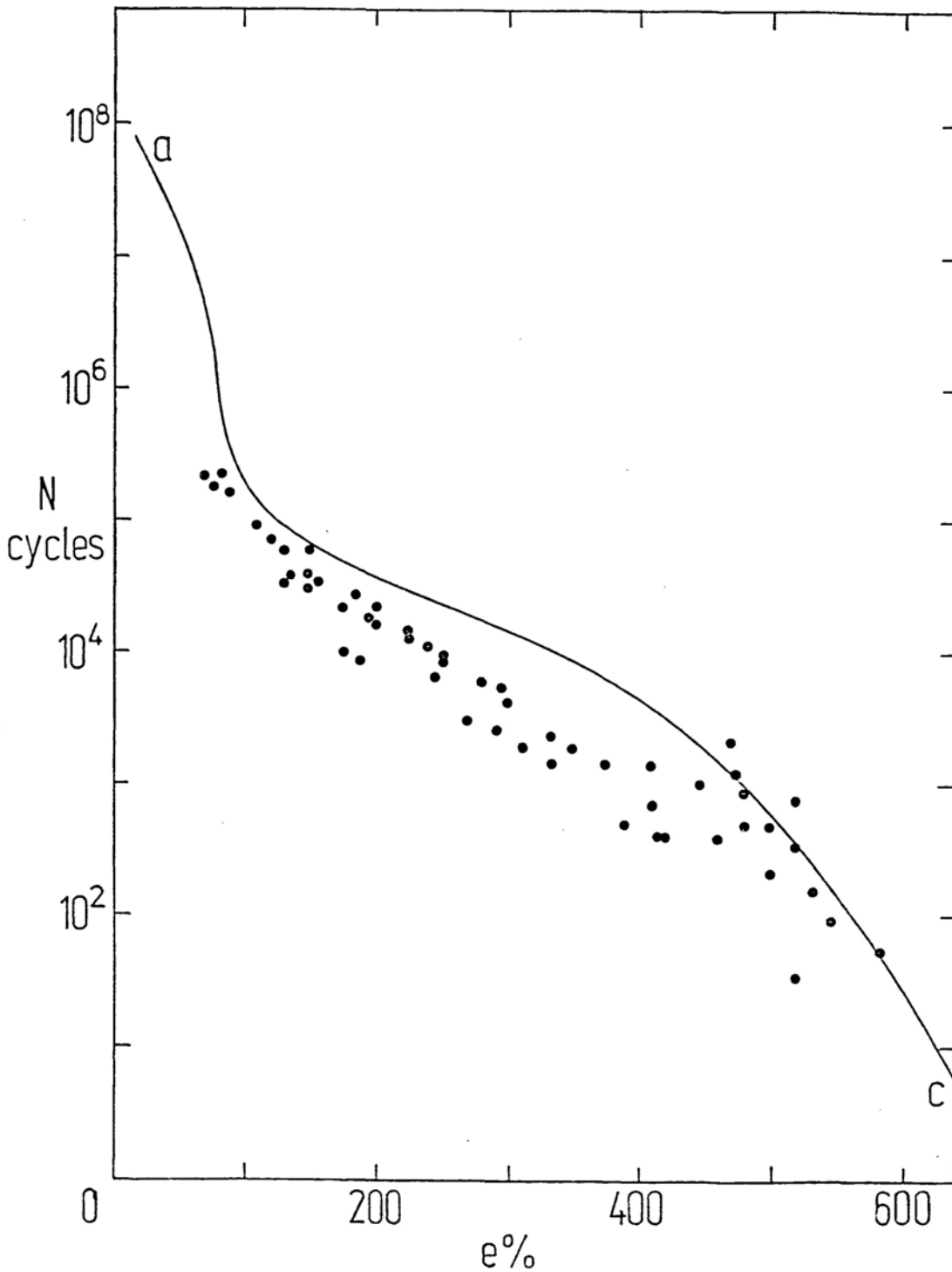


Fig. 6.9 Dependence of fatigue life N on strain e of vulcanizate A at 100°C. Experimental points; curve ac is that at 23°C (Fig. 6.2).

at 23°C, represented by the full line, which is consistent with the crack growth behaviour at the two temperatures. At high strains the lines at 100°C become similar to those at 23°C. The test time is very short in both cases. The crack growth results at high tearing energies do not show this similarity with those at 23°C, probably because the test times were much longer than the high strain fatigue tests.

The fatigue results in Fig. 6.9 show a close similarity to those of unprotected vulcanizate B in Fig. 6.3, ~~represented by the broken line~~. This is convincing evidence that oxidation rather than lessening of the ability to strain-induced crystallization is the dominant factor in the reduction of fatigue life and hence crack growth resistance at 100°C.

6.8 Fatigue tests at 120°C and 140°C

The results up to 100°C illustrate that temperature affects both crack growth and fatigue resistance to similar extent. For convenience, only fatigue testing was carried out at temperatures above 100°C.

The results of fatigue tests at 120°C and 140°C are shown in Figs. 6.10-6.11. The full line is that at 23°C. Lines parallel to that at 23°C can be drawn through the experimental points at 120°C and 140°C indicate that the fatigue life at these temperatures shows the same dependence on strains as that at 23°C up to 400% strain at 120°C and 300% strain at 140°C. A similar parallel line can also be drawn through the fatigue results at 100°C up to 500% strain. For amorphous rubbers, the dependence of fatigue life on strain is very much stronger than that of strain-crystallizing rubber such as natural rubber (13). This strongly suggests that

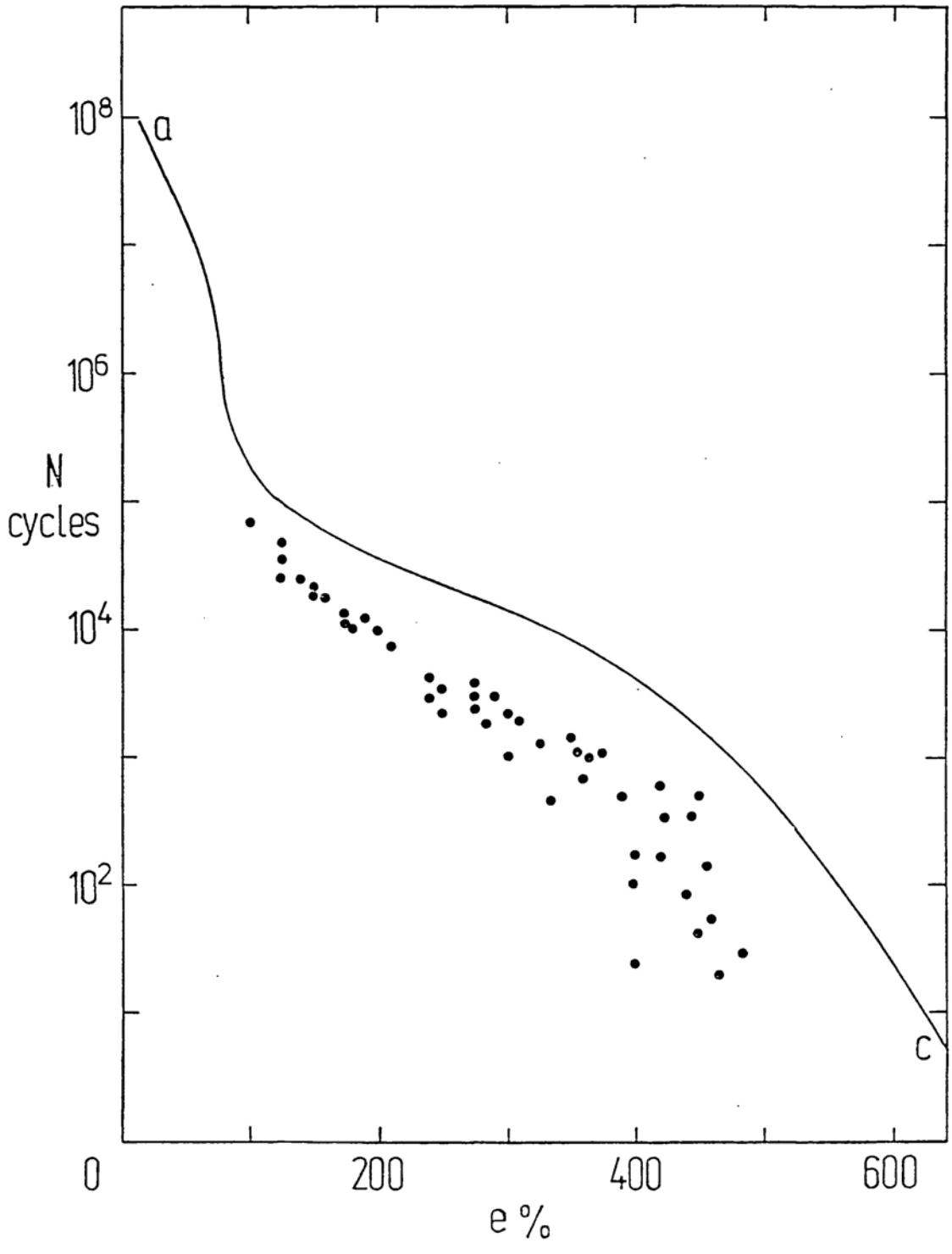


Fig. 6.10 Dependence of fatigue life N on strain e of vulcanizate A at 120°C. Experimental points; curve ac is that at 23°C (Fig. 6.2).

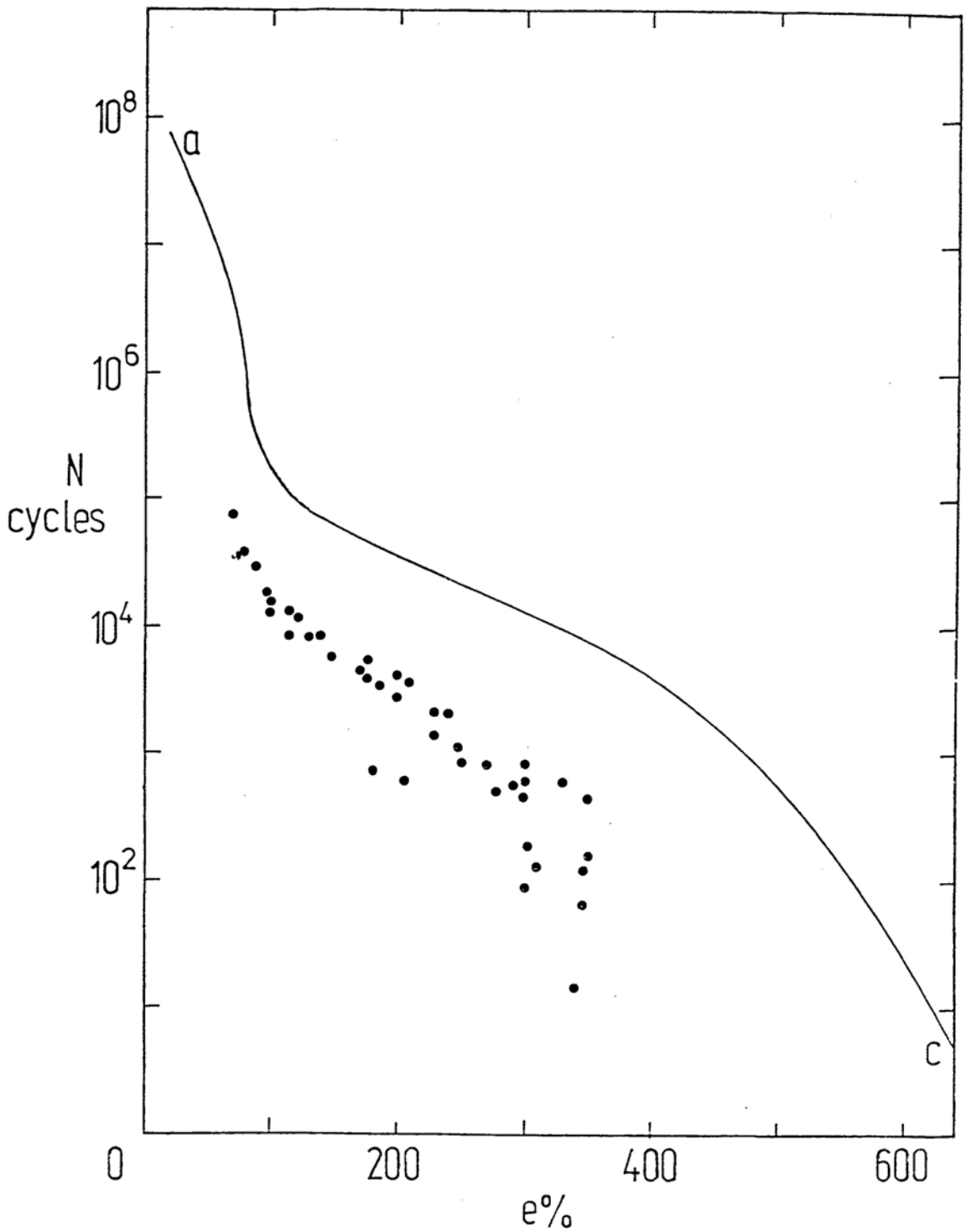


Fig. 6.11 Dependence of fatigue life N on strain e of vulcanizate A at 140°C. Experimental points; curve ac is that at 23°C (Fig. 6.2).

oxidation is still the major cause in the reduction of fatigue life at these temperatures. The fatigue life at 120°C and 140°C is reduced by a factor of about 5 and 13 respectively compared to that at 23°C.

At high strains, about 400% at 120°C and 300% at 140°C, there is a sharp reduction in the fatigue life. Since these are very close to the breaking strains at these temperatures, the reduction could be attributed to the near-amorphous nature of the rubber as discussed in Section 6.4.

6.9 Summary

From the relaxing crack growth behaviour of the natural rubber vulcanizate A, it has been shown that, as with other vulcanizates, it is possible to predict the fatigue life of dumbbell test pieces under the same condition up to 225% strain.

Raising the temperature of 70°C has negligible effect on the fatigue and crack growth behaviour of vulcanizate A which is protected with 2 parts per hundred by weight of the antioxidant Nonox ZA.

At 100°C, however, the fatigue and crack growth resistance are weaker by about a factor of two compared to that at 23°C. The reduction in the resistance is attributed mainly to oxidative effects since the fatigue resistance at this temperature is similar to that of vulcanizate A without the antioxidant at 23°C.

At 120° and 140°C, the fatigue resistance is reduced by about factors of 5 and 13 respectively when compared to 23°C. The dependence of the fatigue life on strains at these temperatures is similar to that at 23°C, and is not as marked as that of amorphous rubbers. This strongly suggests that

oxidation as opposed to lessening of strain-induced crystallization is the main cause of the reduction of relaxing fatigue resistance at these temperatures.

The tests at elevated temperatures show a limitation of the time for which the thin test piece can be used without significant change in the material properties. However, in practice, the thickness of rubber springs is many times that of the 1 mm thick test pieces used here. The behaviour of thin test pieces may not be representative of that of bulky components. It thus seems worthwhile to investigate the ageing behaviour of thick rubber blocks at elevated temperatures.

SECTION 7 HIGH TEMPERATURE AGEING OF RUBBER BLOCKS

7.1 Introduction

Various types of rubber engineering components operate intermittently, and occasionally continuously, at temperatures substantially higher than normal ambient temperatures. For such components it is necessary to have some method of assessing the probable lifetimes of different rubber vulcanizates at elevated temperatures.

As mentioned in Section 6 , : oxidative degradation is considered to be the most serious problem in the use of rubber at high temperatures, and consequently the oxidation of rubber has been investigated extensively (45). A small amount of oxygen (ca 1%) absorbed by a natural or synthetic rubber vulcanizate is found to have a deleterious effect on its physical properties (41) and much research has been concerned with the mechanisms of the basic oxidation processes, ie the interaction between elemental oxygen and rubbers and/or other organic materials. The understanding of these chemical processes has been derived largely from work on model systems and, generally, on thin sheets of vulcanizate.

From an engineering point of view the chemistry of oxidation has not yet answered the question of how long a bulky rubber component will last at an elevated temperature especially when the rubber is compounded with various vulcanizing agents, fillers and protective agents. Answers or at least predictions must therefore be based on service performance or experimental investigation.

The engineer is concerned with stiffness and strength. In conventional ageing tests, values for these are obtained as the stress at, for example, 300% strain and the stress and elongation at

break of thin rings or dumbbells after oven-ageing for a specific time at a specific temperature. The ageing behaviour of thin rubber test pieces is not necessarily the same as that of thick blocks or indeed of the surface of thick blocks. This is evident from a comparison of the two test samples (one thin, one thick) illustrated in Fig. 7.1, both having been subjected to the same ageing conditions. Elliott (46) has found that dumbbell test pieces prepared from thick blocks of rubber and then aged sometimes have tensile strengths and elongations at break substantially lower than expected. He attributes this to the method of preparing the dumbbells, which is also a time-consuming process. A novel technique was adopted by Knight and Lim (47) for their studies of the ageing of thick blocks. They used ten 2.5 mm thick sheets clamped together and were thus able to obtain tensile strength as a function of depth from the exposed surfaces. Unfortunately, this method cannot be applied to the study of rubber components after varying periods in service.

The conventional tensile test, on dumbbells or rings, is not the only method of obtaining stiffness and strength after ageing, and is not a particularly convenient one for use with thick blocks or components. One type of test piece which does not require such elaborate preparation is that on which hardness tests, especially micro-hardness tests, can easily be carried out. Hardness values are based on the deflections which result when a specially-shaped indentor is pressed into rubber under load (48). There is, however, no restriction on the shape of indentor which can be used on a load-indentation test, from which the material stiffness constant Young's modulus can be found. Moreover, if the indentor is long enough then

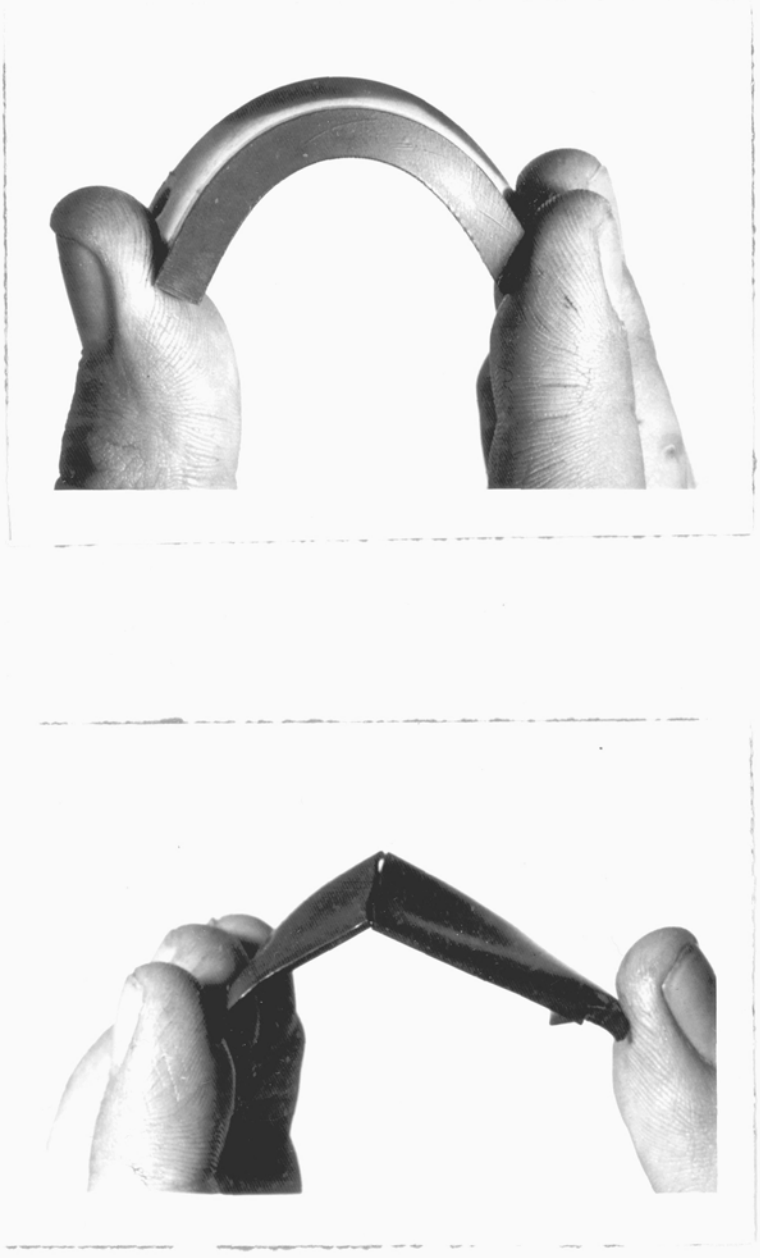


Fig. 7.1 Two pieces of rubber which have been aged for the same time: the thicker piece is still flexible, even at the surface, but the thinner one has become hard and brittle

indentation can be continued until the rubber surface is punctured, thus giving a material strength parameter.

Livingston and Hildenbrand (49) developed the puncture test for routine purposes. They used lubricated cylindrical indentors with flat ends made from music wire 0.36 mm in diameter, and measured the force and indentation at puncture. The indentation reading, raised to the power 3/2, was found to be proportional to Young's modulus. Rounding the edges of the flat ends of the indentor appeared to have no significant effect. Lubrication of the indentor has been found to give better reproducibility (50) of puncture strengths and also reduces the effect of finite block thickness. The puncture strength becomes substantially independent of block thickness when the latter is about twelve times the indentor diameter (51). Livingston and Hildenbrand (49) compared puncture test data with the conventional tensile test results of fourteen different black-filled vulcanizates of SBR at two cure levels. Dozortsev and Nechiporenko (52) also developed a device for determining the mechanical properties of rubber by the puncture method. This device, in which the 0.4 mm diameter cylindrical indentor has a hemispherical end, has been used to study puncture strength (53). Relations have been found between puncture strength and tear strength (54) and sliding wear resistance (55). Using a portable instrument, puncture strengths have also been found to correlate well with the mileage of tyres in iron ore quarries (56).

This section investigates the ageing behaviour of the surface and bulk of small blocks of rubber using a puncture test from which the resistance to indentation and puncture provides quantitative stiffness and strength values.

7.2 Experimental method

Vulcanizate A, pale in colour, used in the crack growth tests at elevated temperatures (Section 6) was used throughout this investigation. Its composition by weight was given in Section 4.2. The test blocks and some 1 mm thick sheets of this rubber were direct-compression moulded for 90 minutes at 140°C. Most of the blocks were hardness pellets, 25 mm diameter by 8 mm thick and made in a 36-cavity mould, but some larger test blocks, 50 mm square by 25 mm thick, were also used.

Ageing was carried out, for various times, in air-circulating ovens set at selected temperatures up to 200°C. One block was used for each combination of ageing time and temperature. After removal from the ovens the blocks were allowed to cool for at least 24 hours at 23°C before being tested at this temperature.

The blocks were cut open with either a razor blade or scissors and several, usually five, puncture tests carried out on both the moulded ('surface') and cut ('bulk') faces.

The puncture tests were carried out on an Instron. A rigidly-located cylindrical indentor was forced into the test block at 5 mm/min and the compressive force recorded graphically as a function of time (and hence of amount of indentation). To minimize any effects of finite thickness an unaged backing block, 25 mm thick by about 100 mm square was placed under the test blocks for all the tests. The indentors were 0.5 mm diameter high speed drills with the plain cylindrical ends ground flat.

Each of the Instron records relating force F and amount of indentation x has a well-defined maximum corresponding to the puncture strength P at which the indentor penetrates the surface

(Fig. 7.2). The initial part of the curve is linear and has been used to determine Young's modulus E from (57)

$$F = Ed\,x\,/(1-\nu^2) \qquad (7.1)$$

where d is the indentor diameter and ν is Poisson's ratio. As values of ν for rubber are generally in the range 0.499 to 0.5 eq. (7.1) becomes (58)

$$E = 3F/(4xd) \qquad (7.2)$$

Although lubrication is reported to improve reproducibility of puncture strengths (50) none was used here as it could have affected the Young's moduli determined from eq. (7.2). Reproducibility of both E and P was generally within $\pm$ 5%. Average values are shown in the results. As a check on indentor performance, indentation tests were carried out at regular intervals on a large block of unaged rubber.

7.3 Variations of stiffness and strength with time of ageing

These tests were carried out on hardness pellets aged in air at 70°C, 100°C, 125°C and 150°C. The variations of Young's modulus E and puncture strength P of the surface and bulk with time of ageing are shown in Figs. 7.3-7.8. The E and P scales are linear; those shown in Figs. 7.3 and 7.6 have depressed zeros. The time of ageing scale is logarithmic.

For 70°C ageing the change in properties is very small over a period of almost 11 months. The surface values after 11 months ageing are inconsistent with the rest of the data. Unfortunately the test block removed after 11 months ageing was the last of the batch.

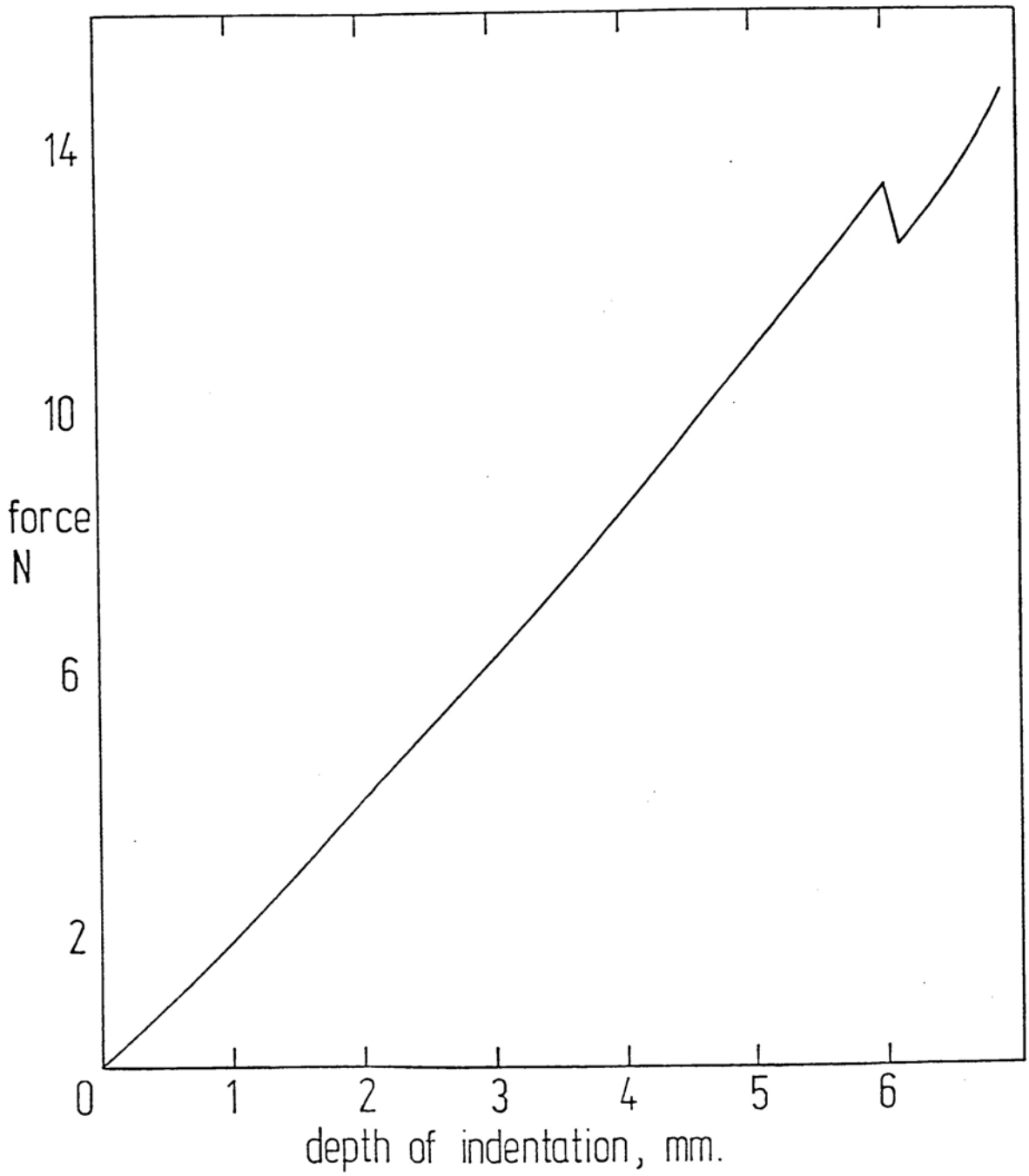


Fig. 7.2 A typical curve showing the relationship between the indentation force and the depth of indentation.

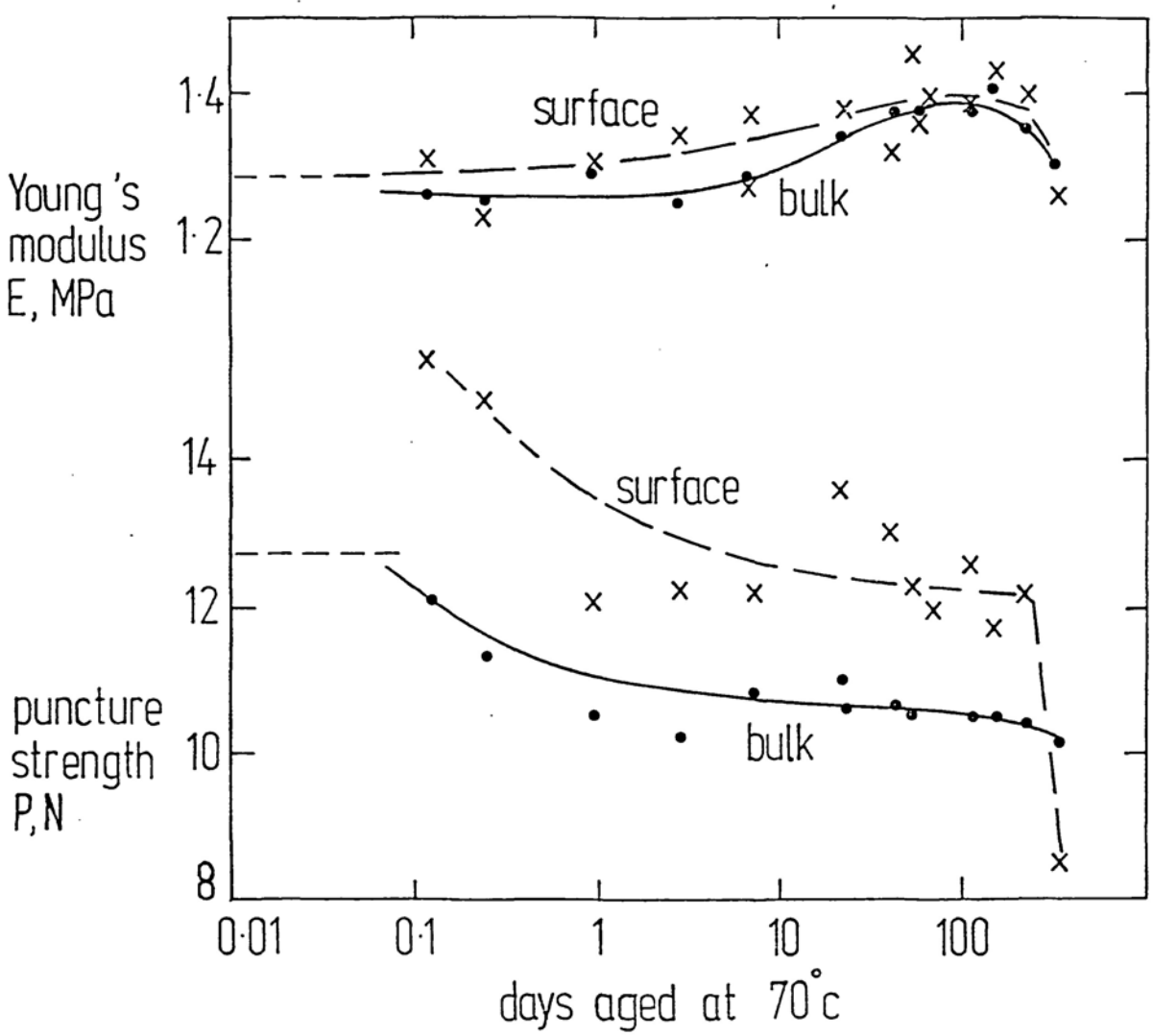


Fig. 7.3 Variation of Young's modulus E and puncture strength P (with ½ mm indentor) of the surface (X) and bulk (•) of rubber disks 25 mm diameter by 8 mm thick with time of ageing in air ovens at 70°C. Unaged values are indicated by the horizontal broken lines at the left.

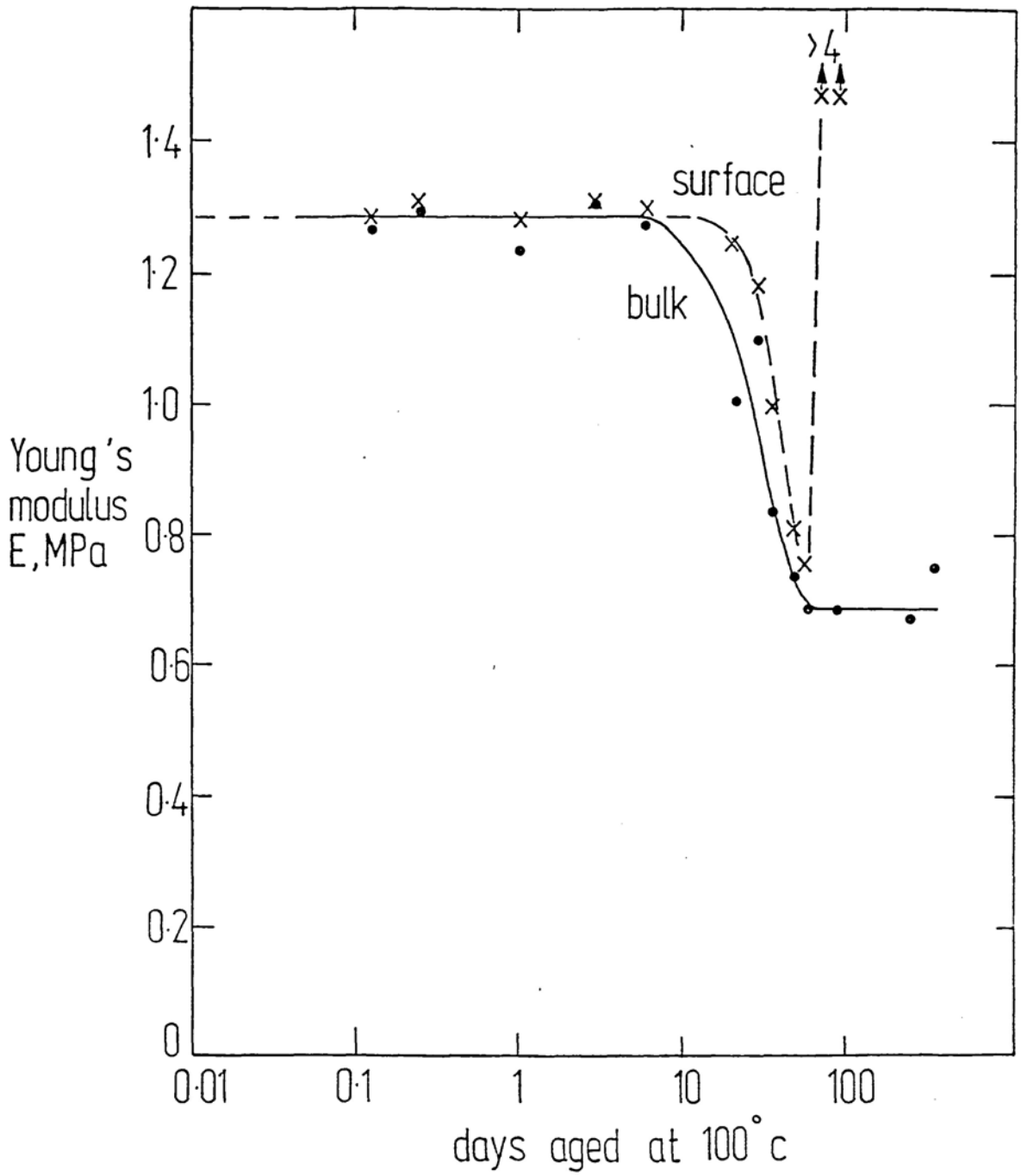


Fig. 7.4 Details as Fig. 7.3 but with ageing at 100°C.

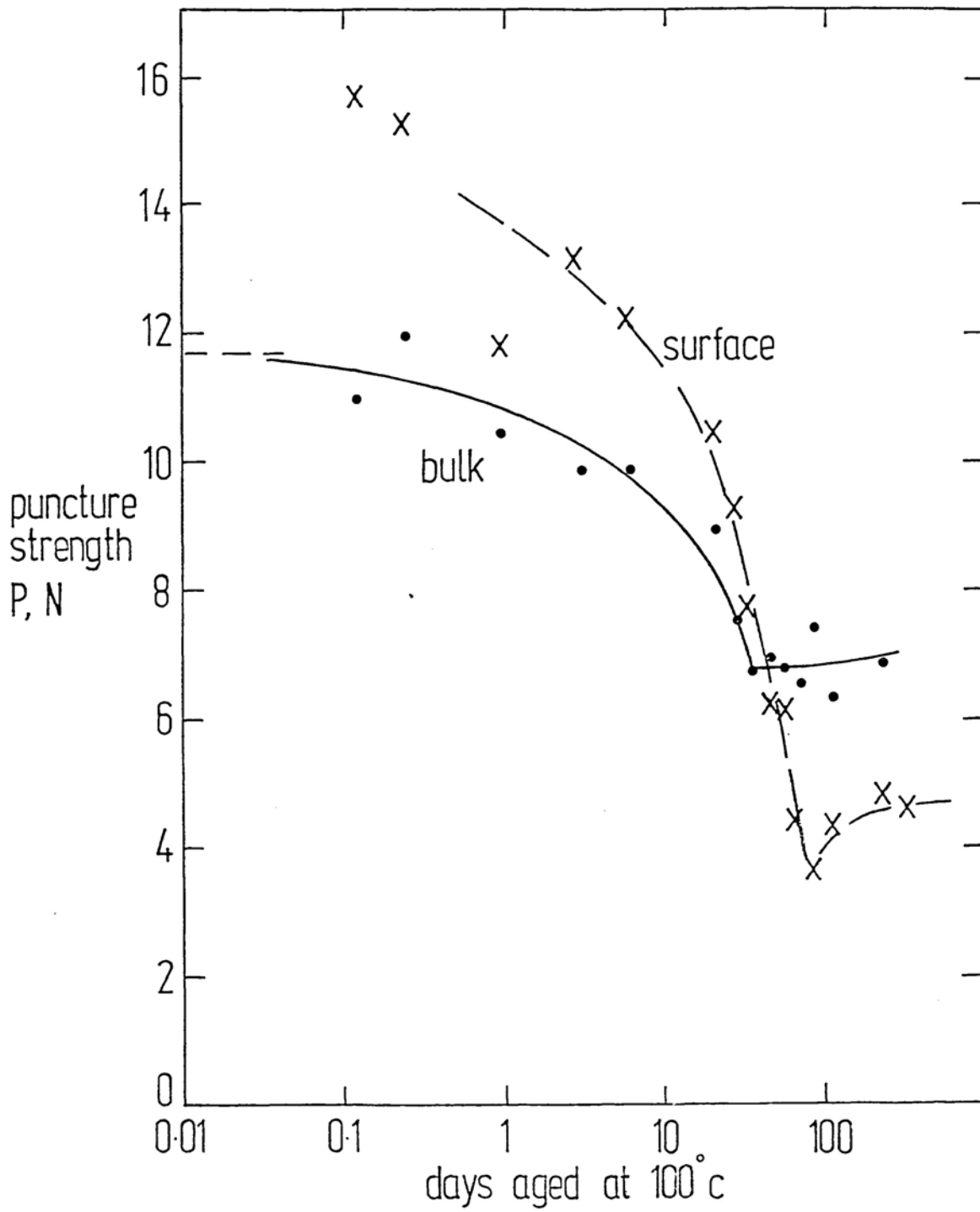


Fig. 7.5 Details as Fig. 7.3 but with ageing at 100°C.

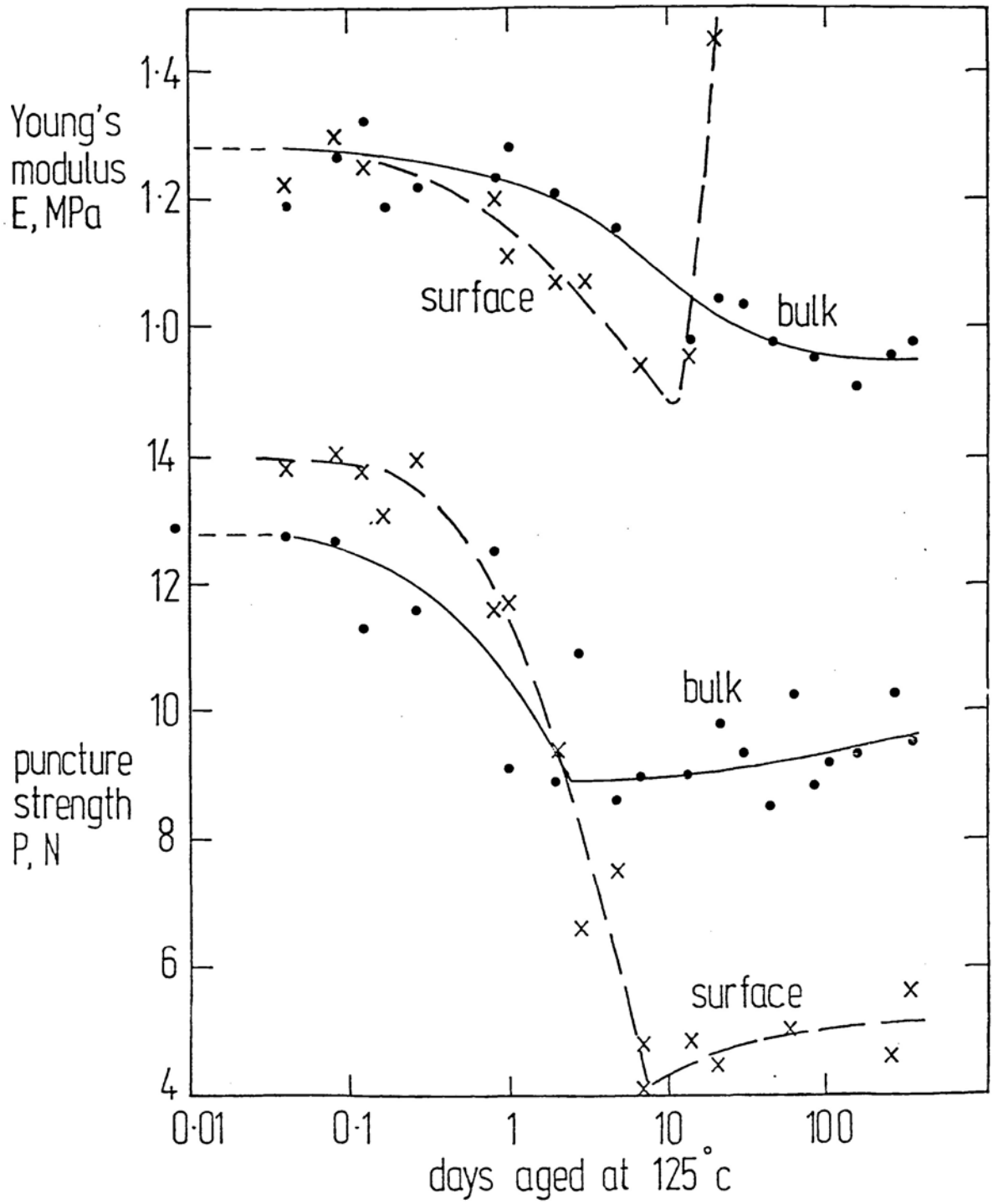


Fig. 7.6 Details as Fig. 7.3 but with ageing at 125°C.

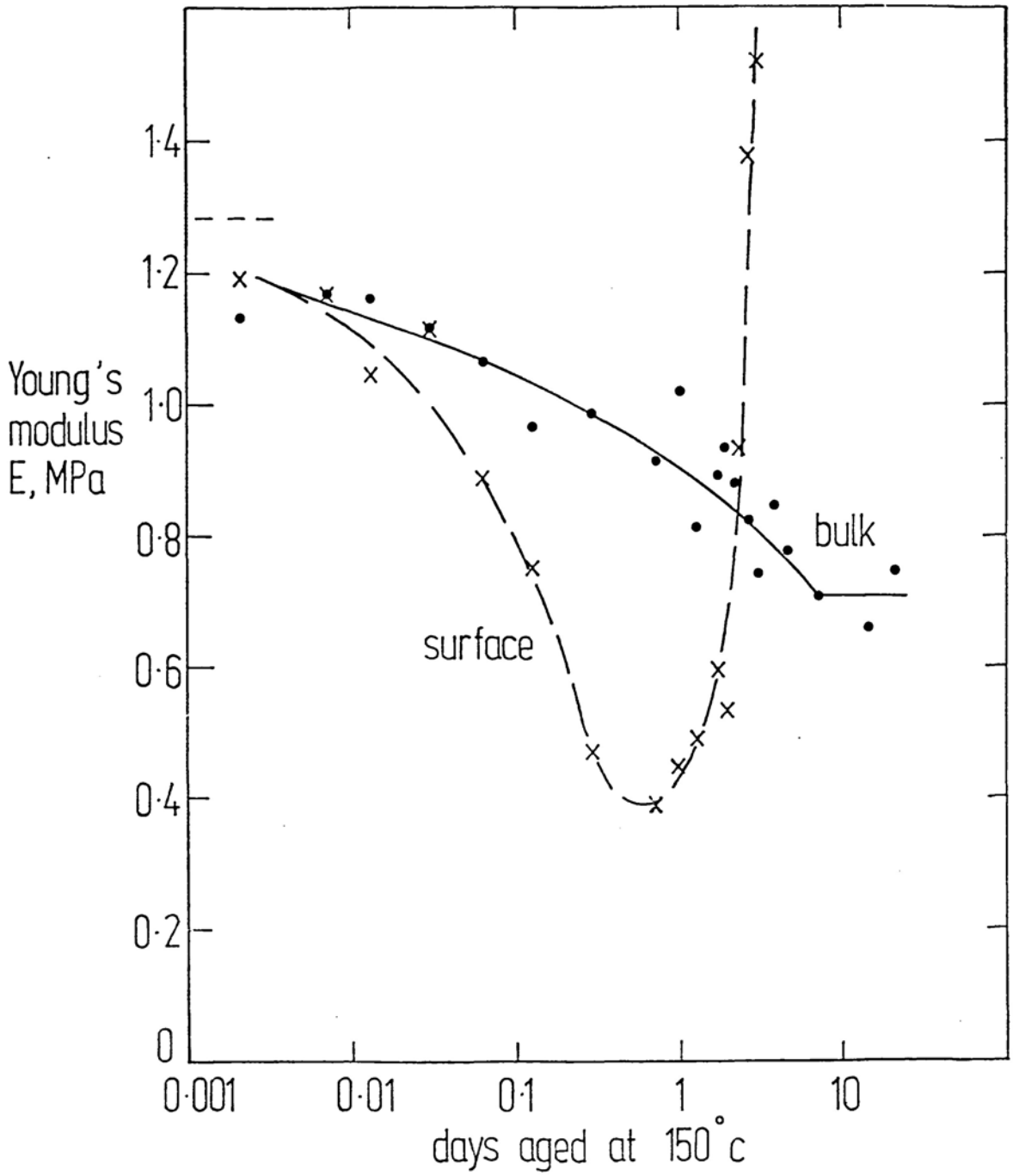


Fig. 7.7 Details as Fig. 7.3 but with ageing at 150°C.

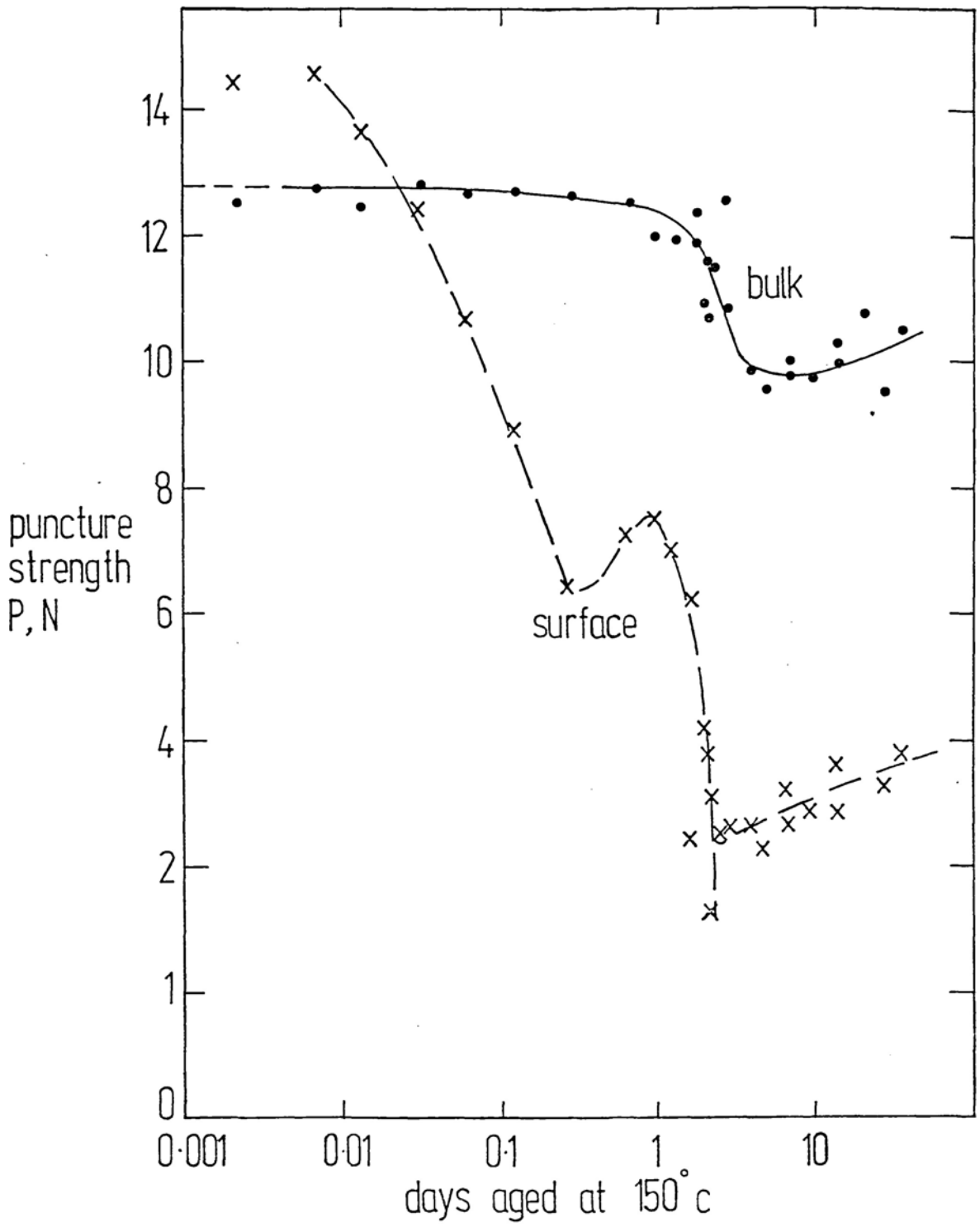


Fig. 7.8 Details as Fig. 7.3 but with ageing at 150°C. At this temperature there was no abrupt drop in force when the indentor penetrated the surface for P values below about 6N, until the hard skin formed. To determine P the indentor was loaded and unloaded with gradually increasing maximum values, until a surface puncture could be seen.

For 100°C ageing Young's moduli of both surface and bulk start to fall after about two weeks. Minimum values of about half the original values, are reached after 8 weeks when the surface E increases rapidly (to over 4 MPa) while the bulk E remains at its minimum value. Puncture strengths also decrease markedly between 2 weeks and 8 weeks after which the bulk P levels off while the surface P decreases for several more weeks before reaching a minimum, then increases slightly before levelling off.

The characteristics for 150°C ageing are similar to those for 100°C except that the times are very much shorter and the bulk changes (ie reversion) occur much less rapidly than those of the exposed surface. The results for 125°C ageing are intermediate. A few results obtained for 175°C and 200°C ageing (not illustrated) appear to be similar to the 150°C ageing results except for a reduction in the time scales.

Considering that on each of Figs. 7.3-7.8 a different block was used for each ageing time the scatter is quite small, which means that ageing behaviour is reasonably well defined by the lines drawn through the experimental points. The lines on these figures have been transferred to Figs. 7.9 and 7.10 where the effect of temperature on the surface and bulk values respectively can more readily be seen. These results appear well-behaved with respect to temperature, apart from the curves in Fig. 7.10 for the bulk properties at 100°C for which an explanation is given in Section 7.5.

7.4 Brittle skin formation

At the minimum values of E and P (in Fig. 7.9) the surface of the rubber is soft and tacky. The rapid increase in Young's modulus, at a time of ageing t^*, corresponds to the formation of a very thin

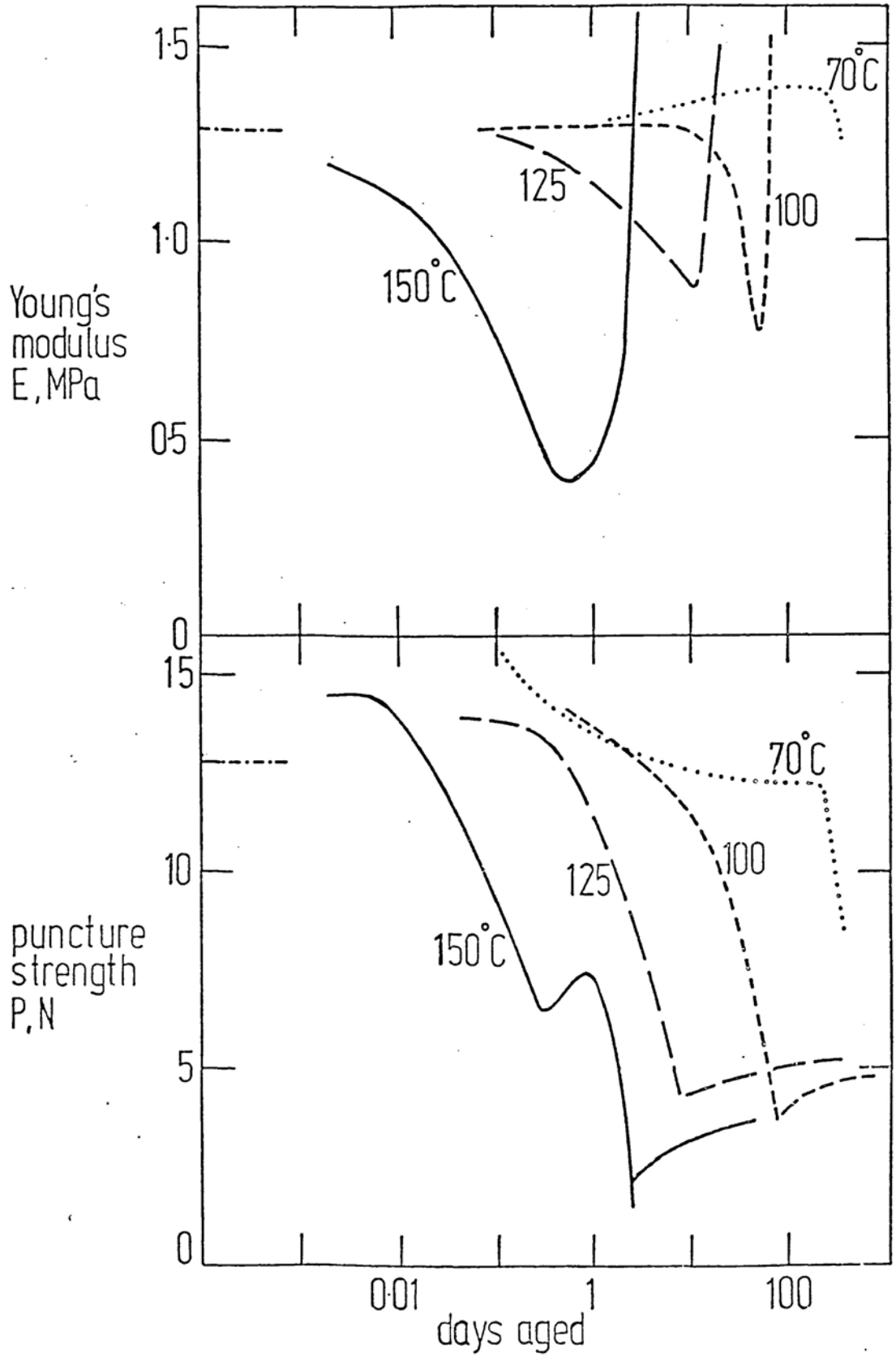


Fig. 7.9 Curves from Figs. 7.3-7.8 representing surface values of E and P.

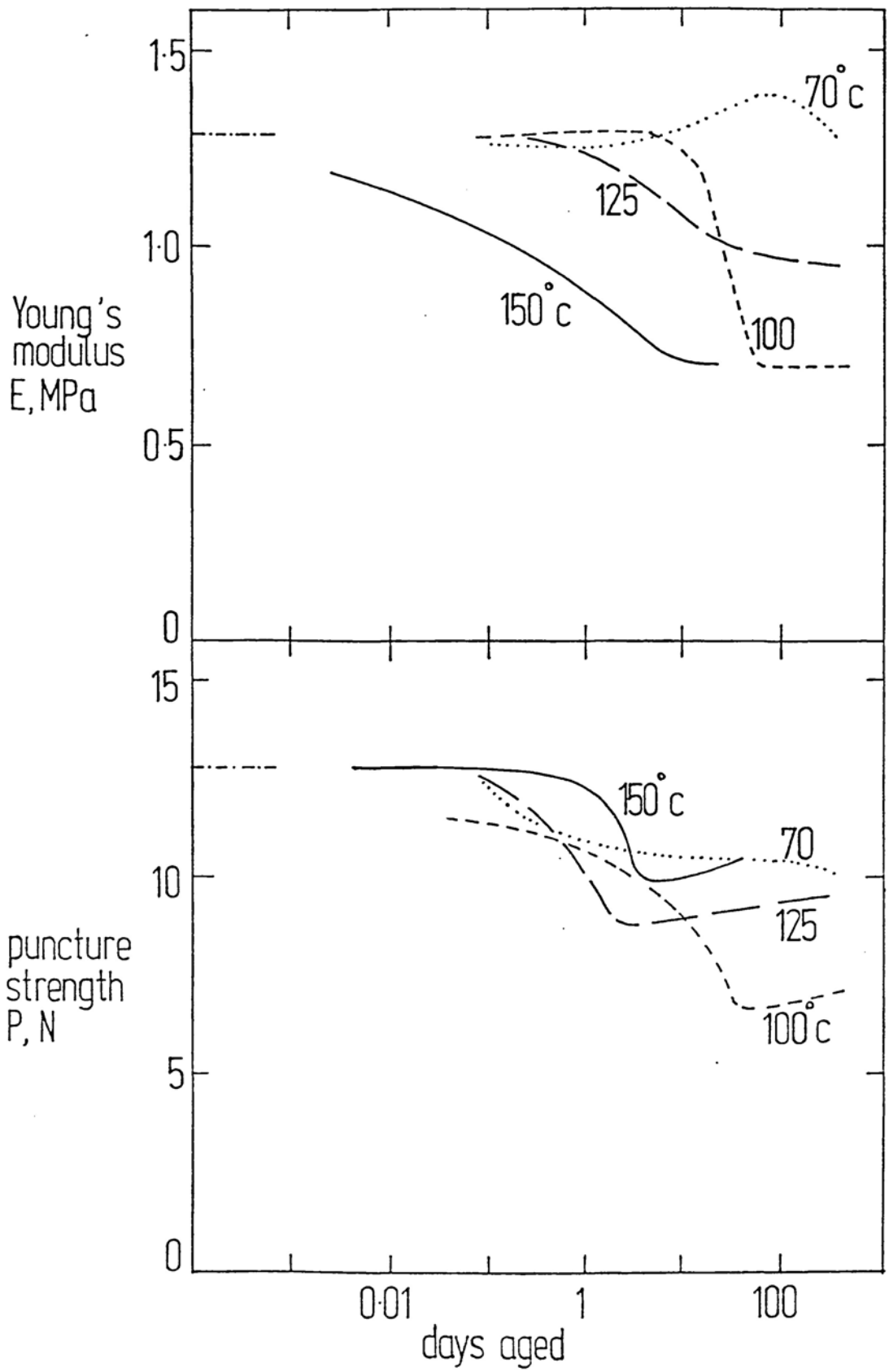


Fig. 7.10 Curves from Figs. 7.3-7.8 representing bulk values of E and P.

hard skin (59) which is smooth and brittle. The thickness of this skin is about 0.1 mm. As it rests on a soft substrate it is unlikely that the Young's moduli, derived from eq. (7.2) are valid, but there appears to be no necessity for these values of E to be known accurately.

The change in nature of the surface layer is probably due to a chemical reaction for which $1/t^*$ is proportional to the reaction rate k. Many chemical reactions obey the Arrhenius equation

$$\ln k = -E_a/RT + \text{constant} \qquad (7.3)$$

from which

$$\log_{10} t^* = \frac{1}{T} \frac{E_a}{2.303R} + \text{constant} \qquad (7.4)$$

where E_a is the activation energy of the reaction, R the gas constant (1.987 cal $mole^{-1}$ deg^{-1}) and T the absolute temperature. The upper points in Fig. 7.11 are an Arrhenius plot between t^* and temperature in the form of eq. (7.4). At 70°C a lower limit is given as no brittle skin formed in 11 months. The points are satisfied by the straight line, from the slope of which and eq. (7.4) E_a is found to be 20.4 kcal/mole. In the next section this activation energy is also found for the rates of oxygen uptake and oxidative degradation of the vulcanizate used here.

According to van Amerongen (59) the brittle skin of oxidized rubber is impervious to oxygen.

7.5 Oxidation of outer layer

A gum vulcanizate was used for this investigation so that colour changes could be observed. When an aged block was cut open the outer layer of rubber was found to be darker than the rubber in the bulk, the discoloration being attributed to oxidation. Consistent with this is the loss of stiffness and strength of the surface prior to the

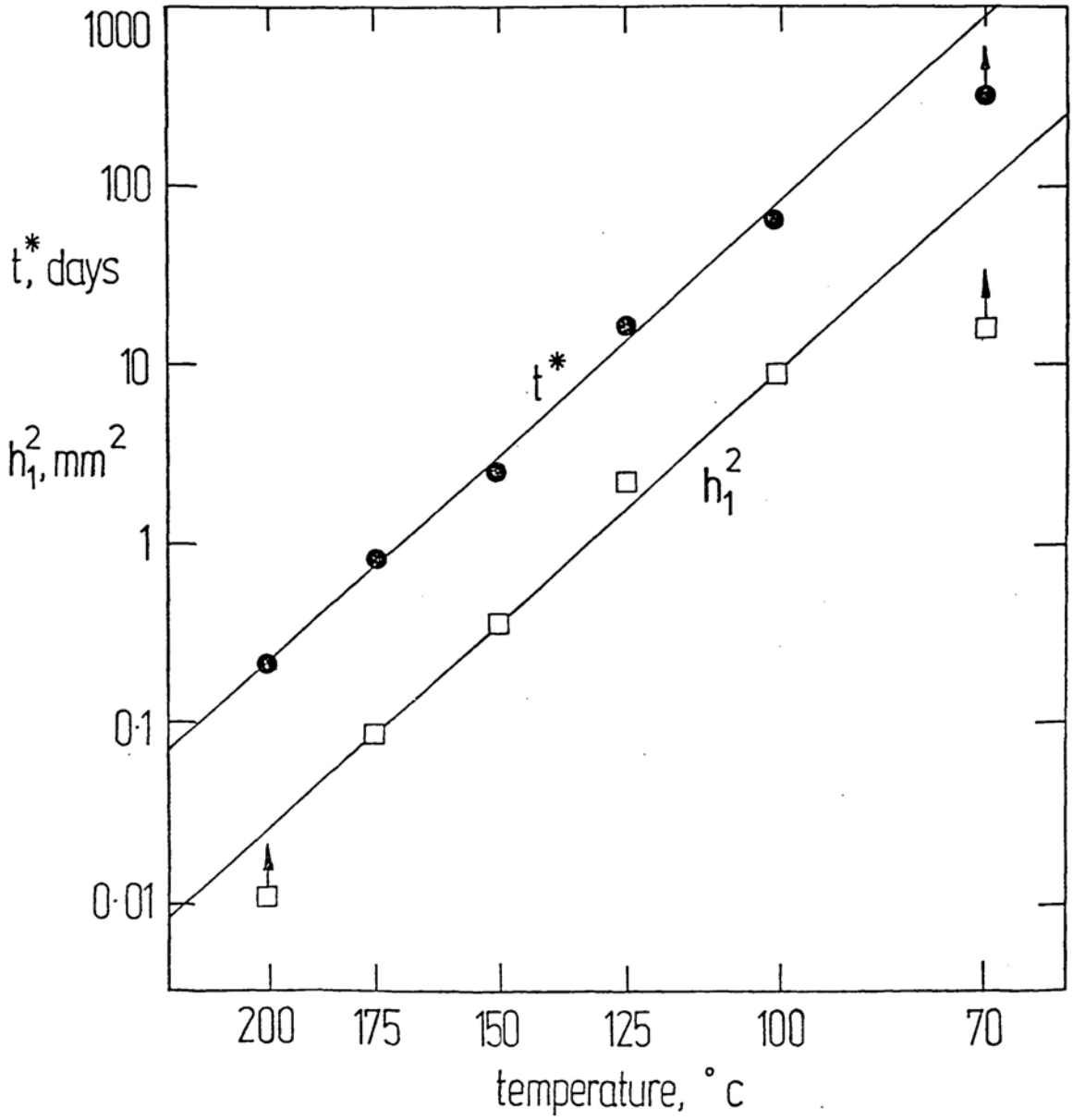


Fig. 7.11 Arrhenius plots of the time for the brittle skin to form (t^*) and the square of the depth of the discoloured surface layer after one day (h_1^2) against temperature. The abscissa covers the reciprocal of the absolute temperature linearly from 0.002 to 0.003.

formation of the brittle skin, probably due to scission of the molecular chains by oxygen. Above 100°C there was negligible change in the colour of the bulk from its colour immediately after vulcanization suggesting that no oxidation had occurred there. Preliminary examination by Knight using radio-chemical analysis showed that the discoloured outer layers of our 50 x 50 x 25 mm blocks aged at 150°C were oxidized and that there was no oxidation in the bulk. Subsequent work by Knight and Lim on black-filled vulcanizates of natural rubber confirmed these findings (47).

Initially the depth h of the discoloured layer increased rapidly with ageing time but then slowed down and appeared to be approaching a limiting depth. Values of h after one day (h_1) and at long times (h_{max}) are given in Table 7.1 for both sizes of test block.

The depth h is the distance that oxygen is able to penetrate into the rubber in a time t. The further it penetrates in a given time the slower the reaction rate. An inverse measure of this rate is the time t to reach a particular depth h. Assuming oxygen penetration to be a diffusion-controlled mechanism with h proportional to the square root of t, the inverse of the reaction rate should thus be proportional to the square of the depth at a given time (59). Taking this time as one day, the penetration depth is h_1. On the Arrhenius plot, Fig. 7.11, h_1^2 is found to have a slope identical to that for t^*. These are thus two measurements from which the rate of degradation of the surface can be determined as a function of temperature. If t^* is the time in days for the brittle skin to form and h_1 is the thickness in mm of the discoloured layer after 1 day, then

$$t^* = 8.7\ h_1^2 \qquad (7.5)$$

Table 7.1 Depth of oxidized layer after 1 day (h_1) and at longer times of ageing (h_{max})

Ageing temperature °C	50	70	100	125	150	175
h_1 of 8 mm-thick rubber, mm	-	>4	3.0	1.5	0.6	0.3
h_1 of 25 mm-thick rubber, mm	-	(a)	2.8	1.4	0.6-0.8	0.3 (b)
h_{max} of 8 mm-thick rubber, mm	-	>4	>4	2.2-2.3	0.5-0.8	-
h_{max} of 25 mm-thick rubber, mm	>12½	10.6	4.9-5.0	2.0-2.3	-	-

(a) Not possible to distinguish

(b) At 175°C, h_1 for the 1 mm-thick sheet is also 0.3 mm

Since a 1% weight uptake of oxygen is considered deleterious, as mentioned in the Introduction, absorption of oxygen by the vulcanizate used in the present work has been measured on automatic apparatus developed primarily for this purpose (60). The times for 1% absorption by weight at 100°C, 125°C and 150°C were 113, 20.5 and 4.6 hours respectively. Substituting t^* by these values in eq. (7.4) gives an activation energy E_a of 20.1 kcal/mole, in excellent agreement with the 20.4 kcal/mole found from t^* and h_1 measurements on the blocks.

Diffusion theory seems to apply to oxygen absorption at least for times up to 1 day, as it predicted the form of eq. (7.5), so in theory it should follow that

$$\frac{h_1^2}{h^{*2}} = \frac{t_1}{t^*} \qquad (7.6)$$

where t_1 is one day and h^* the depth of the oxidized discoloured layer at the time t^* when the hard skin forms. This cannot hold in practice for t^* less than 1 day (ie for $t^* < t_1$) because the hard skin which forms at t^* prevents the ingress of oxygen.

At 200°C the lower limit value for h_1 plotted on Fig.7.11 is the measured depth 0.1 mm, and this must also be h^*. If this value of h^* is used in eq. (7.6), where t^* is about 6 hours, then a theoretical value is obtained for h_1 of 0.2 mm, which compares reasonably well with 0.17 mm obtained from eq. (7.5) and would, therefore, have fallen on the lower line of Fig. 7.11.

By combining eqs. (7.5) and (7.6) h^* is found to be proportional to t^* but the indications are that the diffusion relation, h proportional to the square root of time t, does not hold beyond about a day as h values at long times (h_{max}) are not very dissimilar to h_1 (Table 7.1). Eq. (7.5) may therefore not apply for relatively large h_1 such as occur below 100°C.

At 200°C the discoloured layer appears to be all hard skin, which has the same thickness of about 0.1 mm at all temperatures from 100°C to 200°C. The hard skin is black; the colour of the discoloured layer becomes increasingly lighter as the temperature is reduced below 200°C, and after one day at 70°C its depth cannot be distinguished in the 25 mm thick blocks although it appears to extend through the 8 mm thick blocks. On Fig. 7.11 h_1 is therefore plotted as a lower limit of 4 mm at 70°C.

The colour deepens with time; at 50°C there is obvious discoloration fully through the 25 mm blocks at long times. This applies to the 8 mm blocks at 100°C, but after 1 day h_1 (3 mm) was still noticeably less than the half thickness. The results in Fig. 7.10 for the bulk rubber aged at 100°C show a much greater drop than those for 125°C and 150°C. The sudden drop probably coincides with the penetration of the degraded layer to the centre of the hardness pellet. The limiting depth h_{max} is about 5 mm (Table 7.1), and a 25 mm thick block aged at 100°C for 8½ months shows no oxidative discolouration and no such loss of properties at its centre. Consistent with the above explanation for the pellets at 100°C is the much more marked similarity between surface and bulk values of P and E at 100°C (Figs. 7.4 and 7.5) than at higher temperatures (Figs. 7.6-7.8). The 70°C bulk results (Fig. 7.3) are obviously for oxidized rubber also.

7.6 Anaerobic ageing during vulcanization

For ageing carried out in air at 150°C on a black filled natural rubber vulcanizate Knight and Lim (47) found that the bulk of 25 mm-thick blocks, plied up from 2.5 mm-thick sheets, showed only those physical changes which are consistent with anaerobic ageing. As vulcanization

is also an anaerobic process (surface discoloration only occurring after exposure to air) the changes which occur during vulcanization should be similar to those which occur in the bulk of air-aged blocks. Table 7.2 gives some properties of hardness pellets and 1 mm-thick sheets of Vulcanizate A vulcanized at 150°C for up to 7 hours and for one week. Data for vulcanization at 140°C have already been given in Table 5.3. The broad picture is one of falling stiffness and strength with increasing time of vulcanization.

Press-curing in moulds would appear to be a convenient method of anaerobically ageing rubber but, for two reasons, may be restricted to times of about one week. The first is that the majority of the test sheets of Vulcanizate A which were vulcanized for one week at 150°C had a hard skin on one side, indicating the eventual ingress of oxygen. The second is the considerable time for which the press would need to be occupied.

7.7 Anaerobic ageing of bulk rubber

Anaerobic ageing was carried out in evacuated tubes, for periods of up to 28 days at 125°C and 150°C. Each tube contained hardness pellets from which the puncture strengths P and Young's moduli E of their surface and bulk were obtained and 1 mm-thick sheet from which tensile strength and tear strength were obtained, Tables 7.3 and 7.4. Also tabulated are P and E values for the air-aged pellets. The latter were re-tested with the same indentor used for testing the vacuum-aged pellets (and at the same time) to make comparisons more reliable.

There is, as expected, no significant difference in the surface and bulk properties of the vacuum-aged blocks. However, the results for the vulcanizate vacuum-aged at 150°C show a continuing loss of

Table 7.2 Effect of vulcanization time at 150°C

Time hours	Tensile strength MPa	Elongation at break %	Tear strength kN/m	Microhardness IRHD		Puncture strength N			Young's modulus MPa	
				surface	bulk	top surface	bottom surface	bulk	surface	bulk
½	16.5	693	11.0	34	32.6	12.68	13.57	11.6	1.11	1.16
1	16.1	689	8.8	32.8	33.9	12.8	14.37	11.0	1.25	1.17
2	16.1	689	10.4	32.8	32.5	13.06	12.93	11.4	1.16	1.13
3	15.1	700	9.2	32	32.1	11.87	14.1	11.33	1.04	1.09
5	14.8	704	10.8	31.7	31.4	11.37	14.2	11.37	1.04	1.11
7	12.1	693	9.3	30.8	30.9	9.63	11.0	10.4	0.99	1.08
168	-	-	5.7	28	27.7	10.27	9.33	10.57	0.84	0.88

Table 7.3 Comparison of properties of air-aged and vacuum-aged rubber pellets

Ageing temperature	Ageing time	Air aged				Vacuum aged			
		P,N		E,MPa		P,N		E,MPa	
°C	days	surface	bulk	surface	bulk	surface	bulk	surface	bulk
unaged				1.21	1.21			1.21	1.21
125	14	5.4	9.3	0.94	0.95		9.2	1.12	1.09
	21	2.9	9.4	H	1.03	8.5	9.2	1.08	1.08
	28	2.9	9.6	H	1.03	8.3	8.2	0.92	1.03
150	7	3.2	7.4	H	0.70	6.0	6.6	0.70	0.74
	14	3.8	8.5	H	0.65	5.4	5.0	0.55	0.56
	21	3.6	7.7	H	0.74	4.4	4.5	0.44	0.46
	28[a]	3.7	7.7	H		4.2	4.2	0.39	0.37

[a] 35 days for air-aged pellets

H hard skin

Table 7.4 Properties of vacuum-aged 1 mm thick rubber sheet

Ageing temperature °C	Ageing time days	Hardness IRHD	Tensile strength MPa	Elongation at break %	Tear strength kN/m
	unaged	38	8.94	601	8.3
125	14	35	6.62	613	8.6
"	21	34.5	6.17	613	7.5
"	28	31.8	6.86	641	7.7
150	7	26.7	8.62	780	6.4
"	14	21.3	2.74	722	4.3
"	21	16.4	0.80	501	2.6
"	28	14.1	0.73	494	2.3

properties well beyond the time at which changes cease to occur in the bulk of air-aged blocks.

After a few days ageing at 150°C all the crosslinks in Vulcanizate A are of the thermally-stable monosulphidic type. It seems probable, therefore, that the degradation is not main chain scission, for which temperatures closer to 200°C would be required, but scission of the monosulphidic crosslinks. Moreover, certain materials appear capable of promoting or hindering crosslink scission during anaerobic ageing at high temperatures. It follows from the above that after about 7 days at 150°C such a material must be present either in the bulk of the air-aged blocks, where it hinders this type of degradation, or in the vacuum-aged blocks, where it promotes it. From physical considerations the formation of the hard skin (impervious to oxygen and hence presumably so to materials trying to volatilize from the block) after about three days at 150°C would appear to favour the first alternative but weight losses provide strong evidence in favour of the second.

7.8 Weight losses

Despite the oxygen uptake which would have tended to increase the weight, it was most obvious at short times of ageing and the higher ageing temperatures that the thickness of the hardness pellets was reducing. Changes in weight were therefore obtained using the larger 50 x 50 x 25 mm blocks. Daily weighings for 5 days at 70°C, 100°C, 125°C and 150°C, were converted into percentage weight losses and are plotted in Fig. 7.12 against the square root of time. The straight line relationships at the three lower temperatures are consistent with a diffusion-controlled mechanism.

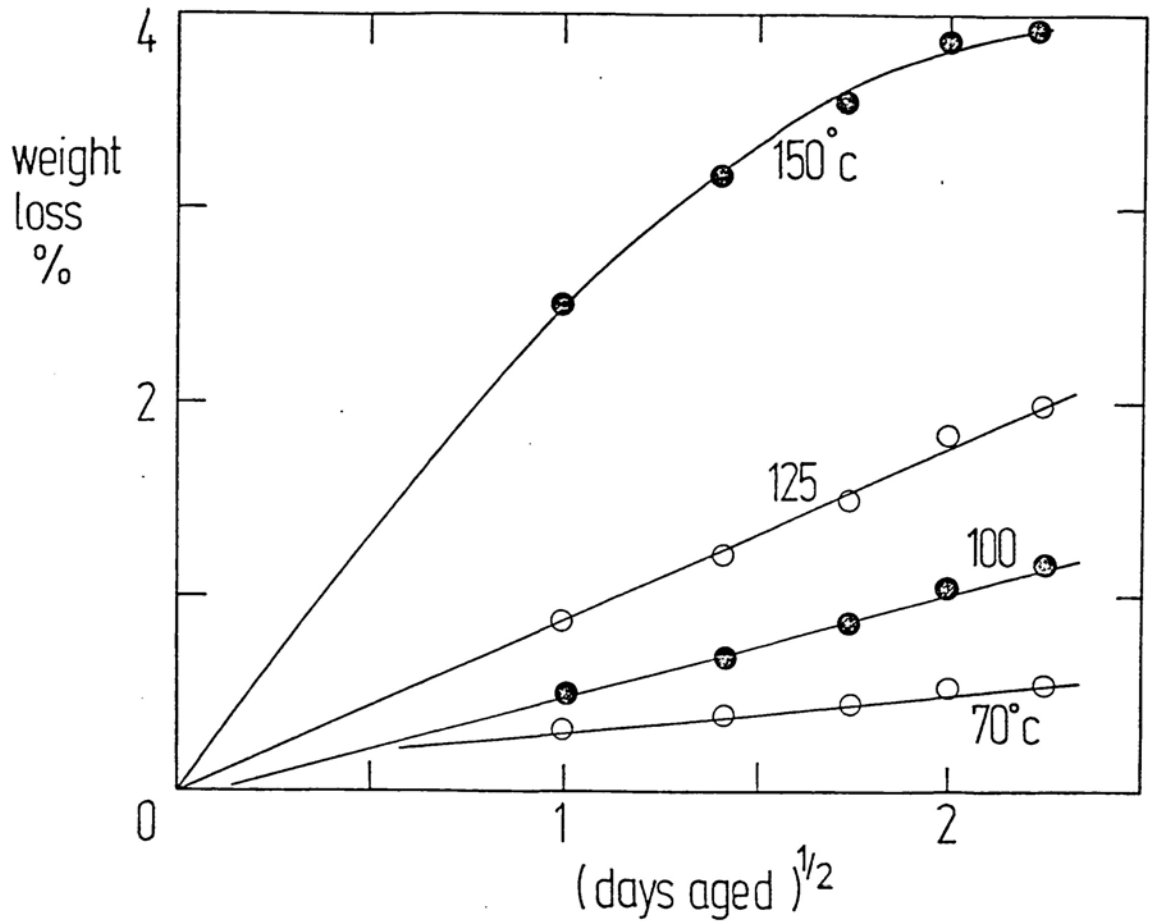


Fig. 7.12 Percentage weight losses as a function of the square root of time in air at different temperatures of 50 x 50 x 25 mm blocks.

The limiting weight loss in air at 150°C is about 4%. If a similar limit is assumed for lower temperatures then the times for limiting weight losses of 4% can be found by extrapolation of the lines on Fig. 7.12. These times give an activation energy of diffusion of about 16.5 kcal/mole. Using these data in conjunction with the t^* of Fig. 7.11, the 4% weight loss should be complete before the brittle skin forms at temperatures below about 150°C but not (by extrapolation) above it. In vacuo the weight loss at 150°C is about ½%.

Analysis to identify the materials lost from the rubber, Table 7.5, indicated that about half the 4% weight loss at 150°C was the antioxidant IPPD which is known to diffuse very rapidly through rubber (47). Some of the balance of the 4% appeared to be MBT and ZDBC.

7.9 'Black hole' oxidation

Air-ageing of the pellets continued after the hard skin had formed, one pellet still being used for each combination of ageing time and temperature. Observations on pellets aged at 150°C were as follows:

3 days	Hard skin formed
5 days	Few blisters formed at surface
4 weeks	Surface cracked
7 weeks	A few black holes formed in bulk, see Fig. 7.13.
12 weeks	More black holes formed
22 weeks	More surface cracks
35 weeks	Black holes throughout most of pellet

Table 7.5 Analysis of aged disks

A Vacuum aged at 125°C for 2 weeks

B Vacuum aged at 150°C for 2 weeks

C Air aged at 150°C for 2 weeks

D Air aged at 150°C for 5 weeks

Samples of the disks were cut into small pieces. For C and D samples were taken from the centre and just below the skin. These were extracted overnight with acetone and the evaporated extracts examined by the thin layer chromatographic (TLC) method, with the following results

A and B	Found:	MBT[a], IPPD[b], low ZDBC[c] in A, unidentified components.
C and D	Found:	trace of MBT[a] in C otherwise completely lacking in additives or their decomposition products.

Notes

(a) MBT mercaptobenzothiozol

(b) IPPD isopropyl-isopentyl paraphenylene diamine (anti-oxidant Nonox ZA)

(c) ZDBC zinc dibutyl dithiocarbamate

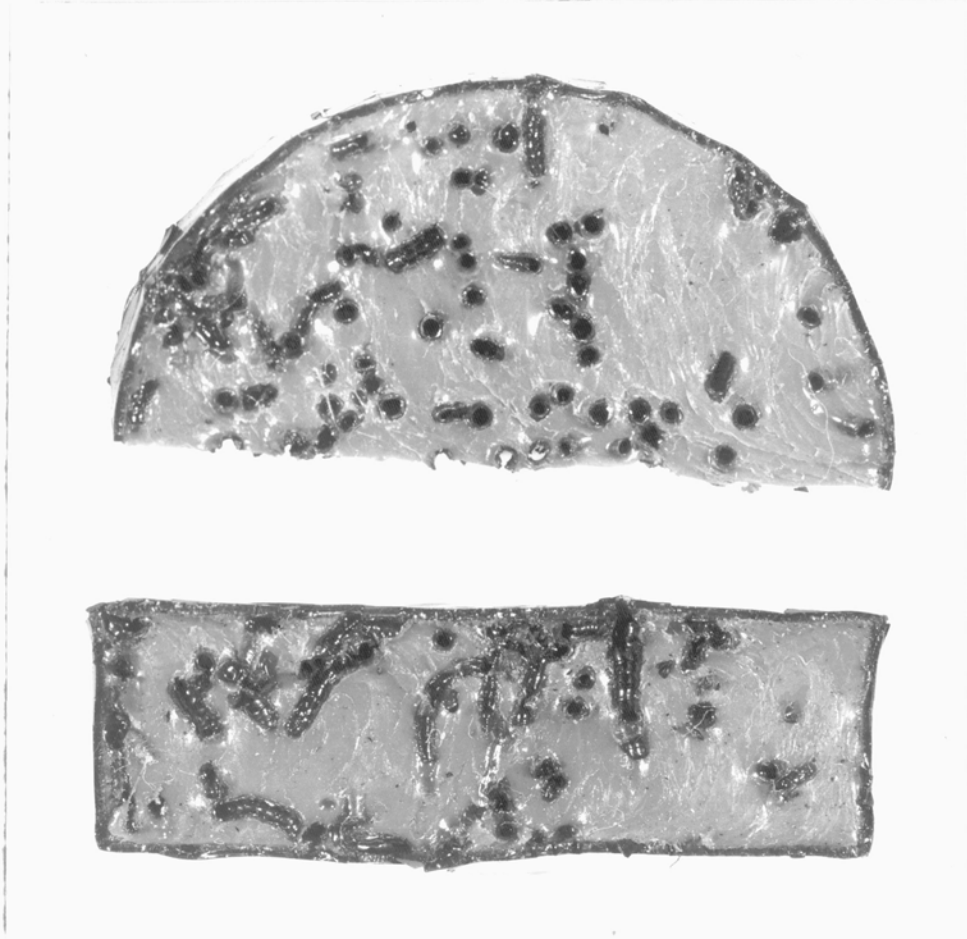


Fig. 7.13 'Black hole' oxidation. Two different sections of the same block (aged for 15 days at 175°C).

The blisters are attributed to gas-pressure build-up as the additives and their decomposition products continue to volatilize after the impervious hard skin is formed. Most of the volatilization occurs prior to hard skin formation (Fig. 7.11) but after 2 weeks there is only a trace of MBT left unvolatilized and nothing after 5 weeks (Table 7.5). The possibility that the degradation processes provide a continuing supply of gas cannot be excluded, although there are no obvious changes in the bulk properties of the rubber after about a week at 150°C (Figs. 7.7 and 7.8).

The initiation of the first cracks at 4 weeks in the weak brittle skin is attributed to the build-up of gas pressure within the block. Gases near the crack are thus released, thereby relieving pressure in those parts of the block remote from the crack. Eventually pressure builds up in the latter sufficient to cause further cracking (at 22 weeks).

The impression given by the photographs, Fig. 7.13, is that volatilizing gases form 'tunnels' on their way to the surface (lower photograph), but that these appear as separate holes when sectioned (upper photograph). It seems probable that, when cracks form, escaping gas is replaced by air and that rapid oxidation of the freshly exposed rubber takes place, producing the black holes. Eventually the rubber pellet becomes hard and crumbly with the appearance and texture of a charred piece of wood.

At 100°C and 125°C surface blisters were observed at 12 weeks and 7 weeks respectively, these being, as at 150°C, the first blocks removed from the ovens after those on which the hard skin first formed. However, surface cracking and the black hole oxidation which accompanies it have only been observed at 150°C and above.

At 200°C the hard skin forms in about 6 hours and black hole oxidation is observed after 24 hours.

Thin sheets of rubber do not exhibit black hole oxidation presumably because all volatile matter can escape before the hard skin forms.

7.10 Thickness effect

The indications are that during ageing most of the protective agent IPPD is lost before the hard skin forms, which may mean that the IPPD prevents or significantly hinders the formation of the hard skin. The thinner the rubber the less IPPD it will contain and the more rapidly will the IPPD be volatilized and lost. Thus the time t^* at which the hard skin forms has, for small thicknesses at least, been noted to increase with increasing thickness. It is possible, therefore, for a thick block to be still flexible and for a thin sheet to have become hard and brittle at the same ageing time and temperature, as illustrated in Figure 7.1. For example, at 150°C, t^* is 33 hours for 1 mm-thick sheet and 3 days for the 8 mm-thick hardness pellets.

7.11 Summary

This has been a preliminary study, from the engineer's viewpoint, of the ageing behaviour of rubber blocks. Thus far only one vulcanizate has been used, and in the unstrained state. The findings will not necessarily apply to other vulcanizates or to the strained state.

The puncture test enables the stiffness (Young's modulus E) and strength (puncture strength P) properties of rubber to be determined. Such tests have been carried out on small blocks of a natural rubber gum vulcanizate aged for varying periods of time at several elevated

temperatures. Relatively reproducible results were obtained for the properties of both the surface, where oxidation occurred, and the bulk of the blocks. The measurements appear to be quite sensitive to changes in the rubber. A major advantage of this method is that it avoids the elaborate preparation of special test pieces.

Measurements were made at various temperatures of the time t^* at which a hard brittle skin formed on the blocks, of the depth h_1 to which the surface layer became discoloured after ageing for one day, and for the time for a 1% weight uptake of oxygen in special apparatus. The activation energy is the same for all of these. When the t^* data of Fig. 7.11 are extrapolated to lower temperatures the following are predicted for the times at which the brittle skin should form:

temperature ^{o}C	20	30	40	50	60
time, years	434	131	45	16	6

Although a linear relation exists between t^* and h_1^2 over the ageing temperatures 100-175^{o}C, it seems unlikely that h_1 will be as large as predicted by eq. (7.5) at lower temperatures, where discolouration in one day cannot be detected. Even at 70^{o}C the oxidation has little effect on surface properties for many months.

The blocks lost weight during ageing, the net loss at 150^{o}C being about 4%. Three substances including the rapidly-diffusing antioxidant IPPD were lost at about 150^{o}C and below before the hard skin formed. Above 150^{o}C the impervious hard skin trapped some of these which volatilized to produce blisters and eventually caused the skin to crack and allow ingress of oxygen. Subsequently

black holes formed in the bulk and ultimately the whole block became like charred wood. With the hardness pellets, some blisters formed below 150°C but did not crack. This may not apply to thicker components in which volatilizable matter may be trapped by the hard skin; there is no evidence that black holes can form in thin sheet.

Prior to the black hole formation, which may not necessarily occur with other vulcanizates of natural rubber, there is no oxidation in the bulk of the blocks beyond the discoloured layer.

PART III

		Page
Section 8	Tearing energies of rubber springs	143

SECTION 8 TEARING ENERGIES OF RUBBER SPRINGS

8.1 Introduction

As indicated in Section 3, the fracture mechanics approach can in principle be used to predict the fatigue life of rubber springs in service, since the relations between crack growth rate and tearing energy are material characteristics and are independent of the shape and size of the springs. It thus has the potential for enabling engineers to design rubber springs with fatigue resistance appropriate to the required service life. The two independent types of information needed for this are (i) the crack growth characteristics of different rubbers under the widest range of conditions obtaining in service and (ii) the strain energy release rates of different shapes of rubber springs for various modes and amounts of deformation.

Many rubber springs, notably those of natural rubber used for anti-vibration purposes, have a sandwich construction with a soft inner block of rubber bonded to rigid outer metal parts. For bonded blocks with square corners, any relative movement of the metal parts produces large stresses at the edges of the bonds so that if crack growth is to occur then these are among the most vulnerable points when the stresses are tensile. In this section tearing energies are determined for different modes of deformation for springs having cracks along the bonds from one or more of the corners. Although the corners are assumed square most springs have some form of strain-relieving fillet but when the crack length exceeds the fillet dimensions the behaviour will obviously tend towards that for a square corner. The methods used for determining T are theoretical, numerical (finite-element analysis) and experimental.

8.2 Experimental method

Vulcanizate A was again used for the experimental part of this investigation. All testing of the rubber was carried out with the laboratory temperature at about 23°C.

The machine used is an old 12-ton Hadley press with jigs to accommodate both the rectangular and the circular shear testpieces. The motion is approximately sinusoidal with a frequency about 2 Hz.

8.2.1 Bonded shear springs

Three types of shear spring were used. Some were double shear units, Fig. 8.1 with circular or rectangular cross-sections, and the remainder single shear units with rectangular cross-sections. The dimensions of the rectangular units were $w = 50$ mm, $t = 25$ mm and $h = 1$ to 6 mm, and of the cylindrical units w (diameter) $= 25$ mm and $h = 3$ to 9 mm.

Bonding was carried out during vulcanization, the metal surfaces being first sand-blasted and then degreased with 'Genklene' before applying the proprietary bonding cements - 'Chemlok' 205 (1st coat), 'Chemlok' 220 (2nd coat) and 'Typly' RC (3rd coat).

The shear stress-strain curves for the springs, obtained on an Instron (rectangular units) and a Servotest dynamic machine (cylindrical units), were essentially linear over the range of strains used in the dynamic crack growth tests. Fig. 8.2 shows a typical shear stress-strain curve. For the rectangular units there was negligible variation with h of the slope of these curves, which was taken as the shear modulus G. For the cylindrical units bending (as with encastré beams) gave an effective shear modulus G_e which decreased slightly from G with increasing h (61).

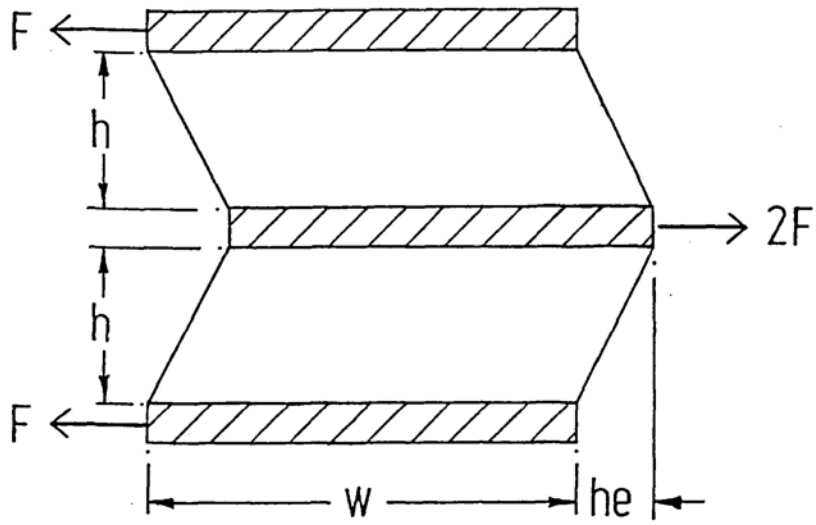


Fig. 8.1 Double shear spring. Each of the two individual bonded rubber blocks (which corresponds to a single shear unit) is shown sheared by an amount he under shear force F. In the case of a double cylindrical shear unit, w is the diameter of the rubber disks.

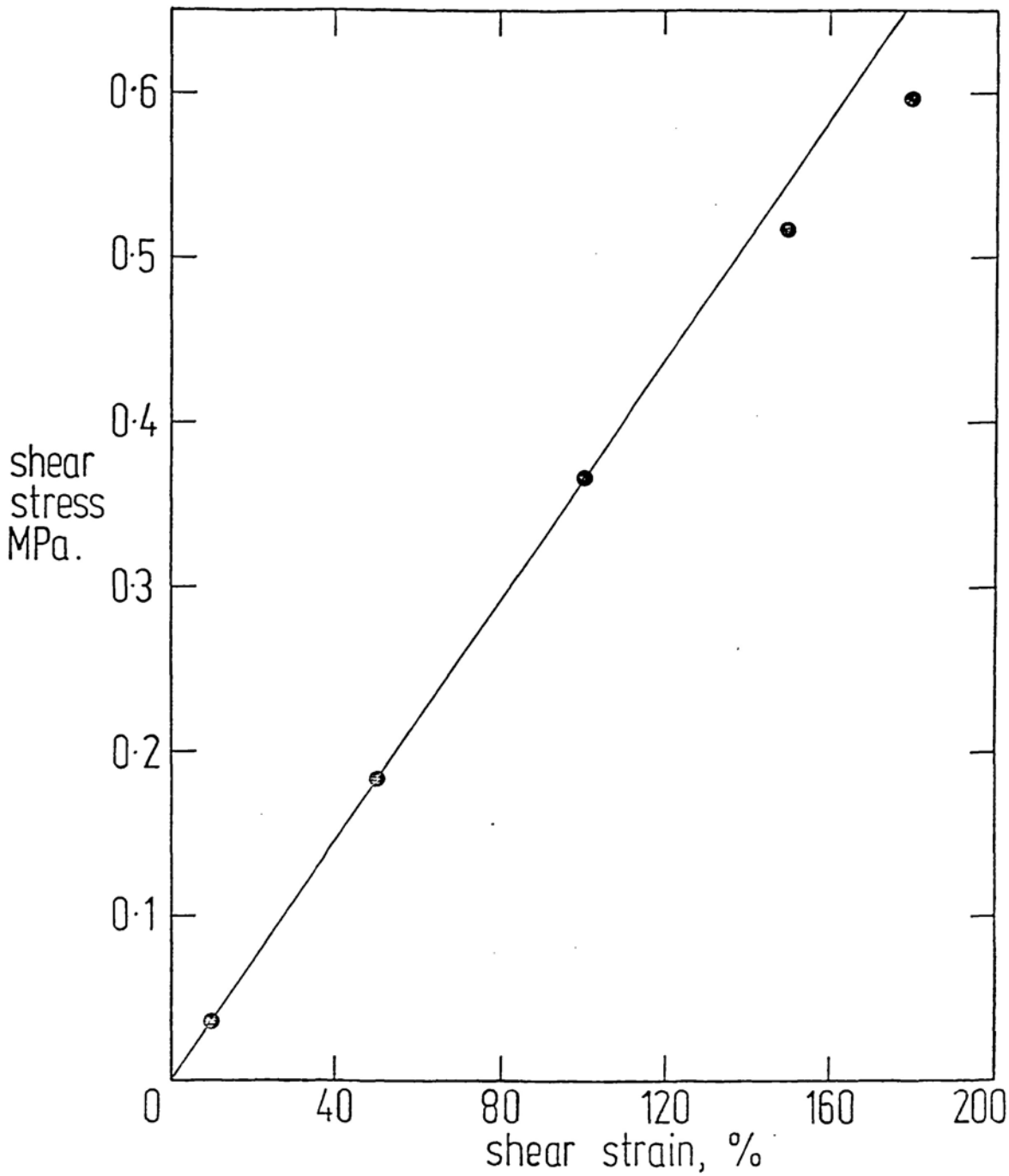


Fig. 8.2 The shear stress-strain curve for natural rubber gum vulcanizate A.

8.2.2 Shear crack growth tests

Cracks were initiated, to ensure they were along the bond, using either a razor blade or acetone (62). Shear tests were carried out at about 2 Hz with the shear strain varying approximately sinusoidally between zero and the required maximum value e. For the cylindrical units the crack length c was obtained by pushing a thin steel rule into the crack and noting the rule reading at the edge of the metal. (This is not a very sensitive method of measurement and leads to considerable scatter in the derived crack growth rates). For the rectangular units a reference line was scribed on each side of the metal close to the crack tip and changes in the distance of the tip from the reference lines measured using a travelling microscope. Measurements were made at suitable intervals of numbers of cycles n. Crack growth rates (dc/dn) were obtained from smoothed curves through c-n plots. Tearing energy T is that applicable to the maximum shear strain e.

Under continuous cycling at about 2 Hz there is a slight temperature rise in the shear units due to hysteresis. Measurements made during 24 hours continuous cycling using an infra-red thermometer and an electronic thermometer showed at most about a 10 deg C limit to the increase in surface temperature. It was observed in Section 6 that such a rise has little effect on its crack growth behaviour.

8.3 Numerical method

Finite-element analysis provides a numerical method of obtaining tearing energies. It has already been applied for this purpose by Lindley (11) to a number of plane-stress shapes of rubber in tension. The plane-stress finite-element computer programme used (40) gave satisfactory results up to 200% tensile strain using triangular elements.

In the plane-strain programme used here (63) the elements are quadrilateral but the programme is restricted, by the long convergence times, to classical solutions only. In plane-strain analyses the rubber cannot be assumed incompressible, as was done in plane stress. The two elastic constants employed are the Lamé constants G (shear modulus) and λ, the latter being taken as 3000G corresponding to a Poisson's ratio of 0.49983.

The finite-element analyses give, among other data, the total elastic strain energies (U_o with no crack or U_c with one or more cracks). The programme enables plane-strain analyses to be obtained in shear, tension, compression and rotation. A minor modification to the programme enables bodies of revolution (disks) to be analysed in tension and compression.

The finite-element idealization both of plane strain sections and of disks is shown in Fig. 8.3. The node on the bond at the bottom left corner (A) is taken as the origin of co-ordinates. By scaling all nodal x-values, any desired w/h ratio can be obtained.

For a section with no cracks, the nodes on the bonds are constrained to move with the rigid plates. Cracks are made in the programme by releasing nodes along the bond from the origin.

When Fig. 8.3 represents the full section, bonded top (DC) and bottom (AB), a single crack can be grown from the bottom left corner (A). When Fig. 8.3 represents a lower-half section (bonded on AB with DC a centre line) the results apply to a full section with cracks at the top and bottom of the left edge. When it represents a quarter section (bonded on AB with DC and CA centre lines), the results are applicable to a full section with cracks at all corners.

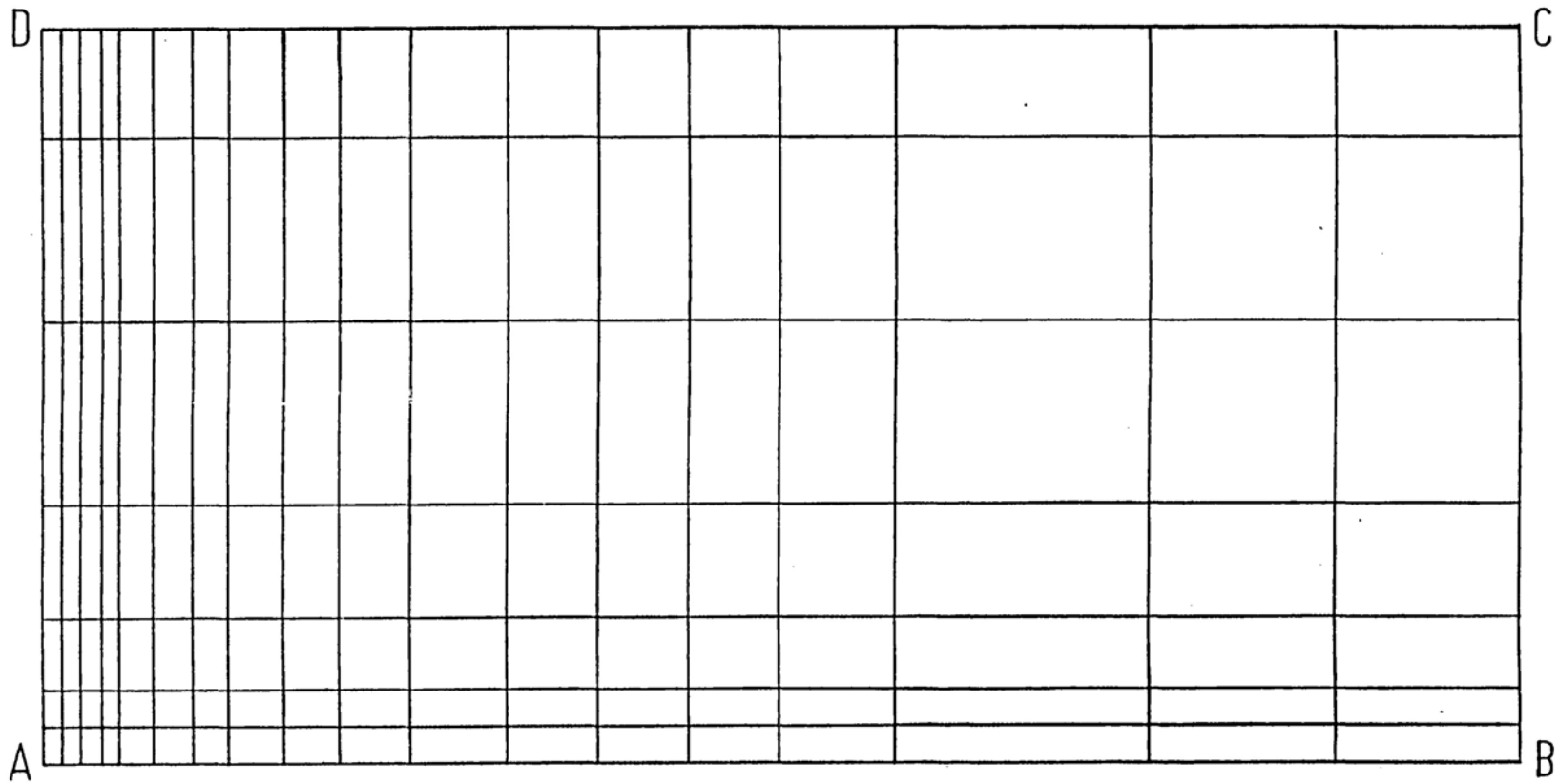


Fig. 8.3 Finite-element representation of a section or part section of a rubber block. In all cases AB is a bond line and cracks are 'grown' from A. For a full section the height AD = h and the width AB = w; the depth, normal to the plane of the figure, is taken as unity in the analyses.

The strains at which the analyses were carried out were 1% in tension and compression, 1% in shear, and in rotation the plates were pivotted about their centres to give an average strain of 1% tension at the left edge (DA).

8.4 Simple shear with long crack

8.4.1 Theoretical

The spring is in the form of a rectangular block of rubber, of width w, height h and depth t (normal to the plane of the figures). When a shear strain e is applied, Fig. 8.4(a), the central region 2, at distances greater than about h from each edge has a uniform strain energy density W. As the stress-strain curve for vulcanizate A in simple shear is essentially linear to strains of the order of 100% or so,

$$W = \tfrac{1}{2} Ge^2 \qquad (8.1)$$

The introduction of a crack extending from the bottom left corner, Fig. 8.4(b), produces an unstrained region 4, a region 3 of constant width but complex strain distribution around the crack tip, a region 2 which is still in simple shear with constant W and a region 1 of constant width but also of non-uniform strain distribution. For an increase in crack length of dc, region 4 increases in width by dc, region 3 moves to the right by dc and region 2 is decreased in width by dc. The net effect is the transfer of a volume of rubber ht dc from the uniform strain energy density (W) state of region 2 to the unstrained state of region 4. The energy loss dU is thus

$$dU = ht\ dc\ W \qquad (8.2)$$

The increase in one surface area of the crack is

$$dA = tdc \qquad (8.3)$$

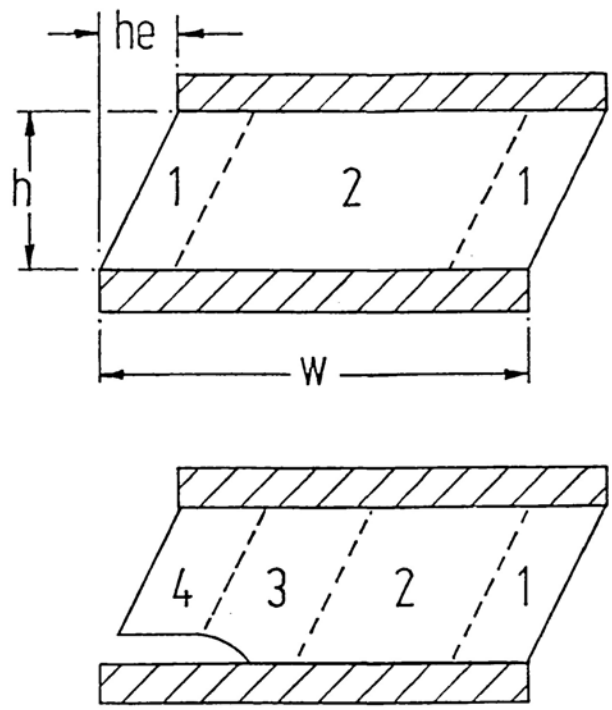


Fig. 8.4 Spring in simple shear at strain e (a) with no crack and (b) with a crack along the bond from the bottom left corner.

Hence, the tearing energy T for the spring in simple shear is derived from eq. (3.1) as

$$T = -\left(\frac{\partial U}{\partial A}\right)_l = Wh \qquad (8.4)$$

This is similar in form to that for the pure shear testpiece in tension described in Section 3.2.

8.4.2 Numerical

Using the mesh of Fig. 8.3 with h (=AD)=1, w (=AB)=10 and 40, $G = 1$, $e = 0.01$ and unit depth, the plane-strain finite-element programme has been used to obtain values of U_o and of U_c for various crack lengths c. The strain energy losses U ($= U_o - U_c$) are plotted against crack length c in Fig. 8.5 on linear scales. The line through the numerical points in Fig. 8.5 has a slope T ($= dU/dc$) of 0.5×10^{-4}, given by eq. (8.4). There is thus excellent agreement for long cracks ($c>3h$) between the theoretical relation for T and T obtained by the plane-strain finite-element analysis.

8.4.3 Experimental

As the depth t (25 mm) of the rectangular cross-section shear springs is sufficiently greater than the height h (< 6 mm), a state of plane strain is assumed when they are deformed in simple shear. The crack growth rates dc/dn, for different strain cycles 0-e, were obtained as averages over a few mm growth ($c>3h$) for the springs of different heights h. Tearing energies were determined from eq. (8.4) at the maximum shear strain e. The experimental results are shown as squares in Fig. 8.6. There is no significant difference either between the results for the single (open squares) and the double (solid squares) rectangular shear units in plane strain or between these results and those for the simple extension testpiece in plane stress taken from Fig. 6.1. (The scatter is about the same for plane strain as it is

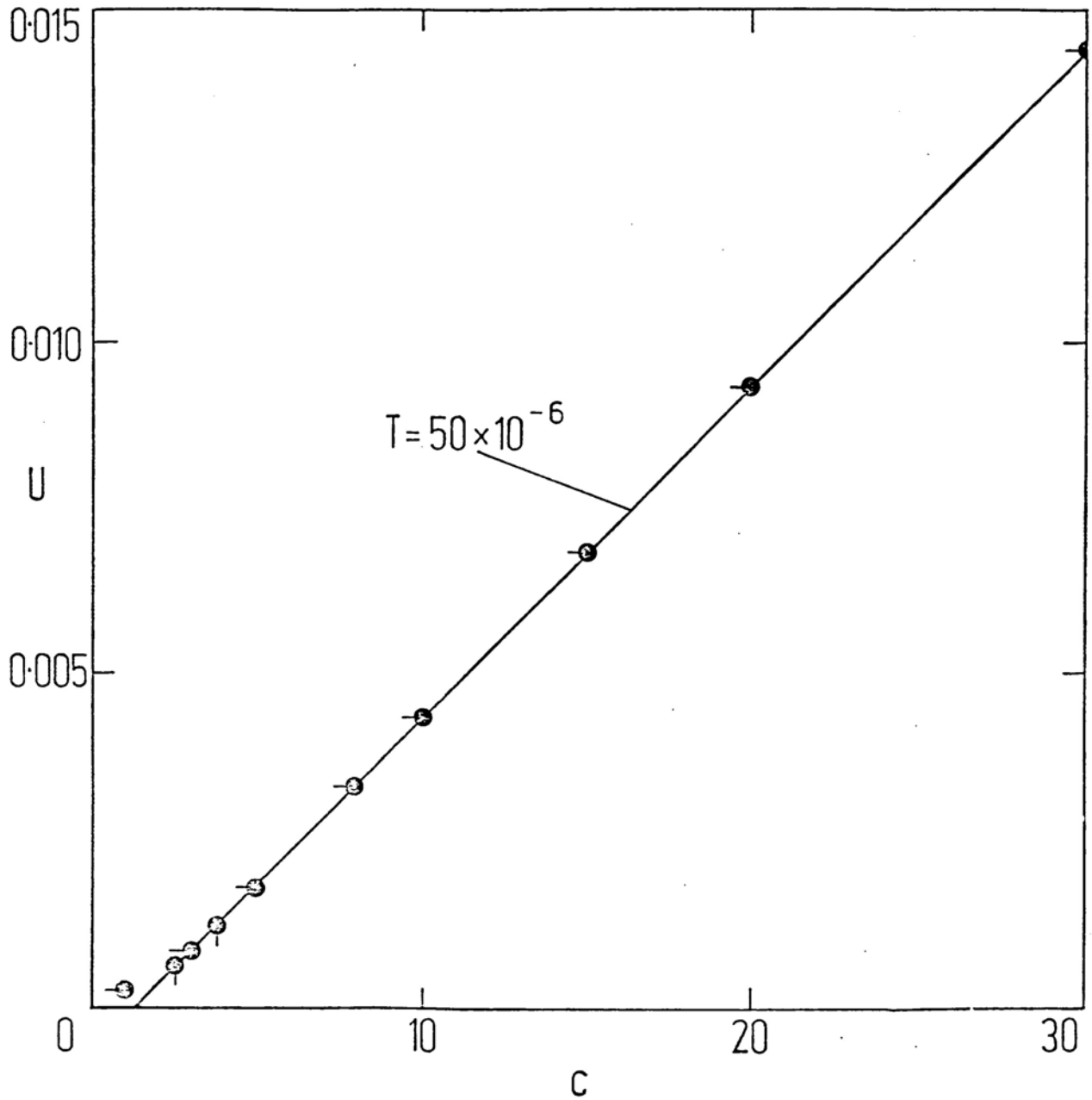


Fig. 8.5 Variation of energy loss U with crack length c (which also equals the crack area A) in plane strain simple shear. The points (w/h values as Fig. 8.7) were obtained using plane-strain finite-element analysis with w = 10 and 40, h = 1, G = 1 and e = 0.01. The slope of the line is given by eq. (8.4).

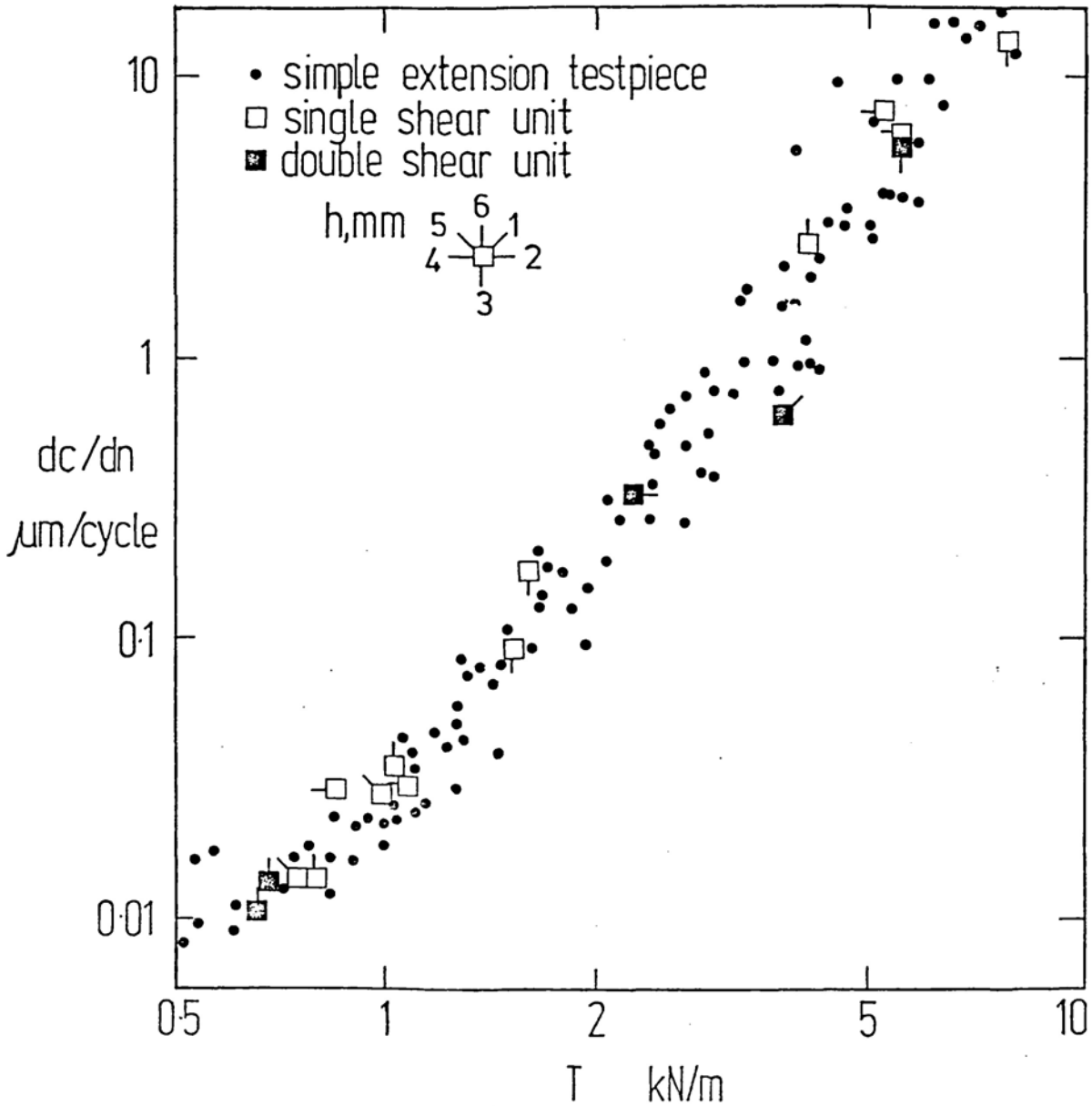


Fig. 8.6 Experimental crack growth rate (dc/dn) against tearing energy (T) characteristic obtained using simple extension testpieces (Fig. 3.1 and eq. (3.4)) and rectangular cross-section springs in simple shear (Fig. 8.4 and eq. (8.4)). For the latter $c > 3h$.

for plane stress). The agreement confirms the validity of the theoretical relation for T eq. (8.4) and, since the numerical data are consistent with theory, the validity of the finite element method also for determining T in plane strain.

8.5 Simple shear with short cracks

Equation (8.4), represented by the straight line in Fig. 8.5, clearly does not hold for cracks less than about 3 h. However, as the central region of the rubber block has a uniform W, a short crack in a wide testpiece ($c \ll w$) may produce an energy loss proportional to c^2, ie

$$U = k_s W c^2 t \qquad (8.5)$$

in a similar manner to that found for the tensile strip in Section 5.1. Figure 8.7, in which $U^{\frac{1}{2}}$ is plotted against c, shows that the numerical data satisfy eq. (8.5) for c values ranging from about h to $2\frac{1}{2}$ h. For this region therefore (vide Section 5.1)

$$T = 2k_s Wc \qquad (8.6)$$

where k_s is 0.21.

The breakdown of eqs. (8.5) and (8.6) at smaller crack lengths is not surprising in view of the stress concentration at the sharp corner. The energy loss U as the crack increases to a length equal to h is shown on linear scales in Fig. 8.8. These finite-element data, like those in Fig. 8.7, are for w/h ratios ranging from 1 to 40 and the relation is extremely well defined. This justifies the scaling of the mesh x-values in Fig. 8.3 to give different w/h ratios.

Some indication of the form of the stress (σ) distribution near the corner can be deduced from the observation that the initial part of the U-c curve in Fig. 8.8 is linear, ie

$$U \propto c$$

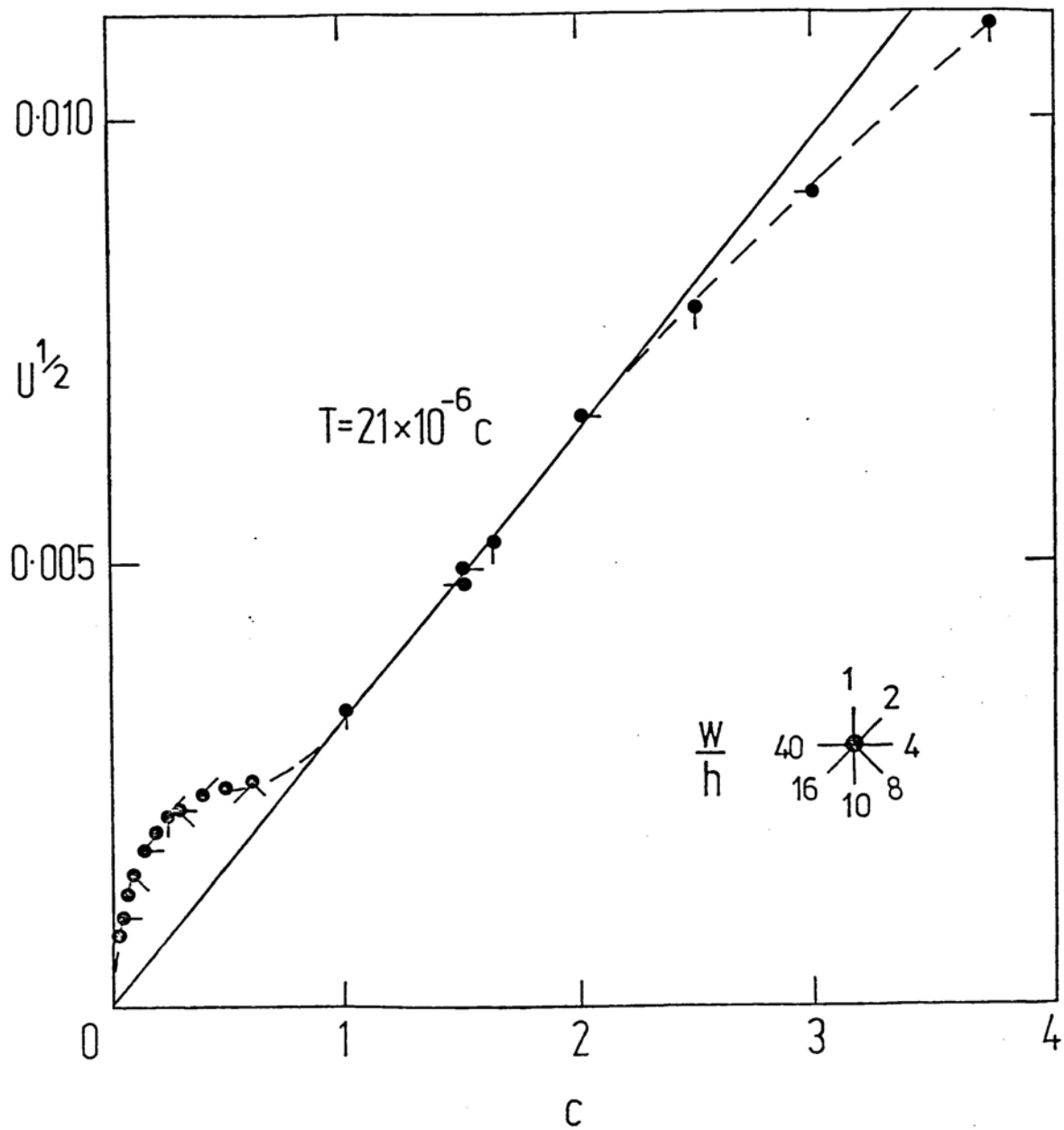


Fig. 8.7 Variation of the square root of the energy loss ($U^{\frac{1}{2}}$) with crack length c in simple shear. Finite-element data: h = 1, w/h as shown, G = 1 and e = 0.01. The full line has the form of eqn (8.6).

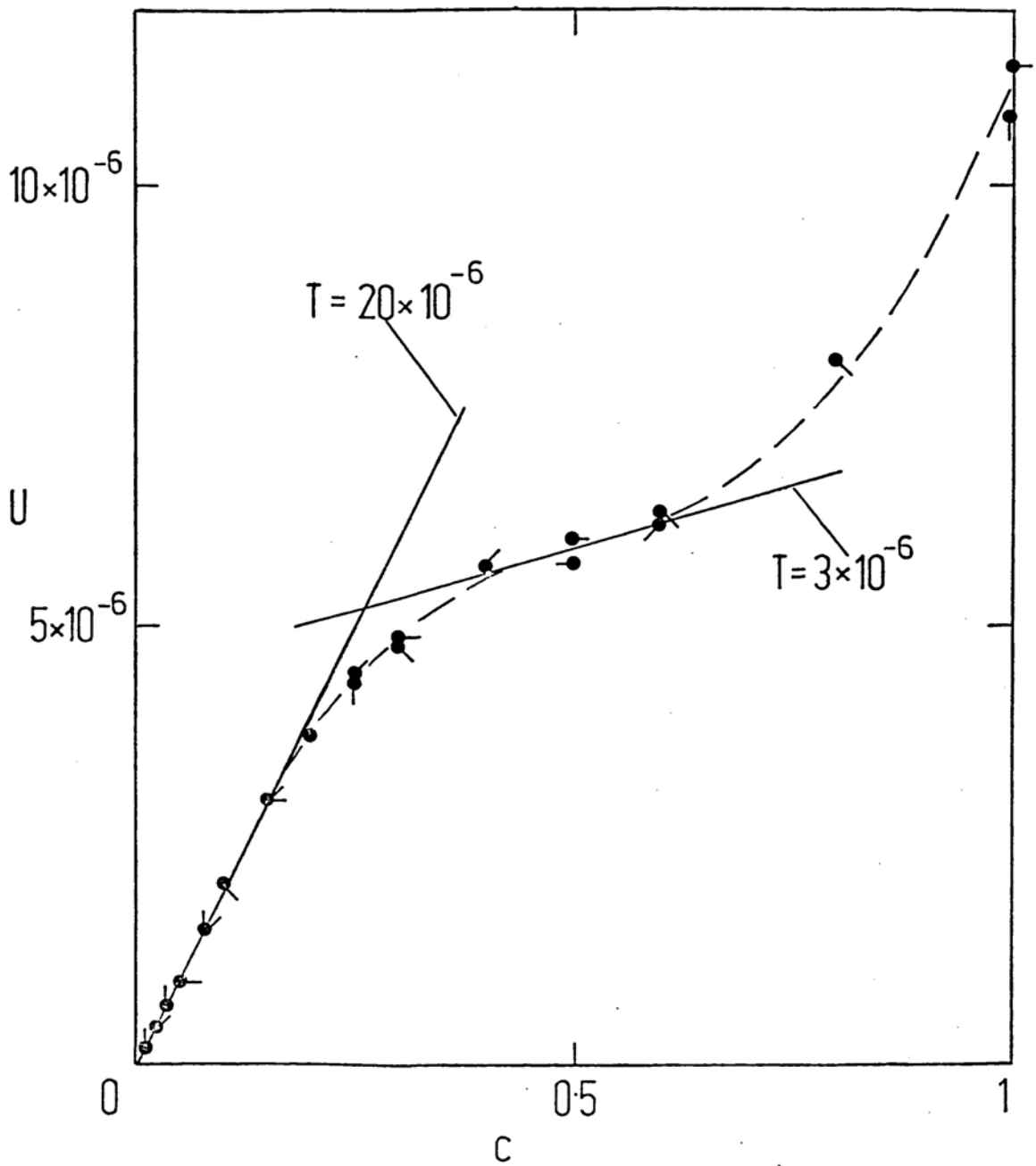


Fig. 8.8 Variation of energy loss U with crack length c in simple shear for $c \leqslant h$. Finite-element data: h = 1, w as Fig. 8.7, G = 1 and e = 0.01.

Consider the stress contours near the corner and take the corner as the origin of co-ordinates. Two assumptions are made: (i) that the co-ordinates of all points on one stress contour are a constant proportion of those on any other contour and (ii) that the energy drop U due to a crack of length c is proportional to the energy originally stored in the volume of rubber bounded by the crack and the contour (this is analogous to the constant stress case in Section 5.1). It then follows that

$$U \alpha \int_0^c W' c \, dc \qquad \alpha \int_0^c \sigma^2 c \, dc \qquad \alpha \quad c$$

since the strain energy density W' is proportional to σ^2. It is evident from this that $\sigma^2 c$ must be a constant, ie that the stress is inversely proportional to the square root of the distance from the corner. In the limit, as this distance reduces to zero, the stress becomes infinitely high in accordance with theory (64).

The slope of the U-c curve is the tearing energy T and Fig. 8.9 shows the variation of T, as a proportion of the tearing energy Wh for long cracks, with the crack length to section height ratio c/h for c/h up to 3. This relation has two interesting features. The first is the pronounced drop in T to a minimum of about 0.06 Wh at c = h/2 which corresponds to the inflexion in the U-c curve of Fig. 8.8. Under certain conditions the drop in T may be sufficient to arrest the growth of a crack which has initiated at the corner stress concentration. The second is that the initial linear region of Fig. 8.8 corresponds to a constant tearing energy (of 0.4 Wh) so that crack growth need not necessarily occur at the theoretically infinite stress at the corner. It may also be noted that the tearing energy Wh of long cracks is the maximum tearing energy that can occur in simple shear.

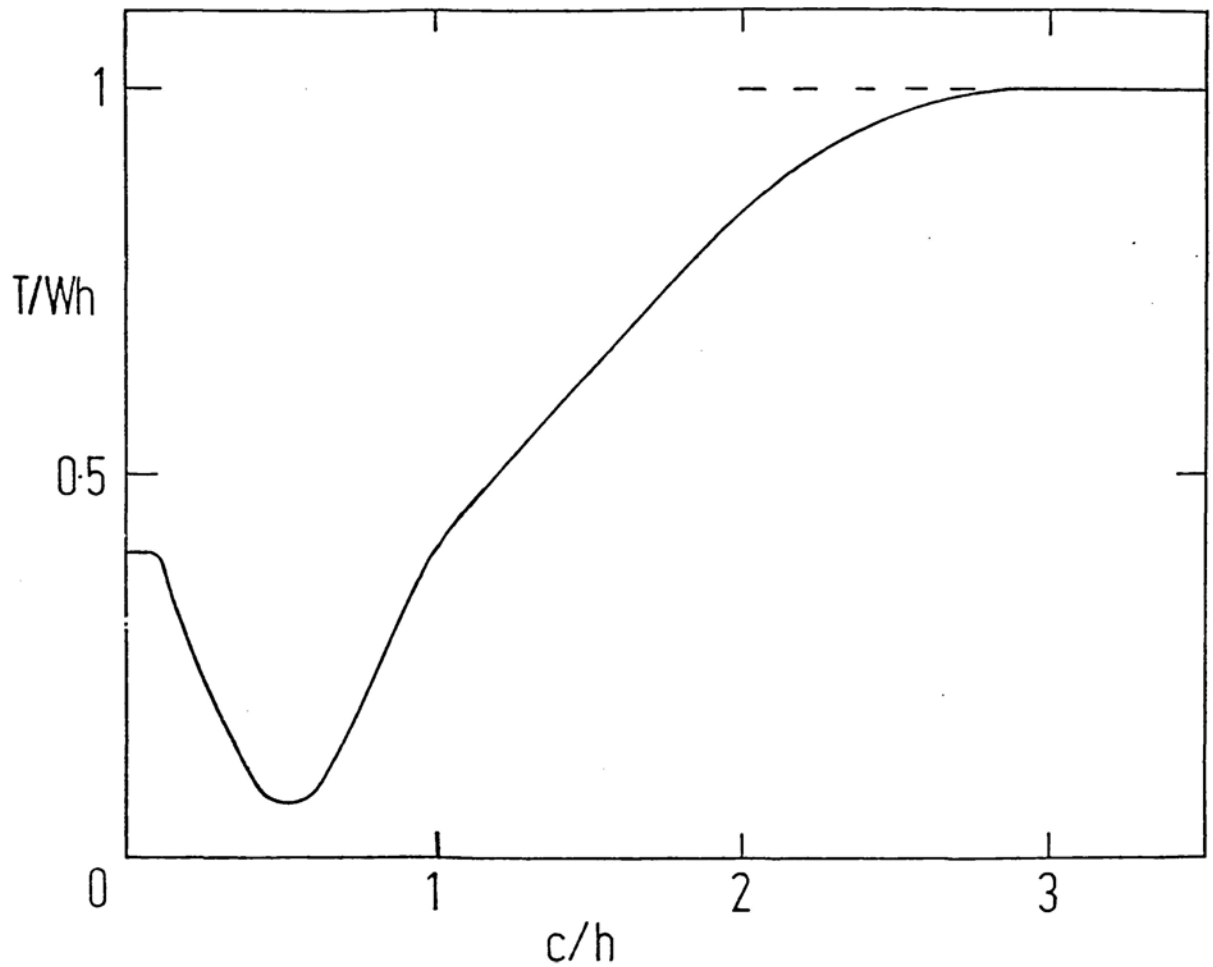


Fig. 8.9 Variation of tearing energy T with crack length c derived from finite-element analyses in simple shear (Figs. 8.7 and 8.8). Wh is the value of T for c > 3h.

8.6 Bonded disks in simple shear

The results of the crack growth tests on the cylindrical shear units are shown in Fig. 8.10. The relation used for the tearing energy is

$$T = 0.7\ Wh \qquad (8.7)$$

the effective shear modulus G_e (see 8.2.1) being used in eq. (8.1) for W.

This relation was obtained by first assuming that T was equal to Wh, as in the case discussed in 8.4.1, and then determining the scaling factor (for Wh) which would bring the points into reasonable agreement with the crack growth characteristic represented in Fig. 8.10 by the small circles obtained using simple extension testpieces. Considering the scatter, due to the method of test (8.2.2), little improvement would appear to be gained by adopting a more complex scaling factor than that of the constant value 0.7 for all diameter/height ratios and crack lengths.

It is not without significance that the coefficient of Wh in eq. (8.7) is less than for plane strain. In plane stress tests in tension when the crack was initiated at a corner in the centre of a long rod of square cross-section, the tearing energy was found by Lindley (11) to be half that given by eq. (5.2) for thin strips of rubber. This arises because the width of the crack tip increases approximately linearly with the crack length. With the cylindrical shear testpieces the width of the crack front also increases with increasing c, although not linearly.

8.7 Plane strain tension

8.7.1 Theoretical model

In the remaining cases to be discussed, ie tension and rotation of plane-strain sections and tension of disks, the theoretical solution is

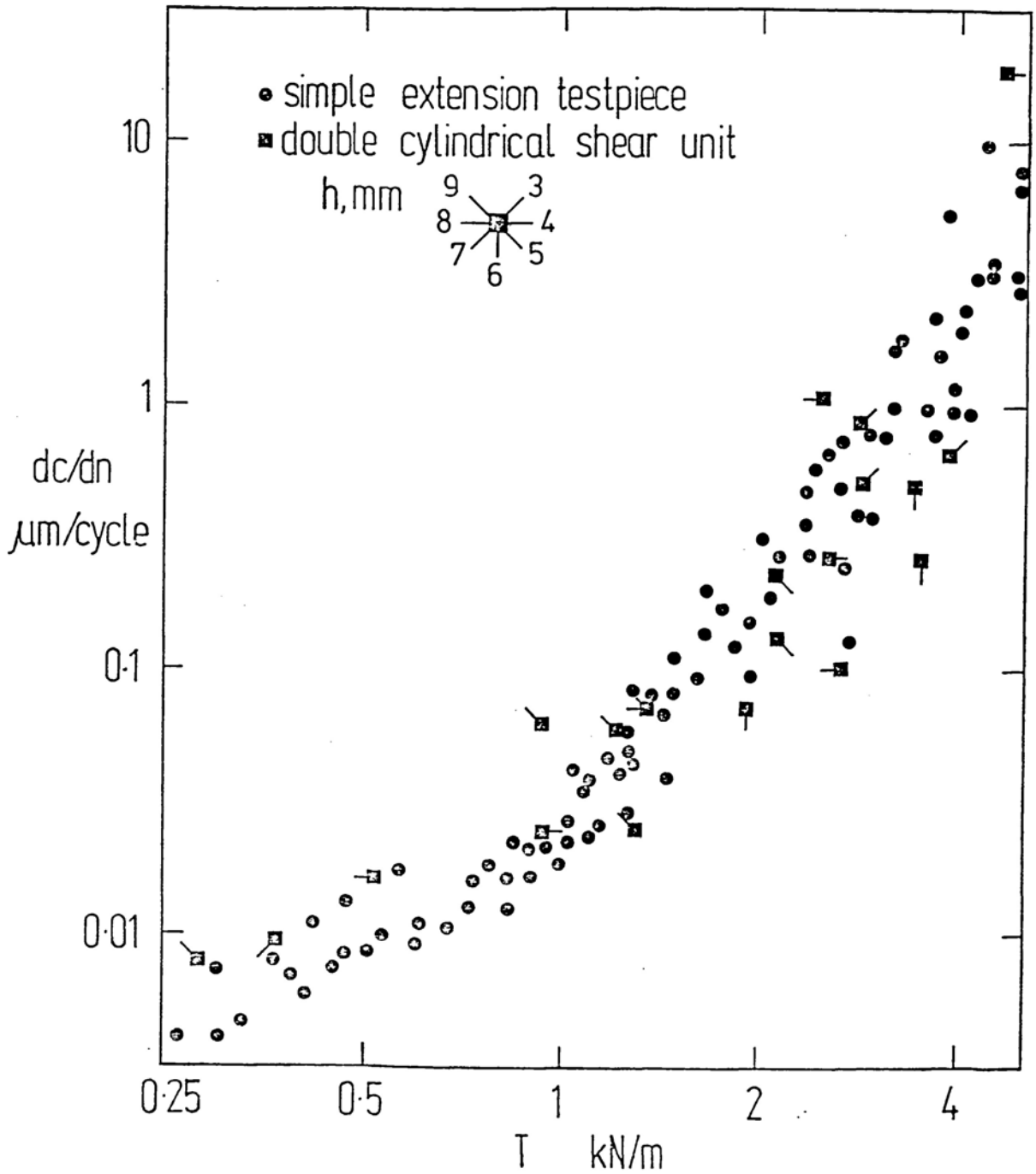


Fig. 8.10 Experimental crack growth data obtained using double cylindrical shear springs in simple shear, with T from eq. (8.7), and simple extension testpieces

based on the following model. For cracks of length c from one or more corners of the section, the top and bottom edges of the rubber still bonded are joined by straight lines and the total energy is then assumed to be that of the smaller section which has these lines as its outer edges, the height remaining unchanged, Fig. 8.11. Where there is only one crack, Fig. 8.11(c), the effective width is assumed to be reduced by ½c, Fig. 8.11(d). Each corner crack thus has the effect of reducing the width by c/2, ie the effective width is w(1-x) where

$$x = mc/2w \tag{8.8}$$

and m is the number of corners at which there are cracks.

A parameter - shape factor, S - is widely used in relations for the compression modulus, and hence stiffness, of rubber blocks. It is defined as the ratio of cross-sectional area to total force-free surface area, eg for the plane-strain section S is w/2h. Since S is proportional to w (for disks also) the effective S for a section containing cracks is S(1-x).

8.7.2 Theoretical solution

A simple theoretical approach for the plane-strain compression modulus E_c of bonded rubber blocks gives (65)

$$E_c = 4G\ (1+S^2) \tag{8.9}$$

As the theory applies equally well for small tensile strains the total energy U_o of a block of volume V (= wht) at tensile strain e is

$$U_o = \tfrac{1}{2}\ E_c\ e^2\ V$$

$$= 2Ge^2\ (1+S^2)htw \tag{8.10}$$

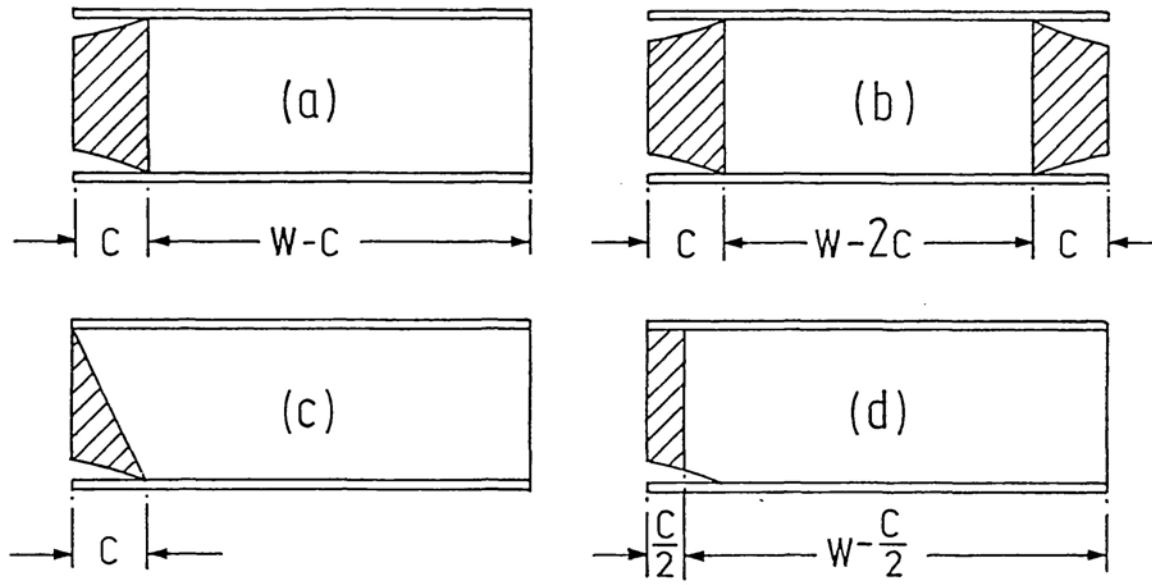


Fig. 8.11 Theoretical model. The shaded areas are assumed to represent the volume of rubber from which all the energy is lost due to the crack(s).

The energy U_c of a block having m cracks of length c at the corners is obtained by substituting w and S in eq. (8.10) by their effective values, ie

$$U_c = 2Ge^2 \left\{1+S^2(1-x)^2\right\} htw(1-x) \qquad (8.11)$$

whence the energy loss U due to the presence of the cracks is

$$U = U_o - U_c$$

$$= 2Ge^2 (1+3S^2) htwx K_1 \qquad (8.12)$$

where

$$K_1 = 1 - (3-x)S^2x/(1+3S^2) \qquad (8.13)$$

The area A of one surface of the crack(s) is, when combined with eq. (8.8),

$$A = mct = 2wtx \qquad (8.14)$$

The tearing energy T is obtained, using eq. (8.14) and either eq. (8.11) or (8.12), from

$$T = -\frac{dU_c}{dA} = -\frac{dU_c}{dx}\Big/\frac{dA}{dx}$$

$$= \frac{dU}{dA} = \frac{dU}{dx}\Big/\frac{dA}{dx}$$

$$= Ge^2 (1+3S^2)h K_2 \qquad (8.15)$$

where

$$K_2 = 1 - 3S^2x(2 - x)/(1+3S^2)$$

When crack lengths c are small compared with w, K_2 is unity, and the initial tearing energy T_i is

$$T_i = Ge^2(1+3S^2)h \qquad (8.16)$$

8.7.3 Numerical solutions

Equation (8.12) for the energy loss can be expressed in terms of T_i as

$$U = 2T_i wx\, K_1 = T_i\, mc\, K_1$$

for unit depth t. Comparison of the numerical results with the above theoretical solution is made on the basis of a parameter u, given by

$$u = U/(T_i\, m\, w) \qquad (8.17)$$

as this enables the results for all widths and shape factors to be shown conveniently on the same figure. For the theory $u = K_1\, c/w$. With $K_1 = 1$, u is the crack length to section width ratio c/w and this is represented in Fig. 8.12 by the dotted lines of slope 1. The broken lines correspond to u with K_1 given by eq. (8.13); these depart very little from the dotted lines. The numerical results are the points joined by the full lines. For S = 2 the number of corner cracks m is 4; in all other cases m = 1.

The slope 1 of the dotted line corresponds to T_i; the numerical value of tearing energy T is obtained by multiplying T_i by the slope of the full line. For the range of S(ie 0.2-20) covered numerically the coefficient of h in eq. (8.16) for T_i varies about 1200-fold. As the numerical and theoretical results differ at most by a few tens of percent the agreement may be considered satisfactory. The normal range of shape factors for blocks used in practice is about ½ to 8, and it is the shape factors outside this range which give the least satisfactory agreement. In most cases the use of the theoretical relation eq. (8.16) introduces a small factor of safety. It may be noted that T_i is independent of the number of cracks.

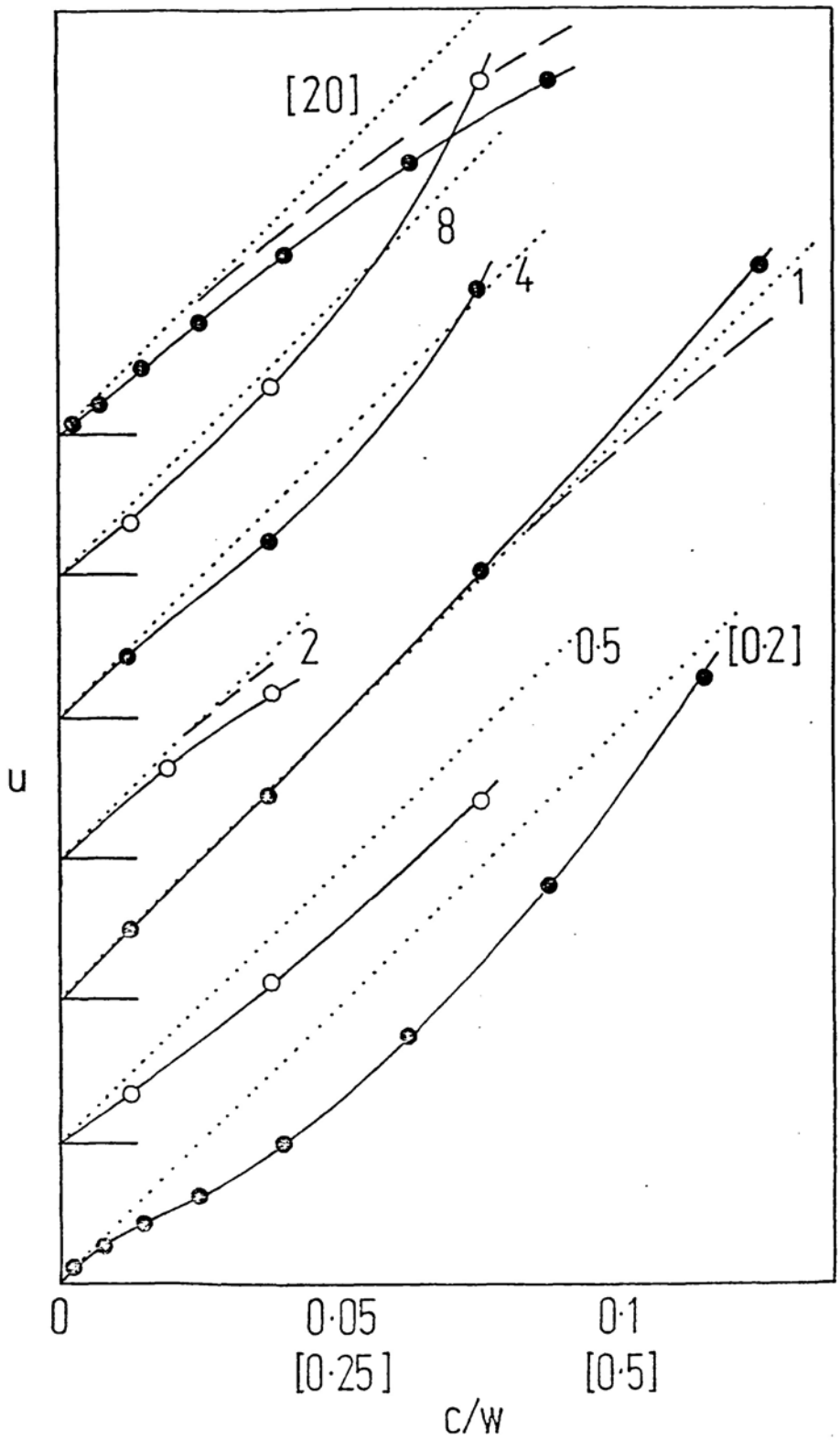


Fig. 8.12 Variation of the parameter u, eq.(8.17) with c/w for plane-strain sections in tension. Values of shape factor S (= w/2h) are shown alongside the curves. The scale for u is the same as that for c/w; the scale in square brackets applies to S = 0.2 and 20. The full lines are drawn through points obtained from finite-element analyses. The dotted lines are theoretical relations (u = c/w) for $K_1 = 1$. Significant departures from the latter, when K_1 is given by eq.(8.13) are represented by broken lines.

8.8 Disk in tension

The tearing energy for a disk in tension is derived in a similar manner to that for the plane strain section in tension. For a disk m can only be 2 (a circumferential crack at one bond) or 4 (cracks at both bonds). The shape factor S is w/4h, where w is the diameter, and the tension modulus E_c is (65)

$$E_c = 3G\ (1+2S^2) \tag{8.18}$$

from which U is derived as

$$U = 0.75Ge^2\ \pi\ w^2h\ (1+4S^2)xK_3 \tag{8.19}$$

where

$$K_3 = 1 - x\left\{\tfrac{1}{2} + S^2(6-4x+x^2)\right\}\ /(1+4S^2) \tag{8.20}$$

and x is again given by eq. (8.8). The crack area A, approximately for m=2, exactly for m=4, is

$$A = \pi\ w^2\left\{1-(1-2x)^2\right\}/4 = \pi\ w^2\ x(1-x)$$

whence

$$T = Ge^2(0.75 + 3S^2)hK_4 \tag{8.21}$$

where

$$K_4 = \left[1 - x\left\{1 + 4S^2(3-3x+x^2)\right\}/(1+4S^2)\ \right]/(1-2x)$$

The initial tearing energy T_i is

$$T_i = Ge^2(0.75 + 3S^2)h \tag{8.22}$$

This is very similar to that for plane strain, eq. (8.16); the coefficient of S^2 is identical.

An example follows to show that the agreement between numerical and theoretical results for disks is not dissimilar to that for plane-strain sections.

When the crack length c is small compared with the diameter w,

$$T_i \simeq U/A$$

For a disk of shape factor S equal to 1, the theoretical value of T_i/Ge^2h from eq. (8.22) is 3.75 and from finite element analysis with c = 0 and 0.15, w = 8, h = 2 and m = 4 the corresponding numerical value is 14% lower at 3.22. It thus appears that tearing energies for bonded rubber disks in tension can be determined using eq. (8.22).

8.9 Plane strain rotation

In rotation, one bonded plate of the plane-strain section is rotated through an angle θ relative to the other, Fig. 8.13(a). The couple M required to maintain this rotation, for a section of unit depth, is

$$M = E_r w^3 \theta/12 \qquad (8.23)$$

where the rotation modulus E_r for the plane strain section is (66)

$$E_r = 4G (1 + S^2/5) \qquad (8.24)$$

The stored energy is

$$U_o = \tfrac{1}{2} M\theta$$

$$= G \theta^2 (1 + S^2/5) w^3/6h \qquad (8.25)$$

When m cracks of length c are introduced at the left edge and there is no tensile or compressive force on the bond plates, U_c is obtained by scaling w and S in eq. (8.25) by 1-x where x is again given by eq. (8.8). The energy loss $U(\theta)$ is then

$$U(\theta) = G\theta^2 w^3 (3+S^2) x K_5/6h \qquad (8.26)$$

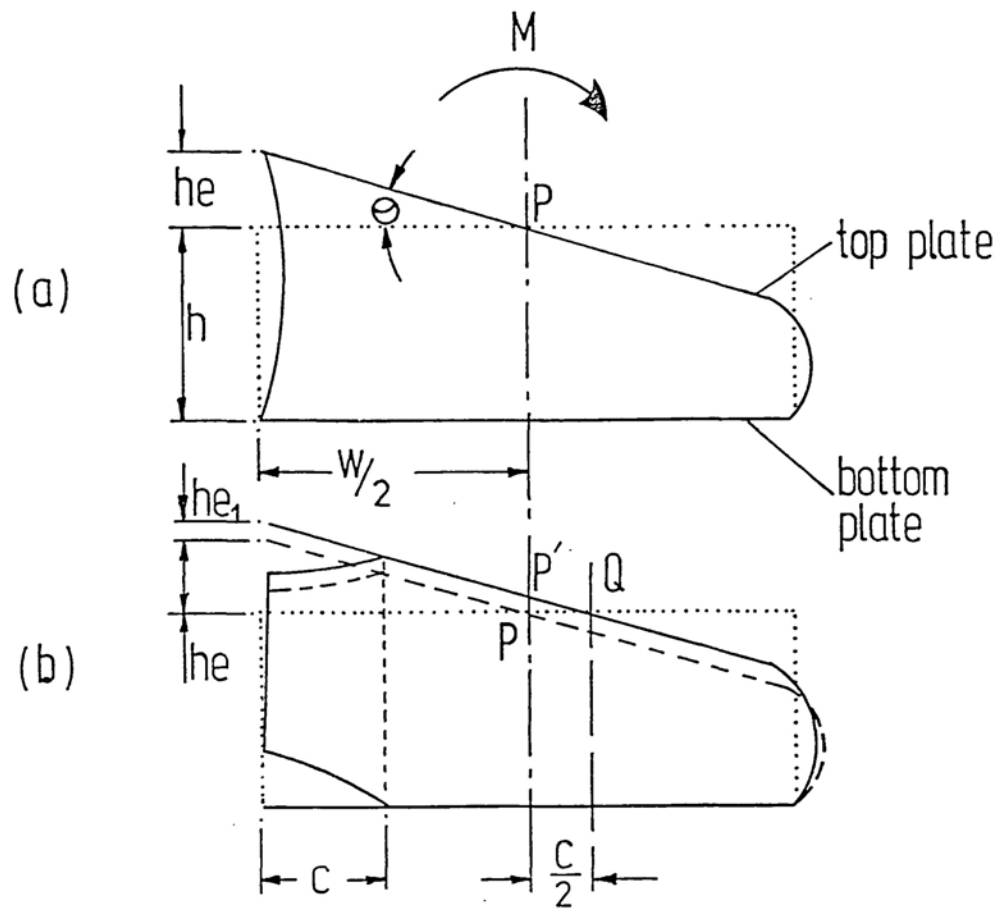


Fig. 8.13 Rotation of a plane-strain section. PP′ is the tensile displacement of P caused by the transfer from P to Q of the centre of rotation of the top plate when cracks of length c are introduced at the left corners.

where

$$K_5 = 1 - x\left\{3-x + S^2(2-2x+x^2-x^3/5)\right\}/(3+S^2)$$

Because U_c above has been determined for a rotation θ about the centre Q (Fig. 8.13(b)) of the bond still remaining intact, the original bond centre P moves to P' which corresponds to a tensile strain e_1 given, for m cracks at the left edge, by

$$e_1 = (mc/4)\theta/h = xe$$

where e, the average initial tensile strain at the left edge, is seen from Fig. 8.13(a) to be

$$e = w\theta/2h$$

To restore the metal parts to the separation they had at c=0 a compressive strain of magnitude e_1 must be applied to the section. The work $U(e_1)$ needed to do this is obtained from the tension U_o, eq. (8.10), with e, w and S replaced by xe, w(1-x) and S(1-x) respectively, ie

$$U(e_1) = 2Ge^2x^2\left\{1 + S^2(1-x)^2\right\}hw(1-x) \qquad (8.27)$$

This energy is additional to that due to rotation and must therefore be added to the rotation U_c, thus reducing the energy loss by the same amount, ie

$$U = U(\theta) - U(e_1) \qquad (8.28)$$

For a section in which G = 1, w = 8, h = 2 (giving S = 2), e = 0.01, m = 2 and c = 0 and 0.15, eqns. (8.26-28) give

$$U(\theta) = 1.382 \times 10^{-4}$$

$$U(e_1) = 0.054 \times 10^{-4}$$

$$U = 1.328 \times 10^{-4}$$

Using the same data, finite element analysis gives 1.192×10^{-4} for U, which is about 10% lower than the theoretical value. It thus appears that tearing energies in rotation, derived from the approximate theoretical analysis, should not be greatly in error.

The initial tearing energy is given by

$$T_i = G\theta^2 w^2 (3 + S^2)/12h$$
$$= Ge^2 h \, (1 + S^2/3) \qquad (8.29)$$

8.10 Summary

By comparing experimental crack growth data for rubber in simple shear, based on an exact theoretical relation for tearing energy ($T = Wh$), with those in simple extension, based on a well-proven relation for T, it has been shown (Fig. 8.6) that the crack growth behaviour of rubber is the same in plane strain (rubber 25 mm thick) as it is in plane stress (rubber 2 mm thick), within the limits of the experimental reproducibility.

It has also been shown (Fig. 8.5) that the numerical plane strain finite-element method gives the same tearing energy as the exact theoretical relation ($T = Wh$) for long cracks along the bond for a plane-strain section in simple shear. It is presumed, therefore, that T values determined by the finite-element method must be substantially true values of tearing energy. The numerical method enables the energy loss U due to one or more cracks of surface area A to be obtained, T being the slope of the U against A curve. This method has been used to determine T for small cracks in simple shear (Fig. 8.9).

For cylindrical units in shear T has been deduced to be about 0.7 Wh by superimposing experimental crack growth rates on the simple extension crack growth data (Fig. 8.10).

In order to determine T for plane strain sections in tension and rotation and for disks in tension, an approximate theoretical method has been used. U values derived from the theory differ at most by a few tens of percent from those obtained numerically (Fig. 8.12 and Sections 8.8 and 8.9).

The energy available for initiating cracks along the bonds of bonded rubber blocks with square corners can be summarised as follows:

Plane-strain shear, at shear strain e

$$T = Ge^2h\ 0.2 \qquad (8.30)$$

Plane-strain tension, at tensile strain e

$$T = Ge^2h\ (1 + 3S^2) \qquad (8.16)$$

Disk in tension at strain e

$$T = Ge^2h\ (0.75 + 3S^2) \qquad (8.22)$$

Plain-strain rotation, with edge strain e

$$T = Ge^2h\ (1 + S^2/3) \qquad (8.29)$$

The differences between theoretical and numerical U values in tension and rotation are seen to be small when compared with the possible range of T due to variations in shape factor. The initial T is proportional, in all cases, to the rubber thickness h. It is also independent of crack length; even for large cracks T departs little from the initial value, except in simple shear (Fig. 8.9) where the initial value is not exceeded for crack lengths of less than the rubber thickness.

PART IV

		Page
Section 9	Strain concentration factors for bonded rubber blocks with radiussed fillets	174

SECTION 9 STRAIN CONCENTRATION FACTORS FOR BONDED RUBBER BLOCKS WITH RADIUSSED FILLETS

9.1 Introduction

Unlike the square cornered models considered in Section 8, many of the rubber components used in engineering applications have a sectional shape similar to that shown in Fig. 9.1, which is the model used in this section. The upper and lower boundaries are considered to be of perfectly rigid material, representing the steel parts to which the rubber block is bonded. Not all bonded rubber blocks have deliberately introduced corner fillets but the method of manufacture invariably ensures that there is one, albeit small. This section describes an investigation of the strain concentration factors k at the radiussed fillets of the model for various height-to-radius ratios (h/r) and width-to-height ratios (w/h) for small 'classical' deformations in shear, tension/compression and rotation of plane-strain sections of width w and also of disks of diameter w in tension. The determinations of k for these shapes and modes of deformation are two-dimensional problems for which numerical finite-element analyses have been used.

A study has already been made by Lindley (33) of the strain concentration factors at the curved corners of rubber sheets in tension using the model of Fig. 9.1 in plane stress. Some of these findings, to which those for plane strain will be related, are given in Section 9.3.

It will be shown that, with minor but explicable exceptions, the strain concentration factor k is linearly related to the product of two independent functions, one (F_s) of the ratio w/h of the major dimensions of the section and the other (F_r) of the ratio h/r of

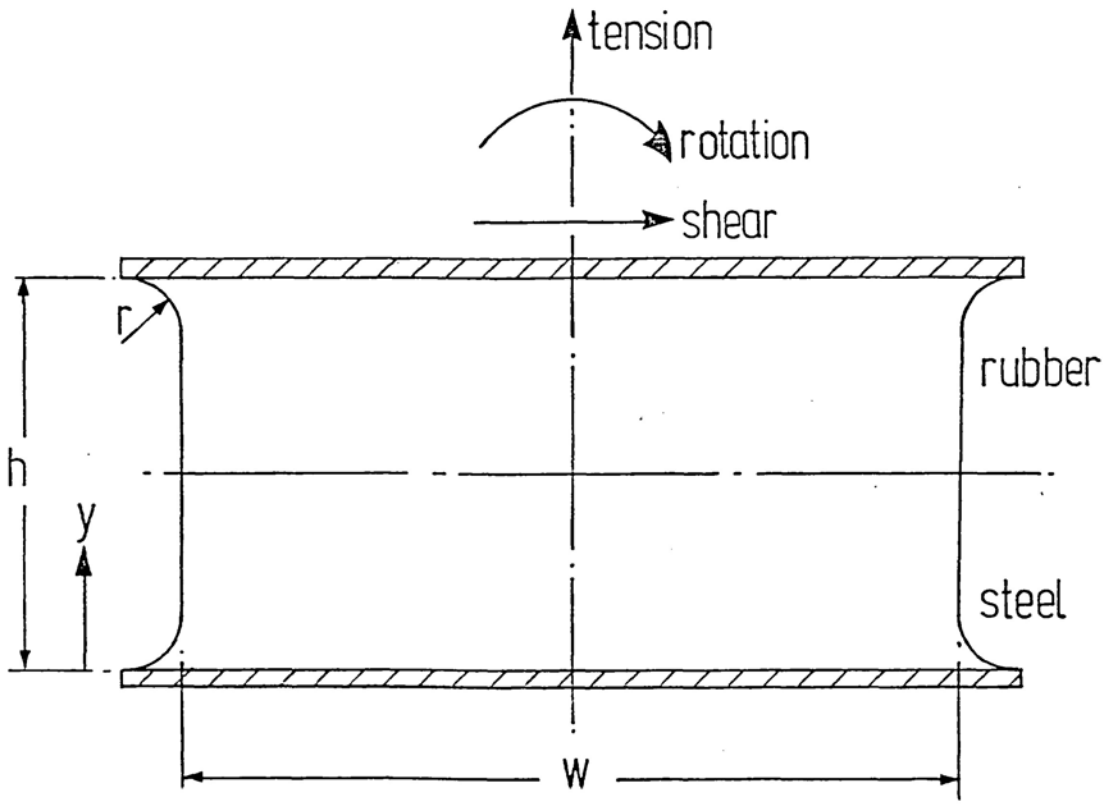


Fig. 9.1 Model section. For plane strain, the depth dimension normal to the plane of this section is infinite. For the purpose of calculation a section of unit depth is assumed. For disks w is the diameter.

section height to fillet radius, ie

$$k - a = F_s F_r \qquad (9.1)$$

where a is a constant.

Blocks with square corners are analysed theoretically and numerically in Sections 9.4 and 9.5 to determine the effect of section shape on k, ie the F_s term in eq. (9.1). As mentioned in Section 8.5 a more rigorous analytical treatment than these by Adkins (64) has shown the strain at a square corner of a deformed block to be infinite - hence the need for some form of fillet - but the infinite strain does not occur in the analyses used here. In Section 9.6 the forms of F_s for blocks with fillets are verified, and F_r is determined using numerical analysis.

Theoretical analyses of rubber are, in general, considerably simplified if the rubber is assumed to be incompressible, ie that its Poisson's ratio ν is 0.5, but in a few cases allowance must be made for the finite compressibility of the rubber. In the numerical finite-element analyses used in this section some compressibility is essential. As discussed in Section 8.3, the two materials constants employed are the Lamé constants G (the shear modulus) and λ, the latter being taken as 3000G (67,68) which corresponds to a Poisson's ratio of 0.49983.

9.2 Numerical method

Two finite-element programmes - one for plane strain analysis of rubber and the other one for analysing axially deformed bodies of revolution - described in Section 8 are also used in this section.

In the programme a grid of rectangular elements is generated to represent the basic rectangular section of the model, similar to that shown in Fig. 8.3. Each edge node is then moved horizontally

to give the required edge profile and the distances from the centre line of other nodes on the same horizontal line are scaled in the same proportion. Computed edge strains are based on the linear distances between edge nodes in the strained and unstrained states, and are given at the mean (unstrained) distance y from the bond. The maximum edge strain e_p can thus be obtained.

Because of symmetry it was not necessary to analyse the whole section except for a few cases in shear, so in tension only the bottom left quarter was analysed, only the bottom half in rotation, and in shear the analyses were mainly of a left section of width between 2h and 4h (Fig. 9.2).

Nominal strains applied to the section are always based on the basic rectangular section, ie the model of Fig. 9.1 without the fillets. The nominal strains e for the three modes of deformation - tension, shear and rotation - are as described in Section 8 and they are shown in Fig. 9.2. In rotation e is the fractional increase in the distance between the left corners of the basic rectangle for a clockwise rotation of the upper metal plate. The nominal strains used in the finite element analyses were 1% for tension and rotation and 10% for shear, the latter being greater because of the small element strains at 1%.

Strain concentration factors k are determined as the ratio of the peak edge strain e_p to the nominal strain e.

9.3 Plane stress

Strain concentration factors k at the corners of stretched rubber sheets, using the model of Fig. 9.1, have been found empirically by Lindley (33) to be approximately proportional to $(h/r)^{1/3}$ from data plotted on logarithmic scales. Some of these numerical data are

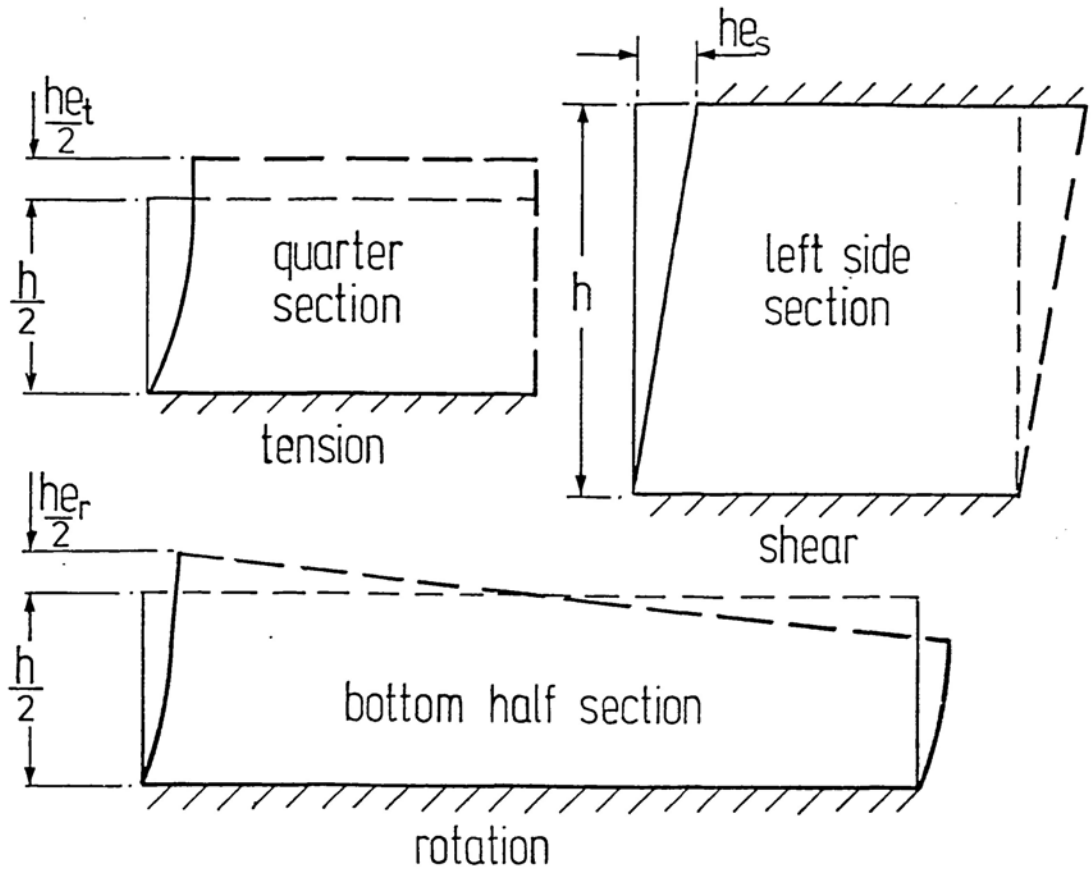


Fig. 9.2 Part sections analysed numerically; in some cases a full section was analysed in shear. The strains are defined as shown for the three modes of deformation.

replotted as k against $(h/r)^{1/3}$ on linear scales in Fig. 9.3 giving an improved empirical relation

$$k - 0.4 = F_s \left\{ (h/r)^{1/3} - 0.4 \right\} \qquad (9.2)$$

where F_s is a function solely of the width-to-height ratio w/h. The form of this relation is that of eq. (9.1).

Minor exceptions to eq. (9.1), and hence to eq. (9.2), were mentioned in Section 9.1. The average tensile stress normal to a plane parallel to the metal end pieces is inversely proportional to the width of that plane. When the section edge-to-edge width of a sheet varies significantly, as is the case for the combination of large r/h and small w/h, so also does the average stress. It is this which leads to departures from the empirical relations.

For relatively wide sheets, at distances greater than about 2h from the edges, the rubber is in a state of uniform strain (pure shear). The width of this central region thus has no effect on the strain distribution in the outer regions (each of width 2h), consequently F_s and hence k are independent of w/h for w/h greater than about 4. Similarly, for relatively tall sheets (or strips) there is a central region for h/w greater than about 4 where the rubber is in uniform simple extension. In this case, however, the size of the corner radius is related to the width, F_r being a function of w/r, with F_s again constant. Because of these limiting conditions there is only a small overall variation in F_s for sheets in tension.

Stress concentration factors k' of shouldered plates in tension have been investigated by Fessler, Rodgers and Stanley (69). The model used was similar to that of Fig. 9.1 except that it was of the same material throughout instead of having the soft centre with rigid outer

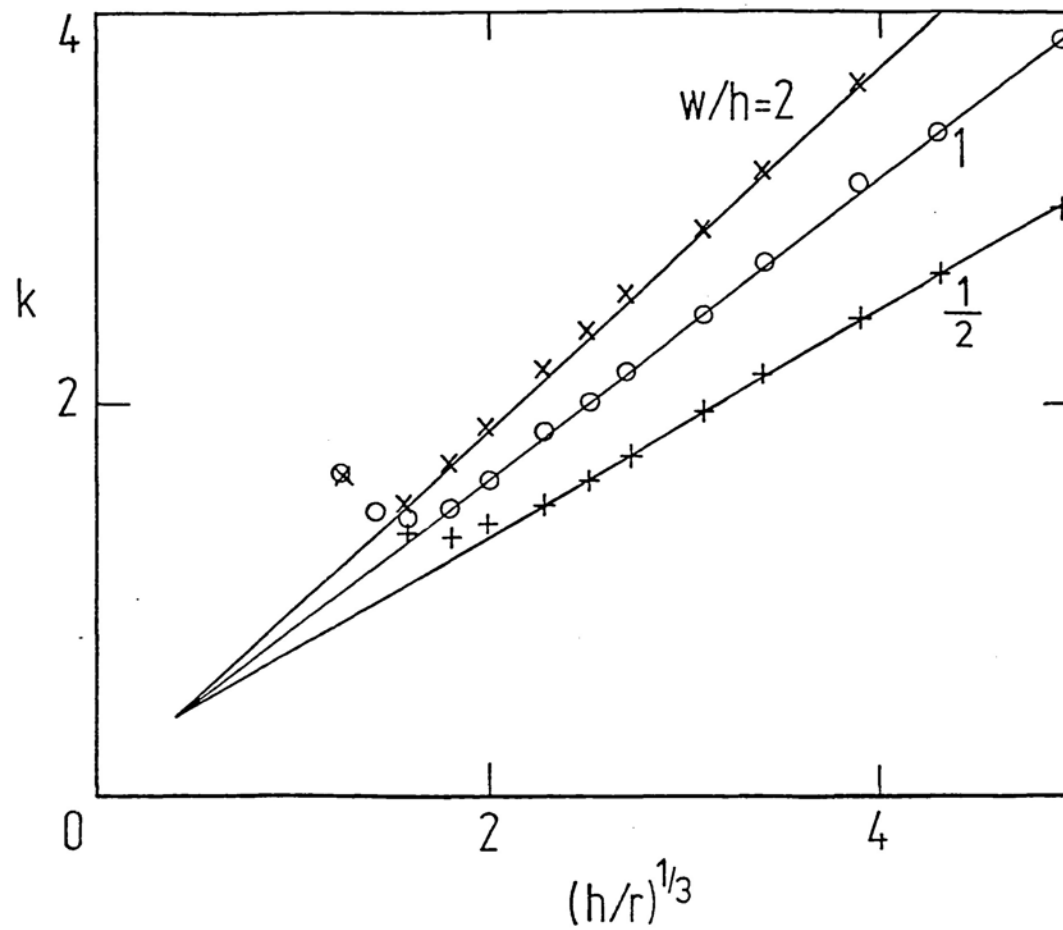


Fig. 9.3 Variation of strain concentration factor k for rubber sheets in tension with the height-to-radius ratio (h/r) for three width-to-height ratios (w/h). (Plane stress data from Lindley (33)).

parts. The empirical relation they proposed is, on average,

$$k' - 1 = 0.465\ (w/r)^{0.38} \qquad (9.3)$$

Their h/w ratio was chosen large enough that F_s was constant and their F_r (expressed in terms of w/r) is not too dissimilar to that for rubber in eq. (9.2). They also found that eq. (9.3) applied to shouldered shafts of diameter w in tension and that for these shafts k' in torsion was about 0.625 of k' in tension.

9.4 Theoretical considerations for F_s

When fillets, meeting the bond at an angle of less than 45^o, are present a finite volume of rubber is involved in the strain concentrations. This precludes the infinite normal stresses and zero shear stresses which, theoretically, would occur in the infinitesimally small volume associated with the strain concentration at a square corner (64). The latter is also avoided, through the assumptions, in approximate theoretical treatments (65,66,70) for the stiffness of blocks with square corners.

9.4.1 Compression

Relations for the stiffness of bonded rubber blocks in compression are often given in terms of the shape factor S which is defined as the ratio of cross-sectional area to force-free areas. For plane strain

$$S = w/2h$$

and for a disk of diameter w

$$S = w/4h$$

The function F_s of w/h in eq. (9.1) may therefore be expressed in terms of S for both plane-strain sections and disks. An approximate theoretical solution by Gent and Lindley (65) for the relation between the compression moduli of blocks with square corners and shape factor S

gives some indication of how F_s depends on S. The three assumptions made by them are (i) that the rubber is incompressible, (ii) that planes parallel to the bonded surfaces remain parallel in the deformed state and (iii) that initially vertical lines become parabolic. For a plane-strain section of unit depth (ie normal to the plane of Fig. 9.1), the volume of rubber displaced by a nominal compressive strain e is whe, which produces parabolic bulges at each edge of peak displacement u and each of volume 2uh/3. Thus

$$\frac{u}{h} = \frac{3}{4}\frac{w}{h}e = \frac{3}{2}Se$$

Gent (71) showed that the maximum shear strain e_{sc} due to compression occurs at the bond and is numerically equal to the slope $2u/\frac{1}{2}h$ of the parabola there, ie

$$e_{sc} = 6Se \qquad (9.4)$$

For a bonded rubber disk u/h is half that for the plane strain section (ie 3we/8h) but as the shape factor is w/4h, u/h is unchanged in terms of S and e_{sc} is again given by eq. (9.4). All other strains at the corner will be proportional to the shear strain there and hence to the shape factor, thus

$$k \propto e_{sc}/e \propto F_s \propto S$$

both for plane strain sections and for disks.

9.4.2 Tension

As classical elasticity theory has been used, a nominal tensile strain of magnitude e will simply reverse the signs of all stresses and strains so the proportionality between F_s and S should also apply in tension.

9.4.3 Limiting values

It may be inferred from the discussions in Section 9.3 that at low shape factors F_s will become independent of S as central regions of the blocks will be in a uniform state of strain (either pure shear for plane strain sections or simple extension for disks) providing F_r is given in terms of w/r. However as the majority of rubber engineering components have w/h ratios greater than about 1 further discussions will be restricted to sections with such ratios. For an incompressible material F_s, as deduced here, is proportional to S for all (high) S.

It is clear from the above that it is the bulging of the rubber which causes the strain concentrations at the corners. For compressible materials there is a limiting value of shape factor, S°, above which the amount of bulging is independent of S. The requirement for this case is that in the central regions of the block lines which are vertical initially must remain vertical in the deformed state, ie lateral strains are zero. The normal stress p° at the bond corresponding to this condition for a compression strain e can readily be found. With the usual notation,

$$p_y = 2Ge_y + \lambda (e_x + e_y + e_z)$$

whence, by putting $p_y = p^{\circ}$, $e_y = e$, $e_x = e_z = 0$,

$$p^{\circ} = (2G + \lambda)e \qquad (9.5)$$

For a block of incompressible material in plane strain the approximate theory by Gent and Lindley (65) gives a normal stress p at a distance x from each corner of

$$p = 1.5\ Ge \left\{ w^2 - (w-2x)^2 \right\} / h^2 + 4Ge \qquad (9.6)$$

which has a maximum value p'' at the centre of the bond of

$$p'' = G(4 + 6S^2)e \qquad (9.7)$$

If this normal stress distribution is assumed to hold for blocks of compressible material for $p \leqslant p'$, then at a shape factor S' the peak stress p'' at the centre given by eq. (9.7) can be equated with the limiting value p' given by eq. (9.5) whence

$$S' = \left\{(\lambda - 2G)/6G\right\}^{\frac{1}{2}} \qquad (9.8)$$

For rubber with $\lambda = 3000G$, S' is 22.3. Although this is a very high shape factor in practical terms, the inference is that for higher shape factors F_s is independent of S. For slightly lower shape factors there will still be some significant compressibility of the rubber which will reduce the amount of bulging and hence the magnitude of F_s below the corresponding values for an incompressible material.

For a disk the normal stress distribution is (65)

$$p = 3Ge \left\{ w^2 - (w-2x)^2 \right\} /4h^2 + 3Ge$$

with a maximum value p'' at the centre of the bond of

$$p'' = 3Ge\ (1+4S^2)$$

Equating this with p' from eq. (9.5) gives the shape factor S', above which no further increase in k may be expected, as

$$S' = \left\{(\lambda - G)/12G\right\}^{\frac{1}{2}} \qquad (9.9)$$

which, for $\lambda = 3000G$, is 15.8.

9.4.4 Rotation

For a rotation of the plane strain section the normal stress at the bonds is given approximately by Gent and Meinecke (66) as

$$p = Ge\ (w-2x) \left\{ w^2 - (w-2x)^2 \right\} /2h^2w$$

which has maxima (when dp/dx = o) of

$$p'' = \pm 4GS^2e/(3\sqrt{3}) \qquad (9.10)$$

at distances from the centre line of $w/2\sqrt{3}$ (66,70). As the shear strains at the maxima of p are zero (70) there is no volume displacement across the verticals at distances $w/2\sqrt{3}$ from the centre. The net volume displacement at each edge is thus found to be hwe/6 and hence, as this is one-third that for compression or tension,

$$k(\text{rotation}) = 1/3\ k(\text{tension}) \propto S$$

assuming the edge profile again to be parabolic.

A shape factor S'' can be found, for a block of compressible material undergoing rotation, above which the proportionality of k with S breaks down. It occurs when p'' from eq. (9.10) has the limiting value p' given by eq. (9.5), ie

$$S'' = \left\{3\sqrt{3}(\lambda + 2G)/4G\right\}^{\frac{1}{2}} \qquad (9.11)$$

For λ equal to 3000G, this S'' is about 62. Unlike S' for tension/compression, S'' is not the shape factor above which the net volume displacement of the edge ceases to increase. However, rubber components with shape factors greater than 62 are extremely rare.

9.4.5 Shear

Simple shear produces tensile surface strains at two diagonally opposing corners of the section and compressive surface strains at the other two. However, as there is none of the volume displacement of rubber which occurs in the other modes of deformation, no marked effect of shape factor can be expected in shear, so that F_s (shear) should be substantially constant, ie independent of S.

9.5 F_s for square-cornered blocks using finite elements

The use of finite elements, where stresses and strains are averaged over a finite volume of rubber, avoids the problems associated with the theoretical stress singularity at a square corner referred to at the start of the previous section.

A series of finite element representations for square-cornered blocks covering a range of width/height ratios from unity upwards were generated such that for each one the corner element was square with sides h/64. These have been analysed, with $\lambda = 3000G$, for the cases discussed in Section 9.4. The principal tensile strains in the corner elements have been divided by the nominal strain e to give an effective strain-concentration factor k. There will be a fillet of radius r* for which the peak edge strain is the same as the principal tensile strain in the corner element. As the corner elements are the same size for all S, h/r^* and hence F_r are assumed constant for each mode of deformation.

The variations of k with shape factor S, for $\frac{1}{2} \leqslant S \leqslant 8$, are shown on linear scales in Fig. 9.4. The following linear relations between k and S are found for plane strain:

$$k(\text{tension}) - 0.9 = 4.78S \qquad (9.12)$$

$$k(\text{rotation}) - 0.78 = 1.68S \qquad (9.13)$$

$$k(\text{shear}) = 1.26 \quad S \geqslant \tfrac{1}{2}$$

These equations have the same form as eq. (9.1) viz $k-a = F_s F_r$, and with F_r constant, the right hand sides are thus proportional to F_s.

9.5.1 Comparison with theoretical predictions

When expressed in terms of the shape factor, F_s in tension is substantially the same for plane-strain sections and disks, and both the tension F_s and the rotation F_s are proportional to S.

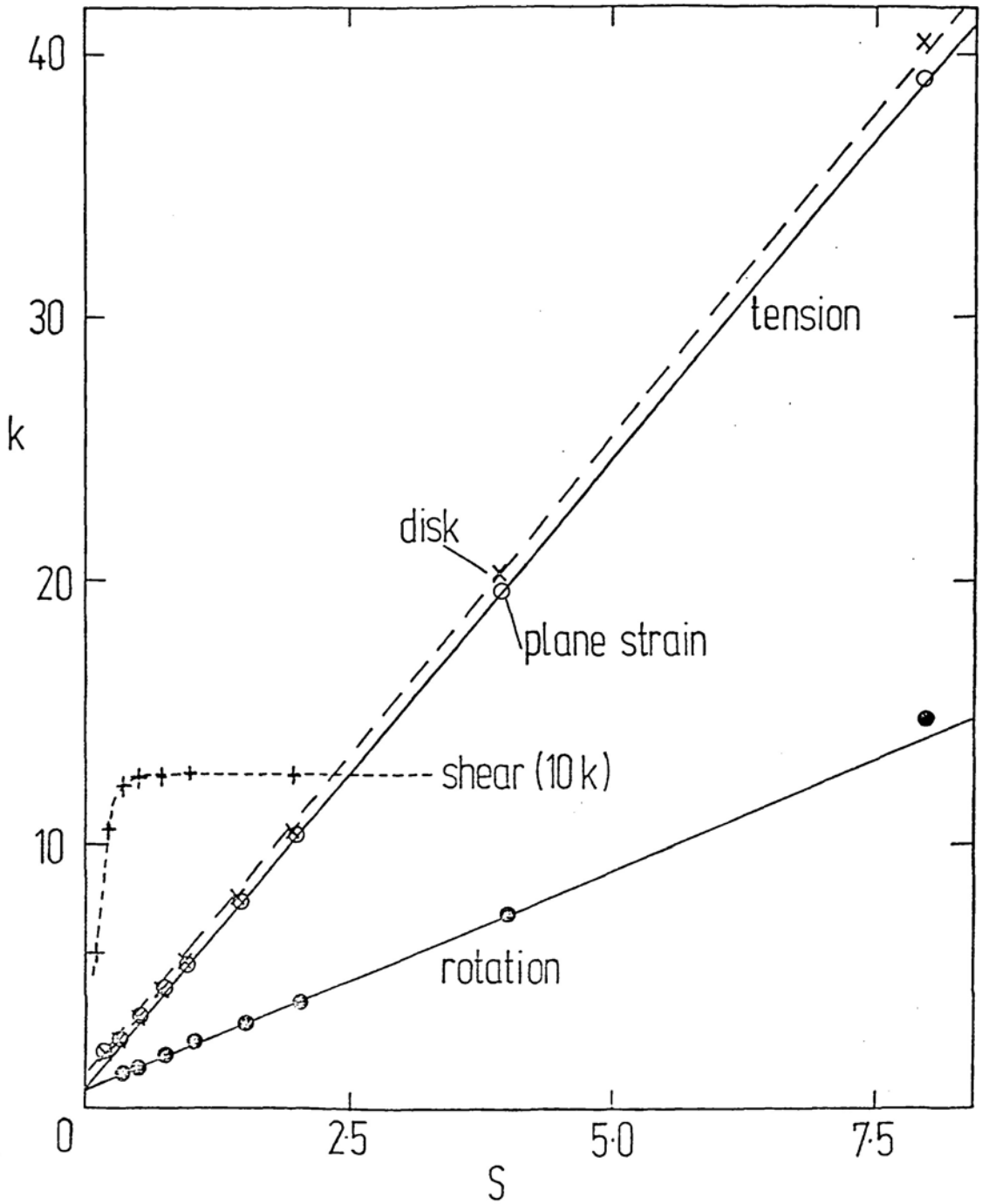


Fig. 9.4 Variation of effective strain concentration factors k at square corners with shape factor S for plane-strain sections in different modes of deformation and for disks in tension. For clarity the k values in shear have been multiplied by 10. (Numerical results.)

For convenience, the coefficient of S in k (tension) is taken as the F_r term so that

$$F_s \text{ (tension)} = S \qquad (9.14)$$

whence, from eqs. (9.12-14),

$$F_s \text{ (rotation)} = 0.35F_s \text{ (tension)} = 0.35S \qquad (9.15)$$

The ratio 0.35 of F_s in rotation to F_s in tension is only 5% higher than the theoretical prediction of 1/3.

These relations for F_s would be expected to apply, for an incompressible material, at higher shape factors than shown in Fig. 9.4. The departures due to the slight compressibility of rubber are shown in Fig. 9.5 where numerical values of F_s (=(k-a)/4.78) are plotted against S on logarithmic scales. The broken lines are drawn through the numerical results; the full lines are given by eqs. (9.14-15). In tension, k was predicted to be constant above a shape factor (S') of 22.3 for plane-strain sections and 15.8 for disks. In rotation, k was predicted to deviate from eq. (9.13) at a shape factor (S'') of 62. These values are indicated in Fig. 9.5; agreement with the numerical data is not unreasonable. Approximate upper limits for k are obtained when S in eqs. (9.14-15) is replaced by S' and S'' respectively. These limits are represented by the dotted lines in Fig. 9.5.

9.5.2 Shear

In shear F_s, Fig. 9.4, is constant for w>2h. This result is very similar to that for sheets in tension (plane stress). Analysis of the finite-element plane-strain data shows that at distances greater than h from the edge the rubber is uniformly deformed in shear and at distances between ½h and h from the edge

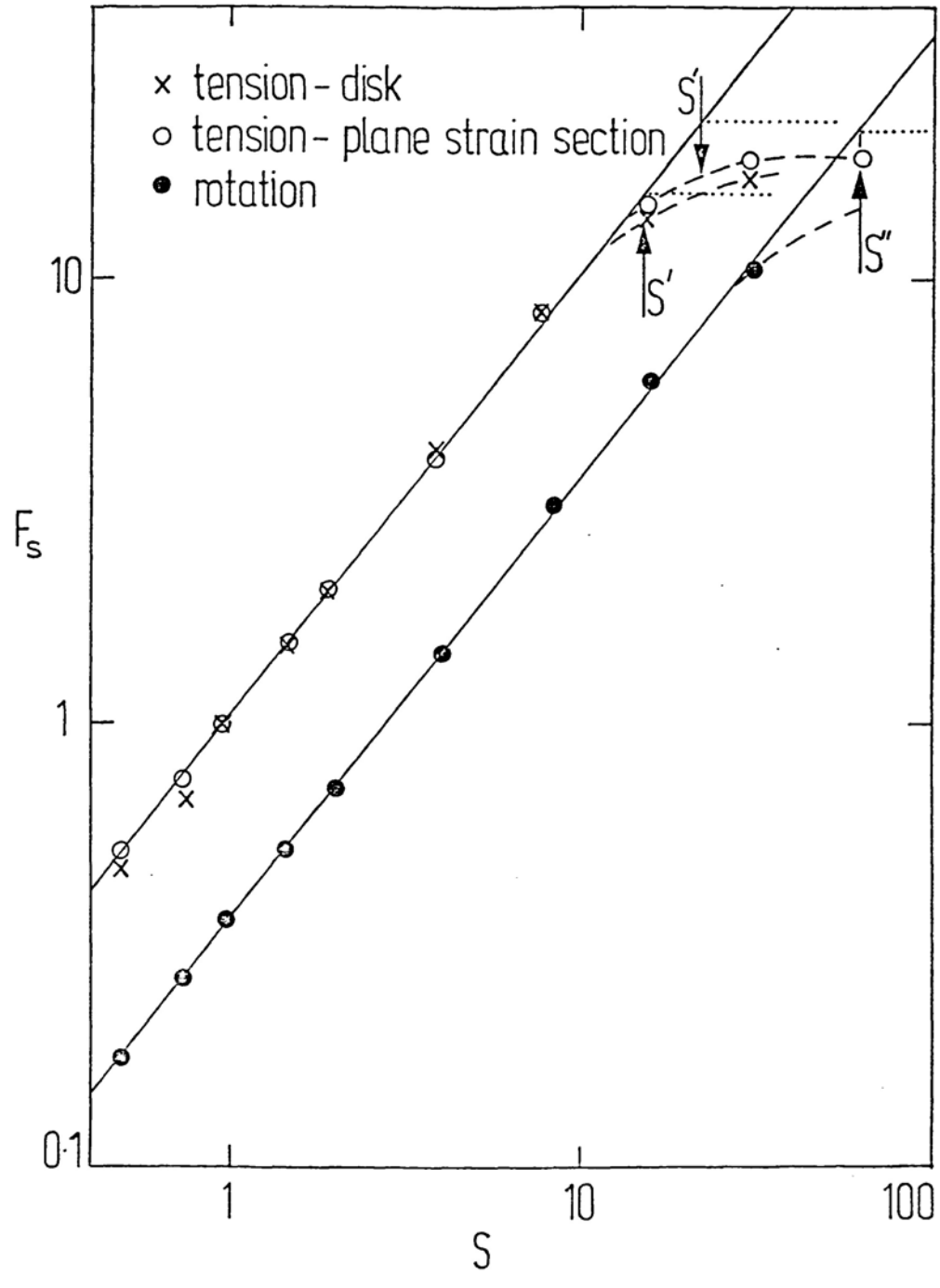


Fig. 9.5 Variation of F_s with shape factor S on logarithmic scales.

the departures from this condition are so slight that there is almost negligible difference between the k values for S=½ and S=1.

9.6 Numerical results for radiussed fillets

9.6.1 Tension

Finite element analyses were carried out, for a 1% nominal tensile strain (e), on plane-strain sections and disks with w/h ratios of 1, 2, 6 and 16 and h/r ratios of 2, 4, 10 and 20. Preliminary analyses showed that the chosen finite-element representation was satisfactory as substantially the same edge strain distributions were obtained with a limited number of finer meshes. The peak edge strains e_p were readily found from these edge strain distributions, and hence the tensile strain concentration factors k (as e_p/e).

It was predicted earlier, from consideration of sections with square corners, that k should be linearly related to the shape factor S (w/2h for plane strain sections and w/4h for disks). When k for the sections with radiussed fillets are plotted against S, linear relations are obtained with an intercept on the k axis of 0.4, ie

$$k - 0.4 = S\ F_r(h/r) \qquad (9.16)$$

To determine the form of the function F_r of h/r, F_r has been determined from eq. (9.16) for each of the k values. The variation of F_r with h/r is shown on logarithmic scales in Fig. 9.6. To satisfy eq. (9.1) F_r should be independent of S, ie be solely a function of h/r, and this requirement is seen to be met, with the exception of the lettered points. The latter correspond to those shapes (low w/h and relatively large radii) for which the cross-sectional area varies markedly, the largest departure being for the disk with w=h and semi-circular edges which has an area four times

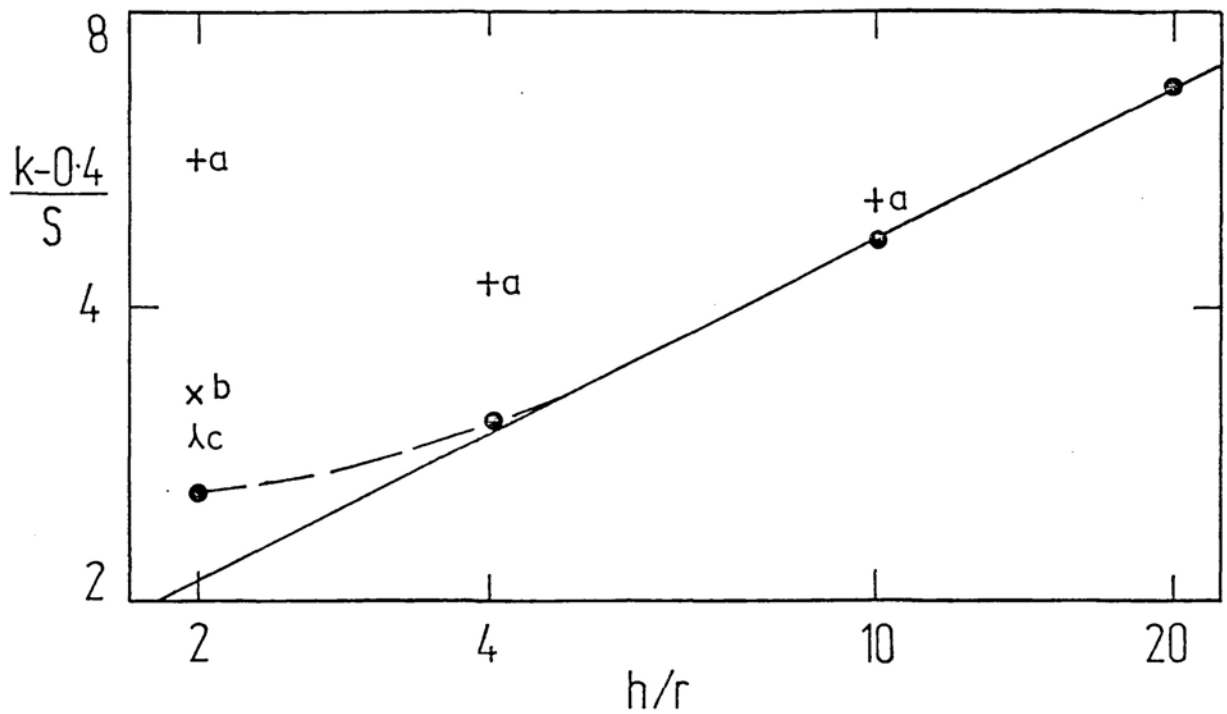


Fig. 9.6 Variation of (k - 0.4)/S with h/r on logarithmic scales for plane-strain sections and disks in tension.

a w/h = 1 (disks)

b w/h = 1 (plane-strain section)

c w/h = 2 (disk)

greater at the bond than at the waist. The plane stress data in Section 9.3 showed similar departures from eq. (9.1).

The full line of Fig. 9.6 is

$$F_r = 1.5\ (h/r)^{\frac{1}{2}} \qquad (9.17)$$

and satisfies $h/r \geqslant 4$. The value of F_r in Fig. 9.6 for semi-circular edges (h/r=2) is 21% higher than that given by eq. (9.17).

In general the peak edge strain occurs at about 0.6r from the bond, the exceptions corresponding to the lettered points on Fig. 9.6 (peak value at centre of edge) and the other shape factors with h/r=2 (peak values less than r/2 from the bond).

Combining eqs. (9.16) and (9.17) gives for k in tension

$$k(\text{tension}) = 1.5\ S\ (h/r)^{\frac{1}{2}} + 0.4 \qquad (9.18)$$

In Fig. 9.7 the numerical values of k are plotted against h/r. The full lines correspond to eq. (9.18), which is seen to be a satisfactory representation of most of the points.

Most rubber-bonded-to-metal sandwich units fall within the range $1 \leqslant w/h \leqslant 16$ covered in Fig. 9.7. For blocks with higher shape factors the substitution of S' for S in eq. (9.18) will give an upper limit for k.

9.6.2 Rotation

From the numerical investigation of plane-strain sections with square corners, eqs. (9.12) and (9.13) give

$$k(\text{rotation}) = 0.35k(\text{tension}) + \text{a constant} \qquad (9.19)$$

The factor 0.35 is the ratio of the F_s values, eq. (9.15). Since the function F_r of h/r is the same for tension and rotation, and eq. (9.19) contains no r term, eq. (9.19) should apply for any ratio of h/r.

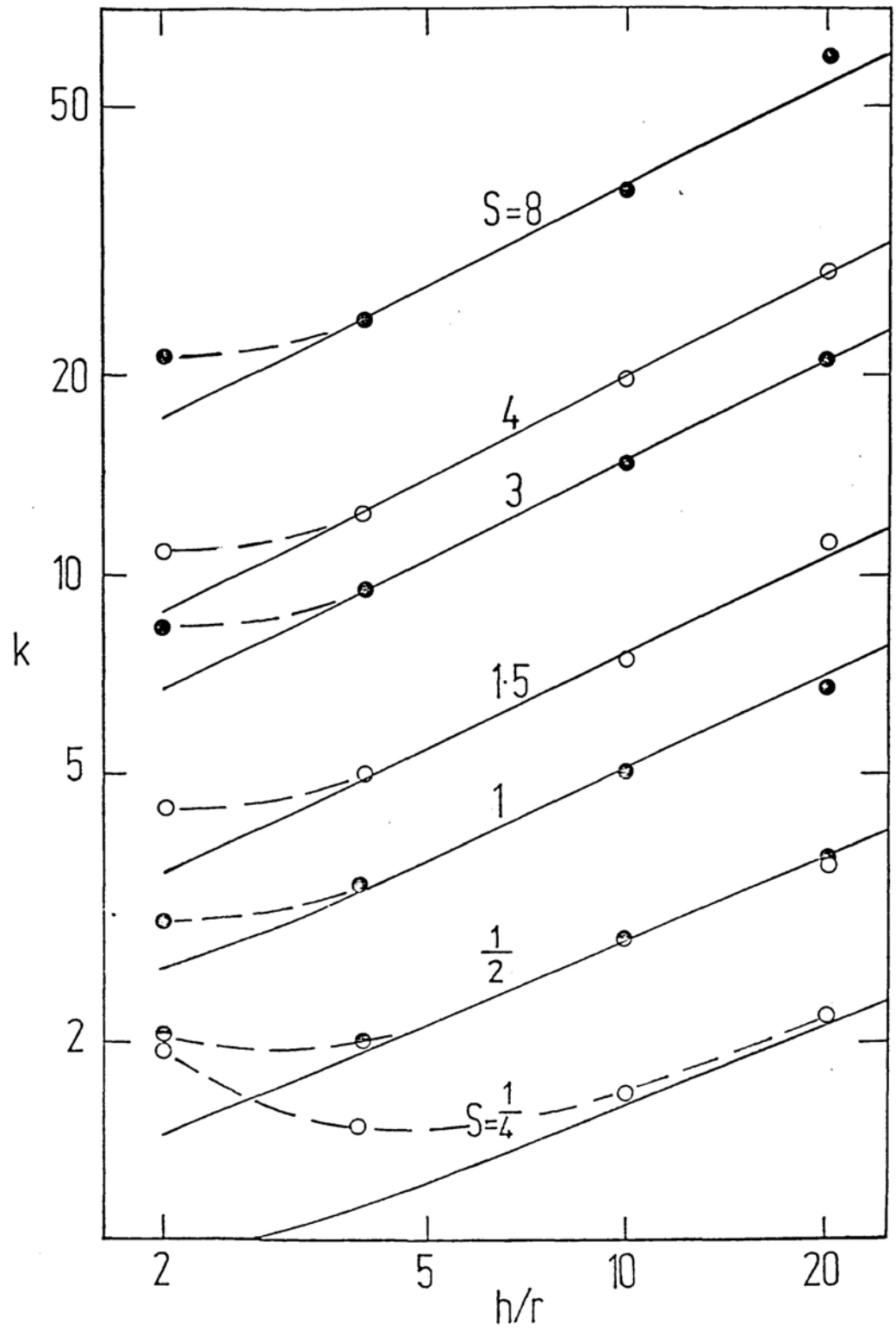


Fig. 9.7 Numerical values of strain concentration factor k in tension plotted on logarithmic scales against the height-to-radius ratio h/r for different shape factors S. The full-line curves are given by eq. (9.18).

Numerical strain concentration factors in rotation were obtained for three shapes: S = 3 with h/r = 2 and 10, and S = 8 with h/r = 4. The results are plotted in Fig. 9.8 against the corresponding tension values.

The two straight lines through the origin of Fig. 9.8 are almost-equally satisfactory representations of the numerical results, ie the final constant in eq. (9.19) can be equated to zero. The slopes are those deduced for square corners. The upper line with the 'numerical' slope of 0.35, eq. (9.19), overestimates k(rotation) by 2.2% on average; the lower line with the 'theoretical' slope of 1/3, (see 9.4.4), underestimates by 2.7% on average. Selecting the latter we conclude that

$$k(\text{rotation}) = 1/3k(\text{tension}) \qquad (9.20)$$

9.6.3 Shear

From the shape factors used in tension, selected full sections have been analysed in shear and no effect of S found; in particular, for semicircular edges, k was 0.667, 0.659 and 0.663 for shape factors of ½, 1 and 3 respectively, an overall variation of 1.2%.

Assuming F_r again to be proportional to $(h/r)^{\frac{1}{2}}$, Fig. 9.9 shows k plotted against $(h/r)^{\frac{1}{2}}$ on linear scales. The straight line relation obtained is

$$k\ (\text{shear}) = 0.238\ (h/r)^{\frac{1}{2}} + 0.34 \qquad (9.21)$$

The peak edge strain occurs at a distance of about 0.6r from the bond, except for semi-circular edges when the distance is about r/2. (The edge strain changes sign about midway between the bonds).

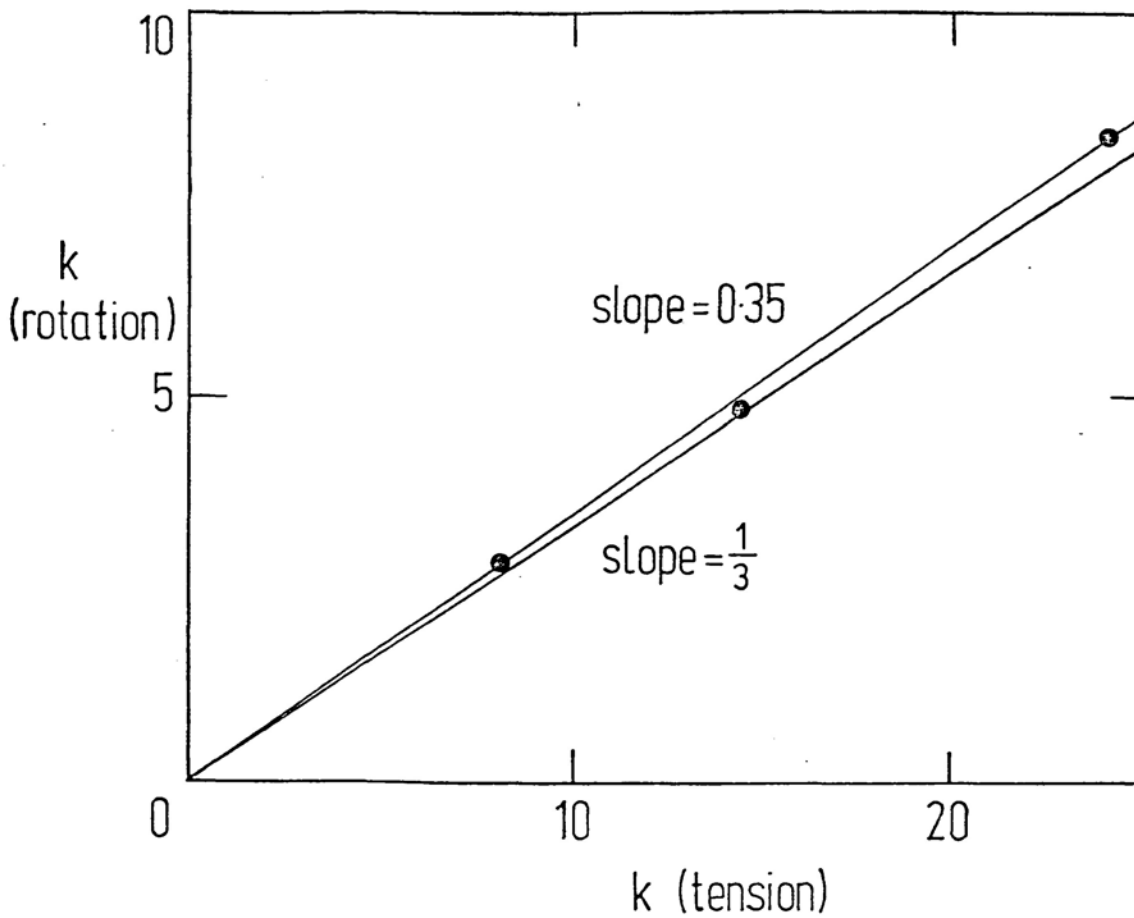


Fig. 9.8 Numerical results showing linear relation between corresponding values of k for rotation and k for tension.

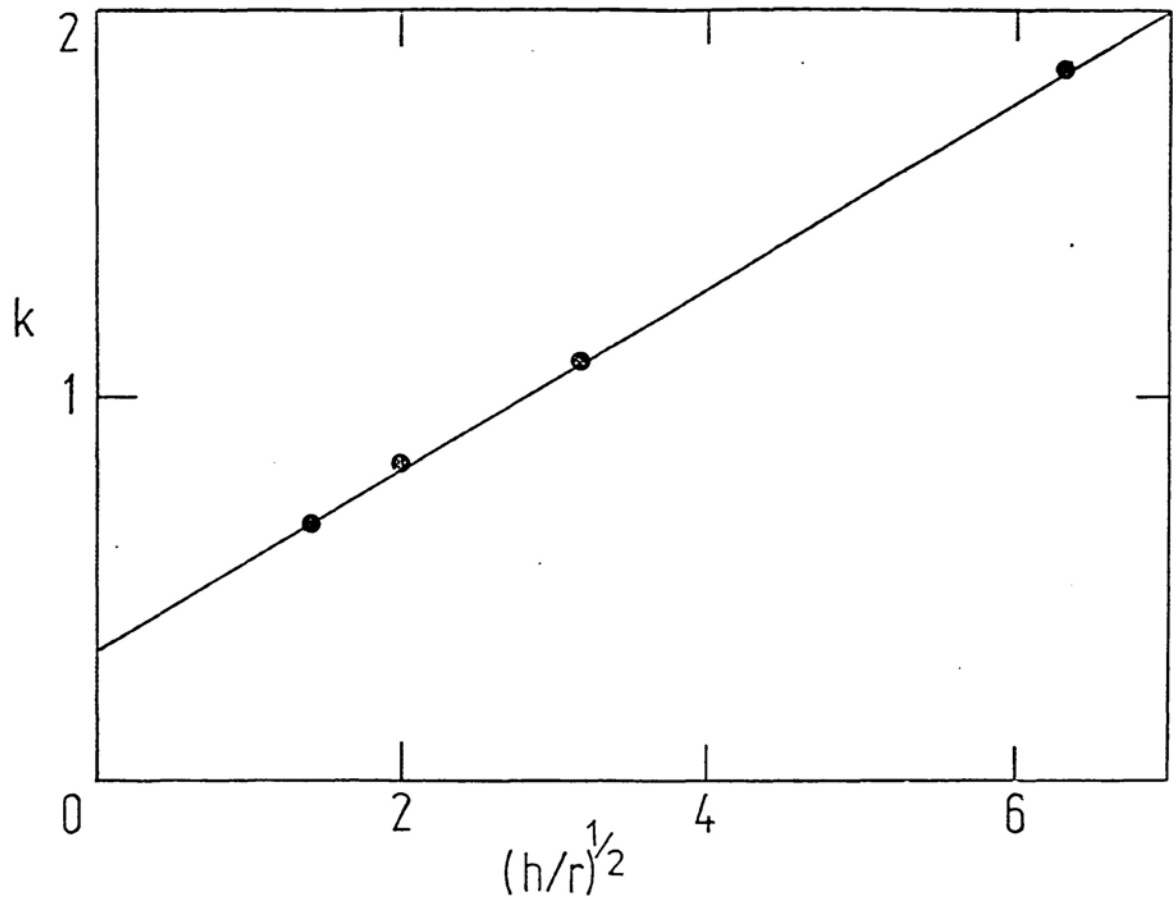


Fig. 9.9 Variation of k with the height-to-radius ratio h/r for plane-strain sections in shear.

9.7 Stress concentration factors

The reason for using strain, rather than stress, concentration factors with blocks of rubber is due to its relatively high incompressibility. For an incompressible material the application of a hydrostatic pressure has no effect on the strain distributions in the deformed state. A high hydrostatic stress can occur in the centres of some bonded rubber blocks, particularly in tension, compression and rotation, whereas at the free edge there is none. This can result in stress concentration factors k' significantly less than unity. (The peak stress at the edge can readily be determined from the peak strain there by multiplying by 4G for plane-strain sections and 3G for disks). As an example, consider a plane-strain section with h/r = 4 in tension. The peak edge stress, using k from eq. (9.18) is $4Ge\ k = 4Ge\left\{(1.5S(h/r)^{\frac{1}{2}} + 0.4)\right\}$ = 4Ge (3S + 0.4) and the applied stress, derived from eq. (9.6), is (65)

$$4Ge\ (1+S^2)$$

giving

$$k' = (3S + 0.4)/(1+S^2)$$

which is less than unity for shape factors greater than about 3.

9.8 Summary

With a few exceptions, due to large variations in cross-sectional area, the strain concentration factors at the radiussed fillets of bonded rubber blocks in tension, rotation and shear are given by

$$k = F_s F_r + a \qquad (9.1)$$

F_s is a function of the shape factor S (defined in terms of the width-to-height ratio in Section 9.4) and F_r is a function of the height-to-radius ratio. For width-to-height ratios between 1 and 16 the following relations for k have been obtained:

$$k \text{ (tension)} = 1.5\ S\ (h/r)^{\frac{1}{2}} + 0.4 \qquad (9.18)$$

$$k \text{ (rotation)} = 0.5\ S\ (h/r)^{\frac{1}{2}} + 0.133 \qquad (9.20)$$

$$k \text{ (shear)} = 0.238\ (h/r)^{\frac{1}{2}} + 0.34 \qquad (9.21)$$

The relative size of the fillet appears in all three relations as $(h/r)^{\frac{1}{2}}$. For a given S, semi-circular edges, which have the lowest possible h/r ratio (of 2), give the lowest k, but for this edge profile the $(h/r)^{\frac{1}{2}}$ term in tension and rotation must be increased by 21% (Fig. 9.6).

When rubber blocks are deformed other than in shear, the displacement of the almost-constant-volume rubber is primarily manifest at the free edges, hence the shape factor terms in tension and rotation. At high shape factors, however, the pressures developed in the rubber can be such that volume changes become significant, and k in tension tends to a limiting value. This limit is obtained from eq. (9.18) with $S = S'$, where for plane strain sections

$$S' = \left\{(\lambda - 2G)/6G\right\}^{\frac{1}{2}} \qquad (9.8)$$

and for disks

$$S' = \left\{(\lambda - G)/12G\right\}^{\frac{1}{2}} \qquad (9.9)$$

There is no theoretical limit to k in rotation, but a working limit, most unlikely to be exceeded in practice, can be obtained from eq. (9.20) with $S = S''$, where

$$S'' = \left\{3\sqrt{3(\lambda + 2G)/4G}\right\}^{\frac{1}{2}} \qquad (9.11)$$

The addition of radiussed fillets to the rubber blocks reduces the edges strains at the bonds to zero, the peak edge strain being at about r/2 from the bond.

PART V

		Page
Section 10	General conclusions and suggestions for further work	201

SECTION 10 GENERAL CONCLUSIONS AND SUGGESTIONS FOR FURTHER WORK

Fatigue in rubber springs is essentially a crack growth process from small naturally occurring flaws which act as stress raisers. It is shown in Section 8 that the crack growth behaviour of rubber is the same in plane strain as it is in plane stress. This finding is of great practical significance as most rubber springs are relatively bulky compared with the thin testpieces normally used to study fatigue in rubber. The understanding of fatigue and crack growth behaviour of rubber under plane stress conditions can now be applied to rubber springs in general.

The fatigue life of rubber springs can be predicted provided the crack growth characteristics of rubbers in service conditions and the tearing energy of rubber springs are known. The work described in Part II of this thesis is an understanding of the fatigue and crack growth behaviour of rubber under the influence of temperature.

As the tensile strip with an edge crack is the testpiece used for the fatigue and crack growth experiments at elevated temperatures, an investigation was first carried out to check that in the tearing energy relation for this testpiece, ie

$$T = 2kWc \qquad \text{(eq. (3.4), page 37)}$$

the k is dependent only on strain. It has been assumed that any changes in the material properties would change the shape of stress-strain curve of the material. Using a numerical finite-element method for plane stress analysis, it is shown in Section 5 that k remains substantially unchanged for various vulcanized rubbers over a wide range of temperature. This has increased the versatility of the tensile strip as a testpiece for obtaining crack growth characteristics of rubber.

Raising the service temperature above ambient has two main effects on natural rubber. It reduces the ability of natural rubber to crystallize under strain and it induces chemical changes in the rubber. In the presence of oxygen, oxidative degradation has a deleterious effect on its physical properties. However, it is shown in Section 6 that the fatigue and crack growth behaviour of a protected natural rubber gum vulcanizate A at 70°C is the same as at 23°C. This means that natural rubber springs can be used up to this temperature without significant loss of strength properties.

At temperatures of 100°C and above, there is a reduction in the fatigue and crack growth resistance of rubber, by about a factor of 2 at 100°C, 5 at 120°C and 13 at 140°C. The reduction in the resistance can be attributed mainly to oxidation as opposed to lessening of strain-induced crystallization.

The fatigue and crack growth tests have been carried out under relaxing conditions. Further investigation should include the effect of temperature on the fatigue and crack growth behaviour of natural rubber under non-relaxing conditions in which strain-induced crystallization plays a major role.

As most rubber springs are relatively thick and bulky compared with the plane stress testpieces, the ageing behaviour of thick rubber blocks has been investigated and this is described in Section 7. For engineering design it is important to know how stiffness, as well as strength, changes with temperature. The puncture test used in this investigation enables both of these properties to be measured. The main advantages of this test method are that it is easy to use, it gives reproducible results and it is sensitive to changes in the rubber.

A summary of the ageing behaviour of rubber blocks with time at several elevated temperatures is given in Section 7.11 (page 140). It is found that oxidation occurs to not more than a few millimetres depth from the surface of the rubber blocks, the depth decreasing with increasing temperature. The oxidized layer can be weak and is thus more susceptible to cracking than the unoxidized rubber. It will be useful to investigate how the fatigue behaviour of blocks is affected by the presence of the weak outer layer and also if the ageing behaviour under both static and dynamic deformations is significantly different to that found in Section 7. However, it is shown in Section 7 that ageing at 70^{o}C for 11 months has no significant effect on the properties of the rubber blocks. This is consistent with the findings in Section 6.

Another feature that merits further investigation is the ageing behaviour of rubber blocks under anaerobic conditions. The presence of certain volatile materials in the rubber appears to have a marked effect in the ageing behaviour of rubber (Section 7.7). As this is basically chemical in nature the investigation would be carried out more effectively by chemists.

Part III of this thesis has been primarily concerned with the determination of tearing energies of rubber springs subjected to three modes of deformation - shear, tension and rotation. Two types of rubber springs are used - plane strain rectangular sections of w wide and h high, and circular disks of diameter w and h high. Both are bonded to metal plates.

It was shown in Section 8 that the numerical plane strain finite-element method gives the same tearing energy as the theoretical relation for long cracks along the bonds of a plane strain section in

simple shear. Using this testpiece, it has been found, as mentioned earlier, that the crack growth characteristic is the same as that obtained using the plane stress testpieces.

When crack lengths along the bonds of the rubber blocks are small the tearing energies are given as follows.

Plane strain shear, at shear strain e

$$T = 0.2\ Ge^2h \qquad (8.30)$$

Plane strain tension, at tensile strain e

$$T = Ge^2h\ (1 + 3S^2) \qquad (8.16)$$

Disk in tension at strain e

$$T = Ge^2h\ (0.75 + 3S^2) \qquad (8.22)$$

Plane strain rotation, with edge strain e

$$T = Ge^2h\ (1 + S^2/3) \qquad (8.29)$$

where the shape factor S is w/2h for plane strain sections and w/4h for disks.

These relations represent the energies available for initiating cracks along the bonds of rubber blocks. In all cases, T is proportional to the rubber thickness h and is independent of crack length. Except in shear, T is also a function of the shape factor S.

The finite-element models used here have square corners at which the strains are high. However, it is good engineering design practice to introduce some form of strain relieving fillet at the edge of a rubber-to-metal bond. The determination of strain concentration factors for bonded rubber blocks with radiussed fillets is described in Section 9, Part IV of this thesis. The two dimensional finite-element analyses are used.

For bonded rubber blocks of width (or diameter) w and height h with corner fillets of radius r, the strain concentration factors k are given as follows.

For shear

$$k = 0.238\ (h/r)^{\frac{1}{2}} + 0.34 \qquad (9.21)$$

For tension

$$k = 1.5S\ (h/r)^{\frac{1}{2}} + 0.4 \qquad (9.18)$$

For rotation

$$k = 0.5S\ (h/r)^{\frac{1}{2}} + 0.133 \qquad (9.20)$$

In all cases k is a function of height-to-radius ratio (h/r). These relations show that at a strain concentration due to a fillet, the strain is linearly dependent on the shape factor S in tension and rotation. It may also be noted that tearing energy T depends on the square of the shape factor S in tension and rotation. This is to be anticipated because T is a measure of strain energy density, and hence the square of the strain, at a strain concentration due to a crack.

This investigation has only covered radiussed fillets. Much useful information would be obtained by extending it to other shapes of fillet, and perhaps also to the tearing energies of rubber blocks with these corner fillets.

REFERENCES

1. Elliott, D.J. and Tidd, B.K., Progress of Rubber Technology, 1974, 34, 83-126, London, IRI.
2. Elliott, D.J., Skinner, T.D. and Smith, J.F., NR Technology, 1970, 1, Part 3, No. 13.
3. Elliott, D.J., Chapter 1 in 'Developments in Rubber Technology - 1', ed. Whelan, A and Lee, K.S., Applied Science, 1979.
4. Greensmith, H.W., Mullins, L. and Thomas, A.G., Chapter 10 in 'The chemistry and physics of rubber-like substances', ed. Bateman, L., Maclaren and Son, 1963.
5. Bateman, L, Cunneen, J.I., Moore, C.G., Mullins, L. and Thomas, A.G., Chapter 19 in 'The chemistry and physics of rubber-like substances', ed. Bateman, L., Maclaren and Son, 1963.
6. Griffith, A.A., Phil. Trans. Roy. Soc.A., 1920, 221, 163.
7. Orowan, E, 'Reports on Progress in Physics', 1948-9, 12, 185-232. The Physical Society.
8. Thomas, A.G., Schweizer Arch. angew. Wiss. Tech, 1968, 34, 182-7.
9. Rivlin, R.S. and Thomas, A.G., J. Polym. Sci., 1953, 10, 291.
10. Greensmith, H.W., J. Appl. Polym. Sci., 1963, 7, 993.
11. Lindley, P.B., J. Strain Anal., 1972, 7, 132.
12. Lindley, P.B., and Thomas, A.G., Proc. 4th Rubb. Technol. Conf., London, 1962, 428.
13. Lake, G.J., and Lindley, P.B., Rubb. J., 1964, 146 (11), 30.
14. Lake, G.J., and Lindley, P.B., J. Appl. Polym. Sci., 1965, 9, 1233.
15. Lake, G.J., and Thomas, A.G., Proc. Roy. Soc. A, 1967, 300, 108.
16. Thomas, A.G., J. Polym. Sci., 1955, 18, 177.
17. Busse, W.F., Ind. Eng. Chem., 1934, 26, 1194.
18. Andrews, E.H., J. Mech. Phys. Solids, 1963, 11, 231.

19. Greensmith, H.W. and Thomas, A.G., J. Polym. Sci., 1955, 18, 189.

20. Mullins, L., Trans. Inst. Rubb. Ind., 1956, 32, 236.

21. Greensmith, H.W., J. Polym. Sci., 1956, 21, 175.

22. Grosch, K.A. and Mullins, L., Rev. Gen. Caout., 1962, 39, 1781.

23. Grosch, K.A., J. Appl. Polym. Sci., 1968, 12, 915.

24. Gent, A.N., Lindley, P.B. and Thomas, A.G., J. Appl. Polym. Sci., 1964, 8, 455.

25. Thomas, A.G., J. Polym. Sci., 1958, 31, 467.

26. Lindley, P.B., Ph.D. Thesis, U. of London, 1972.

27. Cadwell, S.M., Merrill, R.A., Sloman, C.M. and Yost, F.L., Ind. Eng. Chem. Anal. Ed., 1940, 12, 19.

28. Lake, G.J., Rubb. Chem. and Technol., 1972, 45, 309.

29. Ingmanson, J.H. and Kemp, A.R., J. Ind. Eng. Chem., 1938, 30, 1168.

30. Ingmanson, J.H., Kemp, A.R.,and Mueller, G.S., J. Ind. Eng. Chem., 1939, 31, 1472.

31. Lindley, P.B., 'Engineering design with natural rubber', N.R.P.R.A., London, 1964.

32. Gent, A.N., Proc. Rubb. Eng. Conf., London, 1956, 25.

33. Lindley, P.B., J. Strain Anal., 1971, 6, 279.

34. Lake, G.J., Proc. Int. Conf. on Yield, Deformation and Fracture of Polymers, 1970.

35. Clapson, B.E. and Lake, G.J., Rubb. J., 1970, 153, 36.

36. Rivlin, R.S., Phil. Trans. Roy. Soc. A, 1948, 241, 379.

37. Gent, A.N. and Thomas, A.G., J. Polym. Sci., 1958, 28, 625.

38. Mooney, M., J. Appl. Phys., 1940, 11, 582.

39. Gumbrell, S.M, Mullins, L. and Rivlin, R.S., Trans. Faraday Soc., 1953, 49, 1495.

40. Lindley, P.B., J. Strain Anal., 1971, 6, 45.

41. McDonel, E.T. and Shelton, J.R., J. Chem. Eng. Data, 1959, 4, 360.

42. Harwood, J.A.C., Payne, A.R. and Whittaker, R.E., J. Appl. Polym. Sci., 1970, 14, 2183.

43. Andrews, E.H., J. Appl. Phys., 1961, 32, 542.

44. Bell, C.L.M., J. Appl. Polym. Sci., 1965, 9, 3101.

45. Barnard, D., Cain, M.E., Cunneen, J.I. and Houseman, T.H., Rubb. Chem. Technol., 1972, 42, 381.

46. Elliott, D.J., Private communication.

47. Knight, G.T. and Lim, H.S., Int. Rubb. Conf., Kuala Lumpur, 1975, 5, 57.

48. Gent, A.N., Trans IRI, 1958, 34, 46.

49. Livingston, D.I. and Hildenbrand, L.E., Rubb. Chem. Technol., 1964, 37, 14.

50. Livingston, D.I., Yeh, G.S., Rohall, P. and Gehman, S.D., J. Appl. Polym. Sci., 1961, 5, 442.

51. Yeh, G.S. and Livingston, D.I., Rubb. Chem. Technol., 1961, 34, 937.

52. Dozortsev, M.S. and Nechiporenko, A.G., Soviet Rubb. Technol., 1967, 26, (5), 41.

53. Reznikovskii, M.M., Dozortsev, M.S. and Lipskerov, V.M., Soviet Rubb. Technol., 1968, 27, (7), 50.

54. Lukomskaya, A.I. and Dozortsev, M.S., Soviet Rubb. Technol., 1971, 30, (8), 22.

55. Vickers, H.H. and Robison, S.B., Proc. Int. Rubb. Conf., Washington D.C., 1959, 128.

56. Mikhailov, V.G., Panchuk, F.A. and Putankin, K.S., Int. Polym. Sci. Technol., 1975, 2, (8), 53.

57. Timoshenko, S. and Goodier, J.N., 'Theory of elasticity', 3rd edn., (McGraw-Hill, New York, 1970), 408.

58. Waters, N.E., Brit. J. Appl. Phys., 1965, 16, 1387.

59. Van Amerongen, G.J., Rubb. Chem. Technol., 1964, 37, 1065.

60. Cain, M.E. and Knight, G.T., Chem. Ind., 1971, 1125.

61. Rivlin, R.S. and Saunders, D.W., Trans. Instn. Rubb. Ind., 1949, 24, 296.

62. Lindley, P.B., J. Instn. Rubb. Ind., 1971, 5, 243.

63. Lindley, P.B., J. Strain Anal., 1975, 10, 25.

64. Adkins, J.E., MRPRA internal report 1952 (unpublished but summarized by Lindley in Ref. 33).

65. Gent, A.N. and Lindley, P.B., Proc. Inst. Mech. Eng., 1959, 173, 111.

66. Gent, A.N. and Meinecke, E.A., Polym. Eng. Sci., 1970, 10, 48.

67. Wood, L.A. and Martin, G.M., J. Res, Natn. Bur. Stand., 1964, 68A, 259.

68. Holownia, B.P., J. Instn. Rubb. Ind., 1974, 8, 157.

69. Fessler, H., Rogers, C.C. and Stanley, P., J. Strain Anal., 1969, 4, 169.

70. Topaloff, B., Der Bauingenieur, 1964, 39, 50.

71. Gent, A.N., Rubb. J., 1959, 137, 420.

SUPPLEMENTARY REMARKS

On the values of k

In Section 5, the tearing energy for a tensile strip with an edge crack is

$$T = 2kWc \quad \text{(eq. (3.4), page 37)}$$

The value of k is dependent only on strain, at least for rubbers whose stress-strain relationships give W_2/W_1 ratios of 4 or less. This is applicable to relatively low-hysteresis vulcanizates normally used in rubber springs.

According to Andrews' generalized theory of fracture mechanics (72), the theoretical value of k is a complex function of the strain energy distribution around a crack. However, the analytical solution for the determination of the strain energy distribution around the crack appears to be mathematically intractable for highly extensible materials. Consequently Andrews and Fukahori (73) derived k experimentally, by the compliance method (74), for four highly extensible materials, styrene butadiene rubber (SBR), ethylene-propylene rubber, plasticized PVC and polyethylene. The values of k for SBR which is more elastic than the other three materials agree with those in Section 5. However, the values of k for the other three materials increase sharply with strain from the value of π to a maximum value of over 6 and then decrease as the strain is further increased. The values are higher than those in Section 5. This could be due to gross hysteresis and excessive set exhibited by these materials which are not commonly used for springs. It may be noted that the W_2/W_1 ratios for PVC and polyethylene (73) are well in excess of 4.

Recent applications of fracture mechanics

Rubber-cord laminated structures are often used in practice notably in tyres. Under repeated stressing, two common forms of cracking are observed: (1) growth of cracks between the ply layers and (2) growth of cylindrical cracks around individual cords ('socketing').

Using the fracture mechanics approach based on the tearing energy concept, Breidenbach and Lake (75,76) found that the rate of crack growth in two-ply laminates could be predicted in terms of the elastic properties and dimensions of the laminate, the magnitude of the deformations and the basic crack growth characteristics of the ply rubber.

A recent study by Lindley and Stevenson (77) has shown that the fracture mechanics approach can also be used to predict the fatigue life of rubber springs in compression. Fatigue lives were increased by a factor of five when specially shaped fillets were employed.

References

72. Andrews, E.H., J. Mat. Sci., 1974, 9, 887.

73. Andrews, E.H. and Fukahori, Y., J. Mat. Sci., 1977, 12, 1307.

74. Andrews, E.H. and Billington, E.W., J. Mat. Sci., 1976, 11, 1354.

75. Breidenbach, R.F. and Lake, G.J., Rubb. Chem. Tech., 1978, 52, 96.

76. Breidenbach, R.F. and Lake, G.J., Phil. Trans. R. Soc. London, 1981, A299, 189.

77. Lindley, P.B. and Stevenson, A., Proc. of Fatigue '81, Soc. Environmental Engineers, 1981, 233.